2014-12-01

Shear-Dominated Bending Behavior of Carbon/Epoxy Composite Lattice IsoBeam Structures

Kirsten Bramall Hinds
Brigham Young University - Provo

Shear-Dominated Bending Behavior of Carbon/Epoxy Composite Lattice IsoBeam Structures

Kirsten Bramall Hinds

A thesis submitted to the faculty of
Brigham Young University
in partial fulfillment of the requirements for the degree of

Master of Science

David W. Jensen, Chair
Richard J. Balling
Paul W. Richards

Department of Civil and Environmental Engineering

Brigham Young University

December 2014

ABSTRACT

Shear-Dominated Bending Behavior of Carbon/Epoxy
Composite Lattice IsoBeam Structures

Kirsten Bramall Hinds
Department of Civil and Environmental Engineering, BYU
Master of Science

Composite lattice structures known as the IsoBeam™ made with unidirectional carbon/epoxy were manufactured and tested in shear-dominated bending. The manufacturing process consisted of placing tows of carbon fiber pre-impregnated with epoxy resin onto a pin-type mandrel to create members with interwoven joints. The members were consolidated with a half spiral aramid sleeve. The IsoBeam structure consists of two main types of members: longitudinal and diagonal members measuring nominally 0.4 in. (10.2 mm) and 0.2 in. (5.1 mm) in diameter, respectively. The hand-manufactured specimens measured nominally 6 in. (152.4 mm) high by 3 in. (76.2 mm) wide by 2 ft (0.61 m) long with 4 bays, each 6 in. (152.4 mm) long. The beams weighed between 1.82-1.86 lbs (8.09-8.27 N). A finite element analysis of the IsoBeam was compared to the experimental results.

The IsoBeam specimens were tested in four-point or three-point bending but were dominated by shear due to short-beam bending because of the low length/height aspect ratio. After testing to failure, individual members that were lightly loaded and appeared to be undamaged were removed and tested in axial compression. The void percentage and fiber volume fraction were also measured. The average maximum strength of the IsoBeam structure was 4.11 kips (18.3 kN), yielding an equivalent shear of 2.06 kips (9.15 kN) and bending moment of 20.2 kip-in (2.29 kN-m). This strength was lower than expected and is attributed primarily to low material quality, insufficient consolidation of members, and inadequate tension on the tows during manufacturing. The structure exhibited ductile behavior absorbing considerable energy after initial failure, as well as exhibiting damage tolerance due to the inherent structural redundancy. The inner diagonal members which are inherently stiffer exhibited higher strains than the side outer diagonal members after initial failure.

The members removed and tested exhibited an average compression strength of 86.9 ksi (599 MPa) and compression modulus of 17.8 Msi (122 GPa) which are both lower than observed in members tested in past research. The diagonal members had a higher strength of 111 ksi (767 MPa) than the longitudinal member's compression strength of 62.5 ksi (431 MPa). Most members were seen to have a high percentage of voids with an average of 4.3% for diagonal members and 6.4% for longitudinal members. The average fiber volume fraction content of members was very low at 38%.

The linear finite element analysis of the IsoBeam structure predicted failure at a load of 34 kips (151 kN). Without considering buckling, the first member predicted to fail was a vertical outer diagonal. This research demonstrates that increasing the manufacturing quality should yield an IsoBeam structure that is strong, ductile and damage tolerant.

Keywords: IsoBeam, IsoTruss, shear, composite lattice, carbon fiber, finite element analysis

ACKNOWLEDGEMENTS

I am so grateful for the opportunity to research this subject and for the great learning environment provided by Brigham Young University and the Civil and Environmental Engineering department. I would like to thank Dr. David W. Jensen for this research opportunity and for his genuine guidance and expertise. I know he put in countless hours to assist me in my success. Thank you to all of my fellow students and research assistants that aided me in my research. I would also like to thank Dave Anderson and Rodney Mayo. Thank you to TCR Composites for donating the material used in this research.

Thank you to my family and friends who were encouraging and supportive. Specifically, my husband, who not only assisted me, but showed me love and support throughout. Most importantly, thank you to my Heavenly Father who I most definitely owe gratitude for blessing me during this process.

TABLE OF CONTENTS

LIST OF TABLES

LIST OF FIGURES

1 INTRODUCTION

The IsoBeam™ is a rectangular, lattice structure made of unidirectional composites. This research provides an analytical and experimental investigation of the IsoBeam (Figure 1-1) loaded in shear-dominated bending. A finite element analysis was created to predict the strength and stiffness characteristics. Three specimens were tested in short-beam bending and individual members analyzed for material properties. This analysis and experimentation provide an initial evaluation of the quality of hand-manufactured, composite structures to be utilized in beam applications.

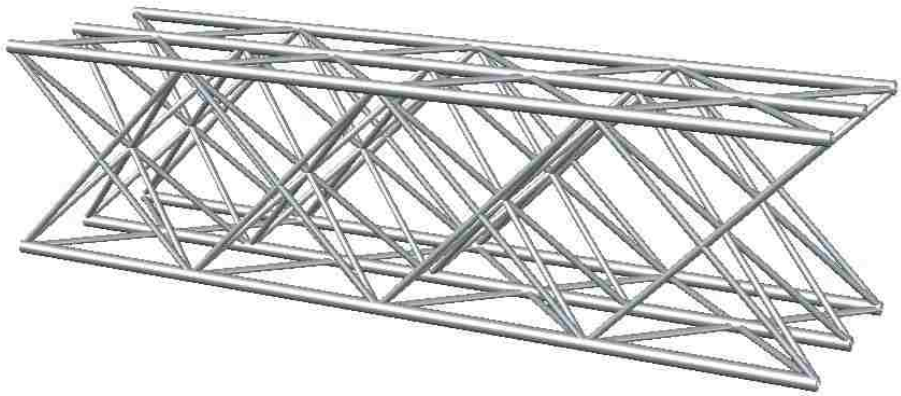

Figure 1-1: Model of IsoBeam™ Structure

This research defines the process for weaving and consolidating an IsoBeam structure by hand as well as analytically predicts the strength of a properly manufactured and consolidated IsoBeam. The characteristics of a carbon/epoxy IsoBeam structure loaded transversely to failure

are determined and the compression strength, void content and fiber volume fraction of hand-woven members are compared to machine-woven members from past research. Lastly, the quality of hand-manufactured IsoBeam specimens is analyzed to provide suggestions for improved manufacturing processes.

Composite structures can provide substantial strength in addition to light-weight characteristics. The IsoTruss®, which consists of unidirectional composite members and interwoven joints, demonstrated this behavior [1]. To create an IsoBeam™ structure, the underlying structure, the IsoTruss, has been slightly distorted to create a similar structure with a rectangular cross-sectional shape. The IsoBeam provides comparable benefits to the basic IsoTruss, mainly the open lattice structure, redundancy and high strength-to-weight ratio, but may be used in other applications, where a rectangular cross-section is preferred.

This research examines the structural characteristics of a hand-manufactured IsoBeam structure. The IsoBeam specimens were tested in flexure, because bending is common in beam applications, but due to the complications in fabricating the IsoBeams by hand, the beams were too short to exhibit complete bending behavior. Thus, the beams tested in bending were dominated by shear due to their low length/height aspect ratio. This is referred to as shear-dominated bending. An analysis was performed using a finite element model and the results were compared to experimental testing of IsoBeam specimens.

1.1 **Description of the IsoBeam**

The IsoBeam™ is a composite lattice structure in the shape of a rectangular beam with members intersecting at nodes. This rectangular shape enables more applications of the basic underlying composite lattice structure, the IsoTruss, where flat upper and lower surfaces are

needed or desired. These applications include bridge decks, truck beds, airplane wing boxes and floor beams, or any beam setting where there is an economical advantage to reducing weight.

The IsoBeam geometry is created from a 6-node double-grid IsoTruss where four of the nodes are shifted vertically so they are on the same top and bottom plane. This is shown in Figure 1-2 with the 6-node double-grid IsoTruss and IsoBeam end profiles. This moves more longitudinal fibers further from the neutral axis, increasing the moment of inertia. This increase is a factor of 1.48 over the 6-node double-grid IsoTruss with 12 longitudinal members and an increase of 5.85 over the single-grid 6-node IsoTruss with 6 longitudinal members [2]. Conversely, going from a 6-node single-grid IsoTruss to an IsoBeam adds substantial manufacturing complexity due to the longitudinal member being on the most outer plane of the IsoBeam. This manufacturing complexity is similar to complexity seen when going from a single-gird IsoTruss to a double-grid IsoTruss.

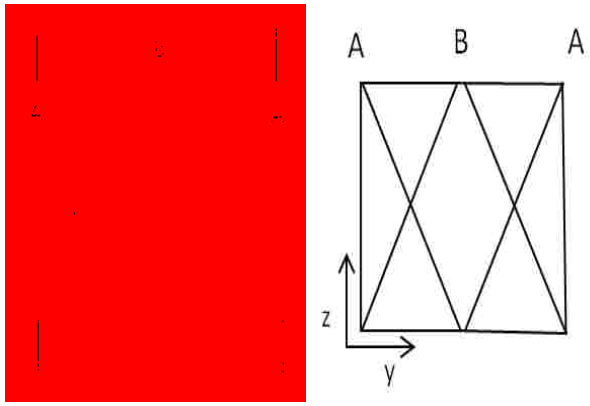

Figure 1-2: End views of a 6-node Double-grid IsoTruss and an IsoBeam structures. Arrows indicate shifting required to change an IsoTruss into an IsoBeam.

The IsoBeam consists of longitudinal and diagonal members. The longitudinal members are the six straight members that run along the length of the beam on the top and bottom. The diagonal members in a conventional IsoTruss can be referred to as helicals, since they are related

to helical members, which create a helix around the longitudinal members. The helix in the IsoTruss is broken up by straight longitudinal members; a definite piece-wise linear helical pattern can be seen on the IsoTruss or a helical pattern broken up by the vertical longitudinal members. This helical pattern is not as evident when converted to the IsoBeam shape. The diagonal members of the IsoBeam act and look more like the diagonal members of a traditional truss. Thus, we refer to these members as diagonal members in the IsoBeam.

The diagonal members consist of three groups: the outer diagonal members in the two vertical side planes, the outer diagonal members in the two horizontal planes, and the inner diagonal members. The vertical outer diagonal members lie in vertical planes on the left and right sides of the IsoBeam, forming an X-shape every bay. The horizontal outer diagonal members lie in horizontal planes on the top and bottom of the structure, also forming an X-shape every bay. The inner diagonal members are inside the structure and consist of four diagonal members intersecting to create an interwoven joint at mid-height that creates an essentially rigid (i.e., fully three-dimensionally constrained) joint. There are two pairs of four inner diagonal members in every bay of the IsoBeam. The IsoBeam nodes are labeled in Figure 1-3. The cross-sections labeled in Figure 1-3 are displayed in Figure 1-4.

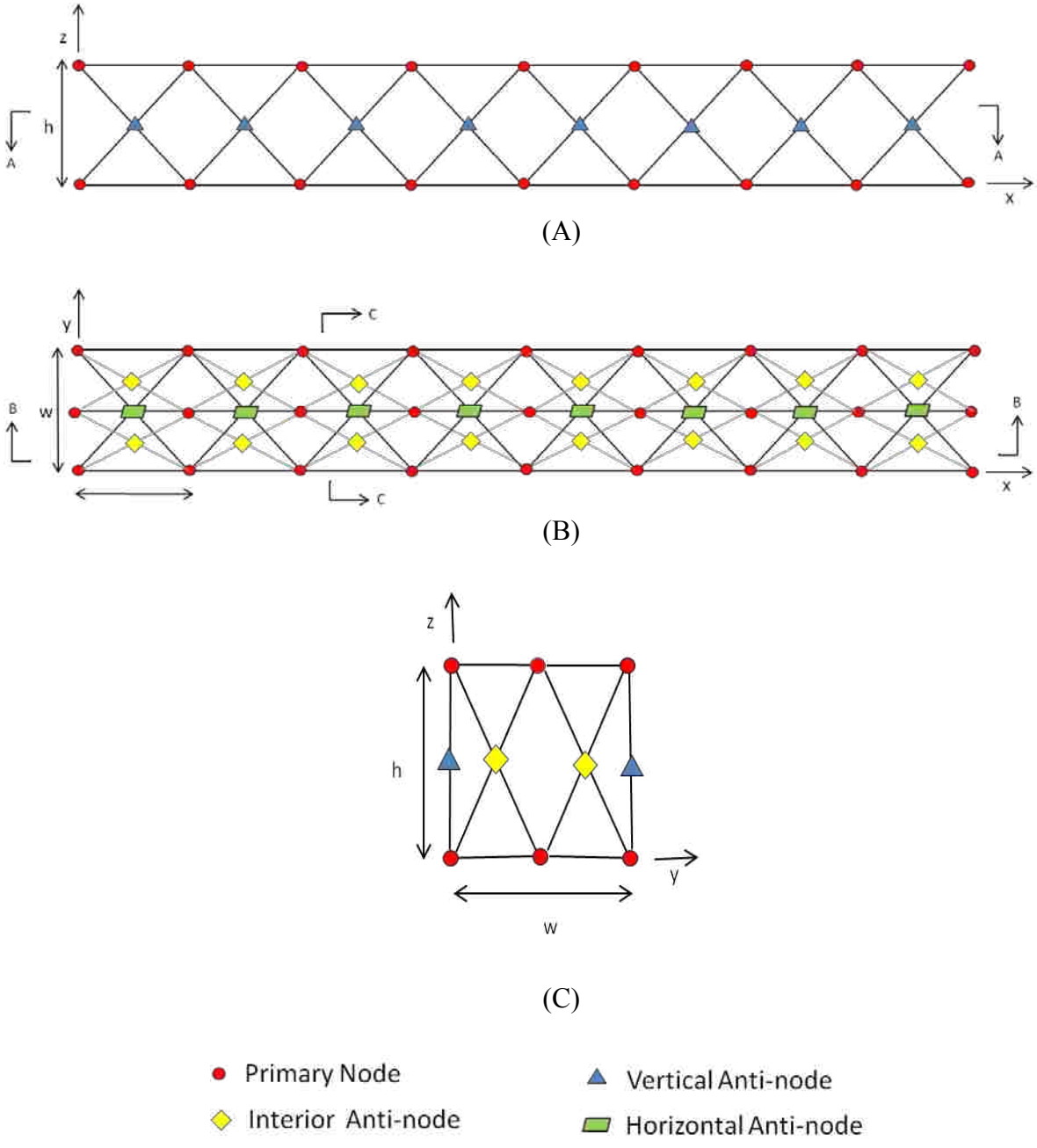

Figure 1-3: IsoBeam Structure with Labeled Nodes: A) Side view; B) Top view; and, C) End view

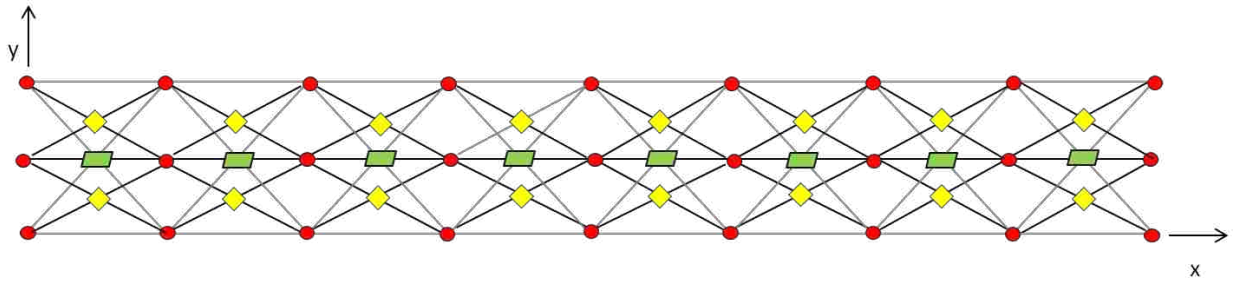

(A-A)

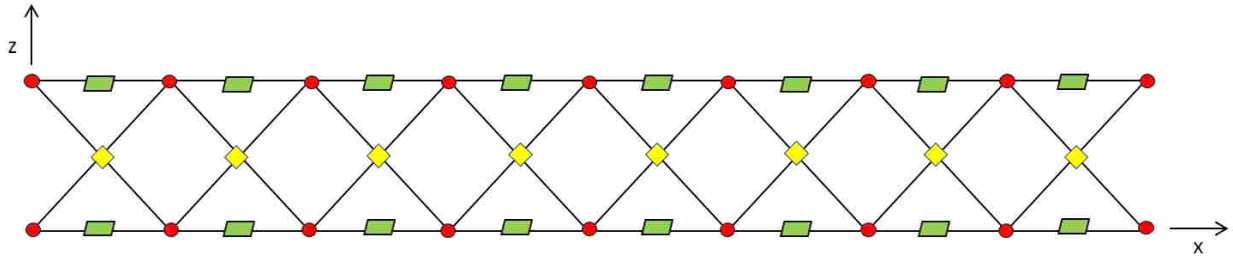

(B-B)

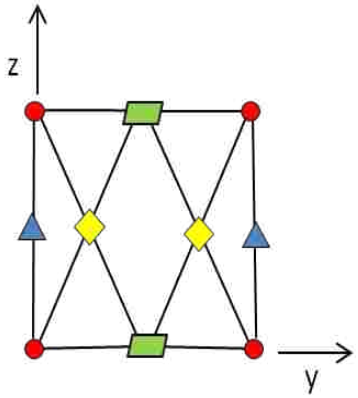

(C-C)

Figure 1-4: Cross-sections A-A, B-B and C-C as Identified in Figure 1-3

The primary nodes or longitudinal nodes are defined as the nodes supported during fabrication and are located on the four outer corners of the cross-section with an additional node in the middle on the top and bottom. The anti-nodes, both horizontal and vertical, are the outer nodes created as the diagonal members in the horizontal and vertical planes intersect. The horizontal anti-nodes are located on the top and bottom while the vertical anti-nodes are located on the sides. Interior anti-Nodes are a subset of anti-nodes, created as several inner diagonal

members intersect, and are the only nodes located in the interior of the IsoBeam. A bay is the fundamental repeating unit, defined from one set of primary (longitudinal) nodes to the next set of primary nodes along the length of the beam.

The IsoBeam overall geometry is defined by the height, h, width, w, bay length, b, and the number of bays, N_b. Given these values, the locations of all the nodes and joints can be described by basic equations.

Equations 1-4 describe the location of all the nodes in the IsoBeam structure as follows.

Coordinates of the Primary (Longitudinal) Nodes:

There are six primary nodes at the beginning of every bay, located on the top and bottom surfaces of the structure. The locations of all primary nodes are defined in Cartesian coordinates (x, y, z), as:

$$\left(b * i, \frac{w}{2} * j, h * k\right) \qquad i = 0, 1, \ldots N_b; \quad j = 0,1,2; \quad k = 0,1 \qquad (1)$$

Coordinates of the Interior Anti-Nodes:

The interior anti-nodes are located every half bay at mid-height. There are two each located at quarter widths. The locations, (x, y, z), are defined as:

$$\left[\left(b * i + \frac{b}{2}\right), \left(\frac{w}{4} + j * \frac{w}{2}\right), \frac{h}{2}\right] \qquad i = 0, 1, \ldots N_b; \quad j = 0,1 \qquad (2)$$

Coordinates of the Horizontal Anti-Nodes:

The two horizontal anti-nodes are located every half bay at mid-width on the top and bottom of every bay. The locations, (x, y, z), are defined as:

$$\left[\left(b * i + \frac{b}{2}\right), \frac{w}{2}, h * k\right] \qquad i = 0, 1, \ldots N_b; \quad k = 0,1 \tag{3}$$

Coordinates of the Vertical Anti-Nodes:

The vertical anti-nodes are located every half bay at mid-height. The locations, (x, y, z), are defined as:

$$\left[\left(b * i + \frac{b}{2}\right), w * j, \frac{h}{2}\right] \qquad i = 0, 1, \ldots N_b; \quad j = 0,1 \tag{4}$$

The members are created using transversely isotropic composite tows of unidirectional carbon fiber, fiberglass, basalt or other fibers pre-impregnated with epoxy resin. The members may be formed using various quantities of tows (meaning a bundle of fibers). The fibers in each tow are either impregnated or subsequently coated with a resin to adhere the fibers to each other upon curing. Before curing, the fibers are consolidated using a sleeve that is either braided or spiral wrapped. This sleeve has most commonly been made with aramid fibers but may also be made of other materials, including shrink tape.

The longitudinal members carry the axial and bending loads while the diagonal members transfer shear and torsion through axial compression or tension in the members. The diagonal members increase the stability of the structure by intersecting and stabilizing the longitudinal members to create shorter buckling lengths.

1.2 **Related Research**

While a substantial amount of work has been completed regarding hexagonal and octagonal IsoTruss configurations, the rectangular IsoBeam structure has not been extensively researched since the development of the structure by Dr. David Jensen and David Jarvis' introduction in his thesis of the IsoBeam as reinforcement for concrete beams [2]. This is due to the difficulty manufacturing the geometry by hand and lack of a braiding machine sufficient in size and capability. Jarvis discusses the creation of the IsoBeam from a 6-node double-grid IsoTruss for the purpose of making the IsoTruss more efficient in flexural loading and designed the mandrel for fabrication used in this research [2].

A description of the IsoTruss and equations similar to those provided in this document for the IsoBeam were documented by Kesler [3], Winkel [4], Scoresby [5] and McCune [6]. Kesler also found that increasing the number of braiders for the consolidating sleeve increased consistency of the braided sleeve and hypothesized that compression failure, rather than buckling, is the preferred failure for individual members [3]. The IsoTruss has been tested in flexure by both Keller [25] and Jensen [26]. IsoTruss was also researched to be used as an aircraft tail section made of polyurethane foam and glass braids [8].

A lightweight, fiber reinforced polymer (FRP) composite triangular truss was examined experimentally and numerically under three-point bending [7]. The structure was similar to those tested in this research, except triangular in cross-section rather than rectangular, and did not contain any inner members. The structure contained members of similar size, but was 19.7 ft (6 m) long. A finite element analysis created in ANSYS matched the experimental data. The members started to buckle at 91.0 lbs (405 N). The structure was optimized using sensitivity

analysis responsive to four key geometric parameters: structure diameter (D), number of bays (N), longitudinal diameter (d1) and helical diameter (d2) [7].

Similar, simplified composite, lattice structures have been researched in many applications. Two flat lattice composite plates were combined to create a three-dimensional panel to be used for spacecraft solar arrays [9]. Isogrid, an equilateral triangular grid, was analyzed and optimized for weight, buckling load, and material failure [10]. Isogrid contains helical ribs similar to the outer diagonal members in this research. The local buckling of the helical ribs has been studied and modeled using finite element analysis to account for the intersecting ribs and hoop sections [11]. Morozov et al. studied the application of anisogrid, composite, lattice, conical shells in applications such as rocket interstages, payload adapters, fuselage components and parts of space antennas [12].

Several sources discussed the modeling of composite, lattice members and structures using finite element analysis similar to the model created in this research. Finite element models of carbon fiber composite hollow cylinders with lattice structures of various geometries have been modeled and analyzed in axial compression, transverse bending, pure bending and torsion [13]. A cylindrical, composite, lattice structure was analyzed using finite element analysis under multiple loading cases including bending, similar to the bending tests in this research [14]. Also, a continuum method was derived for three-dimensional lattice members that are dominated by stretching. The analysis included the compliance of the lattice joints [15].

Hansen [16] studied the pattern and consolidation of interwoven joints similar to the joints formed when the longitudinal and diagonal members intersect in the IsoBeam. He found that longitudinal joints encapsulated with diagonal tows reduces the member compressive strength by only 4.6%; whereas, a joint interwoven with diagonal members in-between the

longitudinal tows reduces member strength by 30.5%. This difference in strength reduction is due to the increased straightness of the longitudinal members. He also concluded, regarding consolidation methods, that sleeves provide the highest strength and Young's modulus for both the encapsulated joints and the interwoven joints. Of the two sleeves types studied, braided and spiral, braided sleeves yielded the highest quality according to consistency, strength and stiffness [16]. This was also later confirmed by Allen [17].

Compression Strength after Impact (CSAI) tests of composite members similar to those created for the longitudinal and diagonal members were conducted by Wisnom [18], Allen [17], Embley [19] and Sika [20, 21]. Embley studied carbon, fiberglass and basalt specimens wrapped with aramid sleeves that were longer than the critical buckling length. His general conclusions included:

- Members with braided sleeves are up to 34% stronger in compression than members with spiral sleeves after being subjected to transverse impact.
- Members with full coverage are up to 38% stronger in compression than members with only half coverage, all after being subjected to transverse impact.
- The buckling strength of carbon/epoxy composites decreases with increasing impact energy. Fiberglass and basalt composites, however, are more flexible, and thus, exhibited less degradation in strength at higher impact energy levels.
- The average buckling strength and stiffness of non-impacted, unidirectional carbon fiber/epoxy was 77.9 ksi (537 MPa) and 17.7 Msi (122 GPa), respectively [19].

Sika studied carbon fiber and fiberglass epoxy specimens consolidated with an aramid sleeve that failed in compression. His conclusions relating to this research are summarized below:

- The compression strength and stiffness of carbon fiber members are unaffected by sleeve type and coverage when members are undamaged, which was also observed by Hansen [16] and Embley [19].
- After impact, however, the ultimate compression strength and stiffness decreased with increasing impact energy level. Increasing sleeve coverage increased the damage tolerance of carbon fiber/epoxy.
- Co-curing a dry fiber sleeve over unidirectional fiber/epoxy effectively consolidates core material.
- The average compression strength and stiffness of non-impacted, unidirectional carbon fiber/epoxy wrapped with a half spiral sleeve of aramid was 139.0 ksi (958 MPa) and 22.3 Msi (147 GPa), respectively [20, 21].

Use of unidirectional carbon, fiberglass and basalt material for members of composite, lattice structures has been investigated [17, 19, 20, and 21]. Each material's damage tolerance was studied including the effect of sleeve coverage and type on the member's damage tolerance. The strength of member joints was examined. The IsoTruss structure has also been extensively studied and characterized [1, 3-6, 16, 24, and 26] along with various other composite, lattice structures [7-15]. This research provides an initial study and description investigating the IsoBeam structure manufactured from unidirectional carbon/epoxy tested in short-beam bending, dominated by shear.

1.3 **Scope of Investigation**

This research presents an investigation of the structural behavior of hand-manufactured IsoBeam structures tested in short-beam bending, dominated by shear to gain insights into the IsoBeam strength and durability characteristics. This research addresses and achieves the following objectives:

- Define the process for weaving and consolidating an IsoBeam structure by hand.
- Analytically predict the strength of a properly manufactured and consolidated IsoBeam.
- Determine the characteristics of a carbon/epoxy IsoBeam structure loaded transversely to failure.
- Compare compression strength, void content and fiber volume fraction of hand-woven members to machine-woven members.
- Quantify the quality of hand-manufactured IsoBeam specimens.

To address these objectives, a finite element model of the beam was created and loaded transversely. This model provides a guide for the expected failure and strength. Three unidirectional carbon fiber IsoBeam specimens (Figure 1-5) were manufactured by hand and tested in short-beam bending, dominated by shear.

After testing the IsoBeam specimens, individual members from each specimen that were lightly loaded and appeared undamaged were cut from the structure, sanded and analyzed. The void percentage and fiber volume fraction were analyzed. These members were tested in compression to compare to similar tests performed by Sika [20] for members produced on a machine with spiral sleeves. This research provides a start to the analysis and characterization of the IsoBeam.

Figure 1-5: Picture of IsoBeam Test Specimen

1.4 Thesis Overview

Chapter 2 describes the experimental approach for testing the IsoBeam specimens with details of the specimen manufacturing process and data collection methods during testing. This chapter also contains information on data reduction and the statistical analysis performed. The test results for the IsoBeam specimens are summarized in Chapter 3. The experimental approach for the members tested in compression is discussed in Chapter 4. Chapter 5 presents the results for the member compression tests. The finite element model and analysis are described in Chapter 6. Chapter 7 contains a discussion of the results comparing the analytical model, IsoBeam experiments, the individual member tests and past research. Chapter 8 details the observations, conclusions and recommendations for further investigation.

2 ISOBEAM TESTING EXPERIMENTAL APPROACH

This chapter details the materials, manufacturing process, specimen preparation and testing procedures used for testing the IsoBeam specimens.

2.1 Materials

A 12k T700 carbon fiber pre-impregnated with UF3369 TCR resin [22] was used to create the specimens in this research. The composite was wrapped by hand with an aramid sleeve to achieve proper member consolidate and decrease voids. A description of the materials used, the manufacturer, and specific type of material are listed in Table 2-1. The filament properties of the carbon fiber used are also listed in Table 2-1. Table 2-2 contains the properties of the material per the manufacturer. The specific batch data for the material used for weaving can be viewed in Appendix A.

Table 2-1: Specimen Material, Manufacturer and Type

Material and Use	Manufacturer	Type	Filament Diameter [in (μm)]	Filament per Tows
Carbon Fiber	Toray	T700SC-12K-50C	2.8E-04 (7)	12,000
Epoxy Matrix	TCR Composites	UF 3369-100	-	-
Aramid Sleeve	DuPont	49-7100 Denier	-	-

Table 2-2: Nominal Material Properties

Material	Tensile Modulus [10^6 psi (GPa)]	Tensile Strength [ksi (MPa)]	Density [lbs/in^3 (g/cm^3)]
Carbon	33.4 (230)	711 (4,900)	0.065 (1.8)
Epoxy	0.445 (3.1)	13.4 (92.4)	0.043 (1.18)
Aramid	410 (2830)	10 (68.9)	0.044 (1.21)

2.2 Fabrication

Fabrication of the IsoBeam specimens consisted of laying tows of pre-impregnated, carbon fiber tows on a mandrel. A single-grid IsoTruss can be filament wound [28], but like the double-grid IsoTruss, the IsoBeam has outer longitudinal members surrounding the inner diagonal members. This requires weaving the inner diagonal members around the longitudinal members and thus, requires manufacturing by hand or by using a 3-dimensional braiding machine [24, 29]. The specimens in this research were created by hand. The members were consolidated using an aramid sleeve wrapped spirally. The specimens were then cured following the manufacturers recommendations. The complete fabrication is explained in detail in the following section.

2.2.1 Manufacturing

Specimens were fabricated by hand using carbon/epoxy with a spiral, aramid sleeve for consolidation. An inner mandrel created by Jarvis was used to create the IsoBeam specimens (Figure 2-1) [2]. The mandrel was waxed in preparation of creating a part with Kiwi® neutral shoe wax to aid in easy removal of the cured specimen. During weaving and consolidation, a

continuous 5 lbs (22 N) of tension was desired, although this was difficult to monitor and maintain. The tension was applied by hand during the fabrication and consolidation.

Figure 2-1: IsoBeam Mandrel

Table 2-3 identifies the pattern used to create each specimen. Each phase consists of placing the number of fibers specified of each type of member (Inner Diagonal, Longitudinal and Outer Diagonal). Where more than one type of member is laid during a phase, the tows of each type of members are alternatively applied to create interweaving. Two tows of longitudinal or outer diagonal members were applied for every one tow of inner diagonal or outer diagonal in phases 2 and 5, respectively. The inner diagonal members were consolidated between phases 4 and 5 since the inner diagonal members are easier to access before applying the outer diagonal members. A picture of the inner diagonal members after consolidation can be viewed in Figure 2-2.

Table 2-3: Specimen Member Creation Phases

Phase	Number of Tows		
	Inner Diagonal	Longitudinal	Outer Diagonal
1	7	-	-
2	7	14	-
3	-	65	-
4	7	7	-
5	-	7	14
6	-	-	15
Total	21	93	29

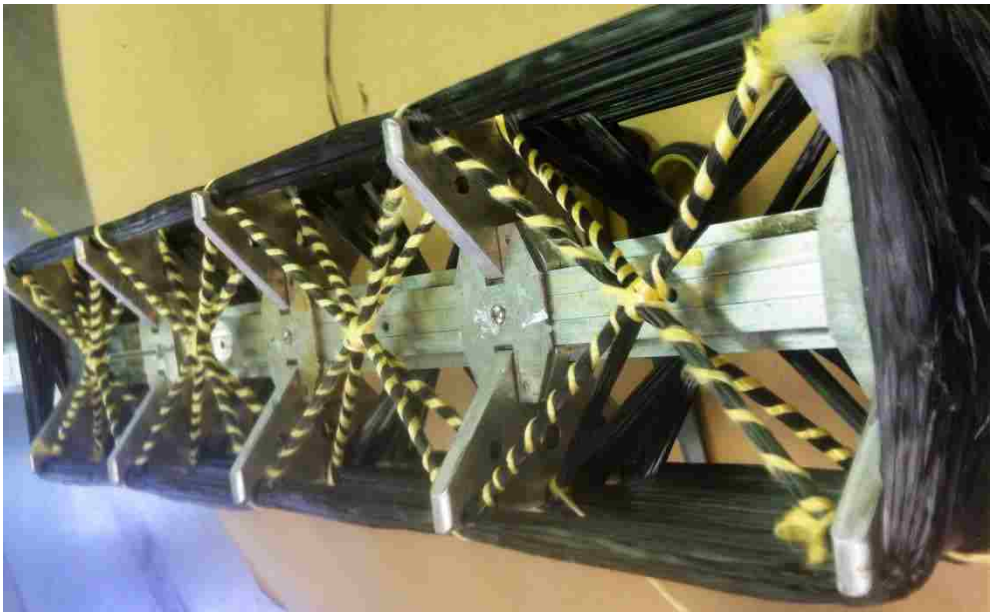

Figure 2-2: Picture of Inner Diagonal Consolidation

This pattern provided an efficient process to create the specimen with interwoven members. Ideally, all types of members would be interwoven (i.e., inner and outer diagonal members), but that creates an incredibly complex pattern to create by hand. This would be more simply achieved by creating the IsoBeam on a three-dimensional braiding machine. Each

specimen took an average of 30 hours of labor to complete. The weaving and sewing of the beams took two or three people at a time depending on the phase.

The most tows were used in the longitudinal members to create a favorable 2:1 ratio in longitudinal member size. The expected sizes were 0.4 in. (10.2 mm) in diameter for longitudinal members and 0.2 in. (5.1 mm) in diameter for diagonal members. The average member sizes can be viewed in Table 2-4. Since the inner diagonal members are braced in all three directions, they are stiffer than the outer diagonal members. Thus, the outer diagonal members were slightly oversized to compensate for this greater internal stiffness. This enabled the outer diagonal members to carry more load. Table 2-4 contains the average dimensions for of each type of member. The average measurements and the description of the measurement method are in Appendix B.

Table 2-4: Average Member Sizes

Specimen	Measurement	Longitudinal		Outer Helical		Inner Helical	
1	Diameter [in (mm)]	0.387	(9.83)	0.214	(5.43)	0.199	(5.05)
	Area [in^2 (mm^2)]	0.111	(71.2)	0.036	(23.2)	0.030	(19.5)
2	Diameter [in (mm)]	0.387	(9.84)	0.212	(5.38)	0.199	(5.04)
	Area [in^2 (mm^2)]	0.115	(74.4)	0.035	(22.7)	0.031	(19.9)
3	Diameter [in (mm)]	0.396	(10.04)	0.218	(5.54)	0.195	(4.95)
	Area [in^2 (mm^2)]	0.119	(76.5)	0.038	(24.2)	0.030	(19.3)
Average	Diameter [in (mm)]	0.390	(9.9)	0.215	(5.45)	0.198	(5.01)
	Area [in^2 (mm^2)]	0.115	(74.1)	0.036	(23.4)	0.030	(19.6)

2.2.2 Curing

A Type-T thermocouple was wrapped on the mandrel in the center of carbon/epoxy with a thickness similar to the specimen's thickest section. This facilitated internal temperature

readings during curing. The parts were cured with a ramp up of 5° F (15° C) per minute from room temperature to 250 °F (121° C) where the specimens were held for 1.5 hours, as specified by the material manufacturer [22]. The temperature was ramped down at 5° F (15° C) per minute to less than 150° F (65.6° C) resulting in a total curing time of about 4 hours.

2.2.3 Final Specimen Preparation

After cooling, the specimens were removed from the mandrel using a Dremel tool with a 543 Carbide cutting wheel head and prepared for testing. The dates that the specimens were cured are listed in Appendix A. The specimens were prepared by cleaning the end nodes with a disk sander. Each member of the specimen was weighed and measured with calipers as detailed in Appendix B.

The final specimens were 2 ft (0.61 m) long with four 6 in. (152 mm) bays, 6 in. (152 mm) high and 3 in. (76.2 mm) wide. Each specimen (1, 2 and 3) weighed 1.833 lbs (8.15 N), 1.824 lbs (8.11 N) and 1.857 lbs (8.26 N), respectively.

2.3 Label Notation

The many members of each specimen were labeled using the system described here to allow easy description of size, strain gage locations, and failure locations. Each member was labeled in a **2FTL3-IF** notation. This example denotes a member from specimen **2** in the **F**ront, **T**op, **L**eft of Bay **3**. The **I** signifies an inner diagonal and the additional **F** or **R** at the end of the inner diagonal notation denotes **F**ront or **R**ear. The Front or Rear is added since there are four inner diagonal members every cross-section.

An example of a vertical outer diagonal label would be **2FTL3-O** with the same description as above. The front (**F**) and top (**T**) are switched to denote horizontal outer diagonal

members. An example of a horizontal outer diagonal labeling would be **2BRL3-O** where the **B** means bottom and the **R** means rear.

An example of a longitudinal member label would be **2FT4-L**. The left or right included in the diagonal member's labels is not included since left or right does not apply to longitudinal members. Table 2-5 contains the notation of each label for each member. Note that the Top and Bottom location category comes first when labeling the horizontal outer diagonal members.

The string potentiometers used during testing are labeled as **2FM**. The **2** or **3** denote which test while the **F** refers to the string potentiometers on the front face and **R** refers to the string potentiometers on the rear face. **R**, **M** or **L** are used for the right, middle or left string potentiometer locations, respectively.

Table 2-5: Member Label Notation Convention

		Inner Diagonal	Outer Diagonal	Longitudinal
Specimen	1	**1**	**1**	**1**
	2	**2**	**2**	**2**
	3	**3**	**3**	**3**
Location	Front (F)	**F**	**F**	**F**
	Middle (M)	**-**	**-**	**M**
	Rear (R)	**R**	**R**	**R**
	Top (T)	**T**	**T**	**T**
	Bottom (B)	**B**	**B**	**B**
	Left (L)	**L**	**L**	**-**
	Right(R)	**R**	**R**	**-**
Bay	1	**1**	**1**	**1**
	2	**2**	**2**	**2**
	3	**3**	**3**	**3**
	4	**4**	**4**	**4**
Member Type	ID	**ID**	**-**	**-**
	OD	**-**	**OD**	**-**
	L	**-**	**-**	**L**
IH Location	Front (F)	**F**	**-**	**-**
	Rear (R)	**R**	**-**	**-**

2.4 Data Acquisition

During testing, data was acquired from the MTS machine loading and displacement as well as strain gages applied to individual members of the IsoBeam. Test 2 and 3 had additional displacement data measured using string potentiometers. The strain gage application and labeling are described below along with the string potentiometer setup and analysis.

2.4.1 Strain Gages

Strain gages were used to acquire data on the beam members during testing. Each member was prepped by applying 5-minute epoxy to fill in the gaps and ridges caused by layering carbon fibers. The epoxy was sanded down using a coarse paper (150 grit paper) until reaching the fibers which created a flat area for the strain gage. The member was then sanded smooth (400 grit paper) and cleaned for application of the strain gage. Figure 2-3 shows a member before sanding (A) and a member after applying the epoxy and sanding flat (B).

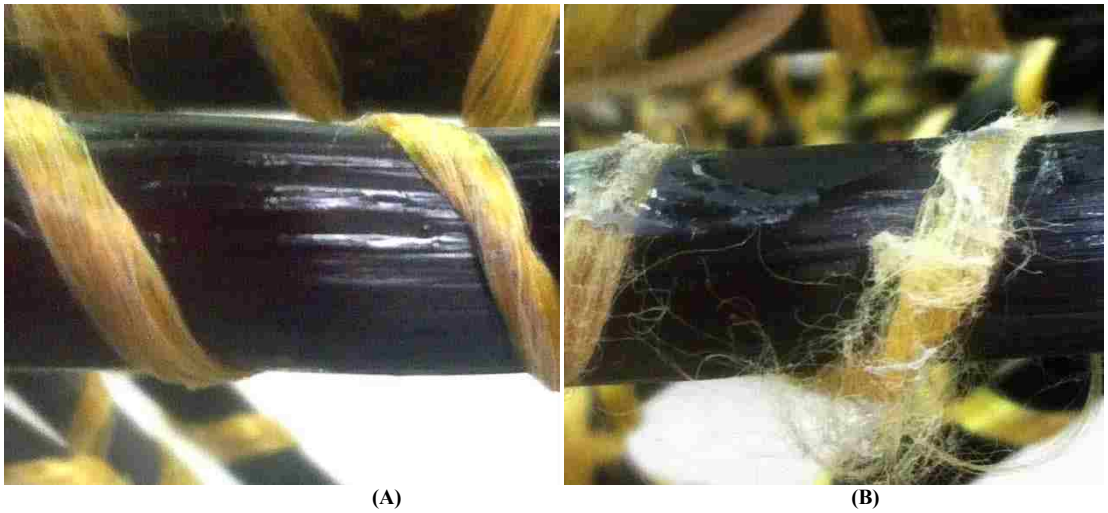

(A) **(B)**

Figure 2-3: Preparation for Strain Gage Application: A) Before; and, B) After Sanding

Strain gages with pre-soldered wires were used on the inner diagonal members because of their inaccessibility. After the first test, these were also used for the top and bottom outer diagonal members since the smaller strain gages were difficult to solder and had to be replaced multiple times. Larger strain gages were used on longitudinal members that required soldering. The types of strain gages used on each member are summarized in Table 2-6. A description of the properties of each strain gage batch is located in Appendix A.

Table 2-6: Strain Gage Information

Strain Gage Type	Member Type	Test
CEA-06-125UN-120	Longitudinal	1, 2 and 3
EA-06-062AK-120	Horizontal Outer Diagonals	1
FLA-2-11-3LT	Horizontal Outer Diagonals	2 and 3
	Vertical Outer Diagonals	1, 2 and 3
	Inner Diagonals	1, 2 and 3

The first test contained extra strain gages to ensure redundant data in case of failure and allowed the important strained members to be identified for the next two tests. Thus, fewer strain gages were used on subsequent tests. A summary of test parameters including the rate of testing, the number of strain gages on each type of member and the method for measuring the displacement are contained in Table 2-7. A description of the strain gage locations and types for each test follows in Table 2-8, Figure 2-4, Figure 2-5 (Test 1), Table 2-9, Figure 2-6 and Figure 2-7 (Tests 2 & 3).

Table 2-7: Summary of Tests

Test	Rate (in/min)	Number of Strain Gages			Displacement Measurement
		Inner Diagonal	Outer Diagonal	Longitudinal	
1A	0.05	12	4	8	Machine
1B	0.1	12	4	8	Machine
2A	0.1	9	2	6	String Pot.
2B	0.1	9	2	6	String Pot.
3	0.2	10	2	6	String Pot.

Table 2-8: Strain Gage Locations for Test 1

Strain Gage	Location
1	FTL4-OD
2	FTL4-IDF
3	FTL4-IDR
4	RTL4-IDR
5	FBR4-IDR
6	FTR3-IDF
7	FTL3-IDF
8	FTR2-IDF
9	FTL2-IDF
10	FTR1-OD
11	FTR1-IDF
12	FTR1-IDR
13	RTR1-IDR
14	FBL1-IDR
15	FT3-L
16	MT3-L
17	RT3-L
18	RT2-L
19	FB3-L
20	FB2-L
21	MB2-L
22	RB3-L
23	TFL3-OD
24	BRL3-OD

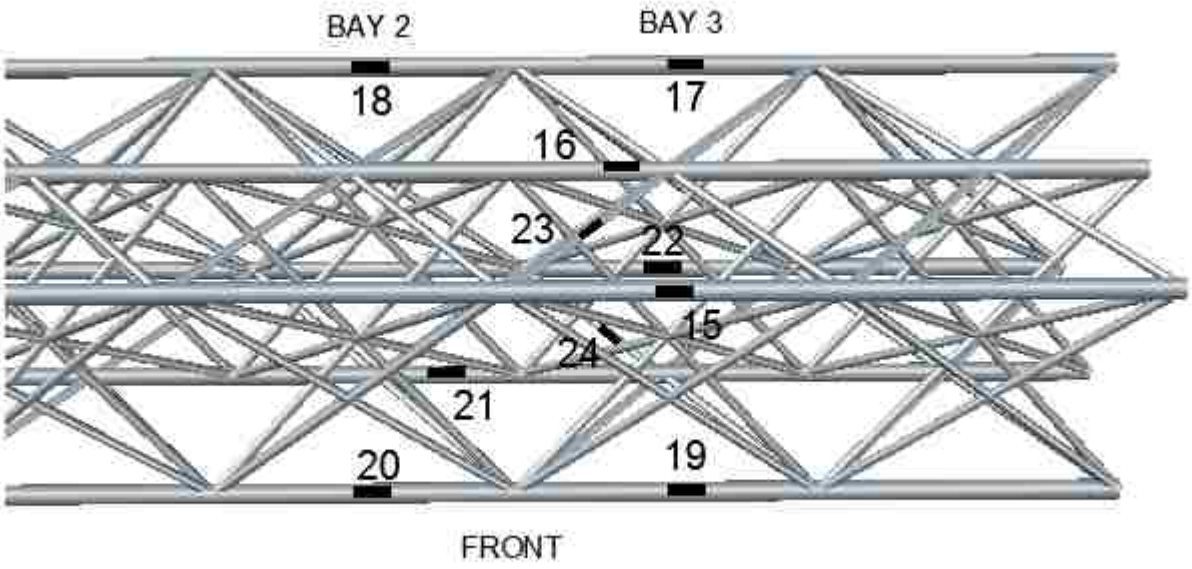

Figure 2-4: Longitudinal and Outer Diagonal Strain Gage Locations for Test 1

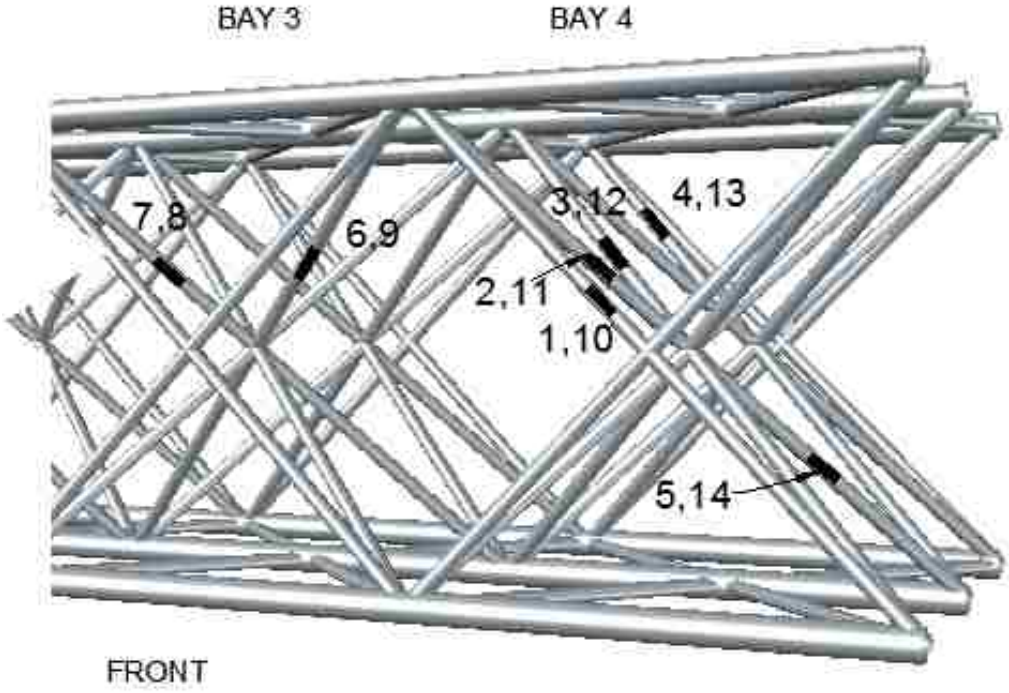

Figure 2-5: Inner Diagonal and Outer Diagonal Strain Gage Locations for Test 1

Table 2-9: Strain Gage Locations for Test 2 & 3

Strain Gage	Location
1	FTL3-OD
2	FTL3-IDF
3	FTL3-IDR
4	RTL3-IDF
5	FBL3-IDF
6	FBR2-IDF
7	FTR2-OD
8	FTR2-IDR
9	RTR2-IDR
10	FBL2-IDF
11	BRL3-OD
12*	FTR3-IDF
13	FT3-L
14	RT3-L
15	FB2-L
16	MB2-L
17	RB3-L
18	RB2-L

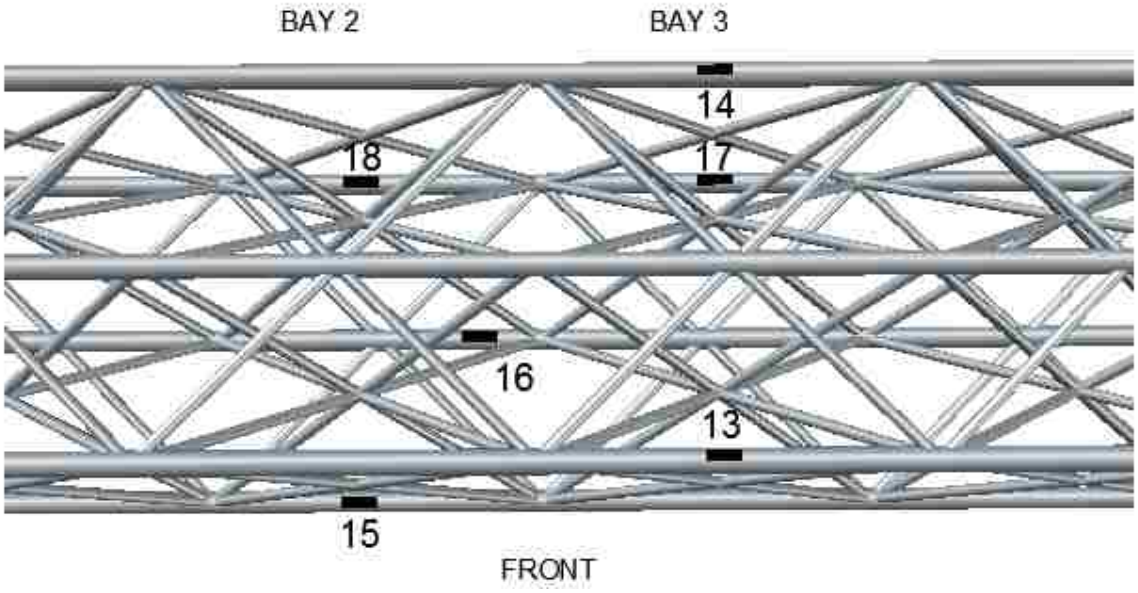

Figure 2-6: Longitudinal Strain Gage Locations for Test 2 & 3

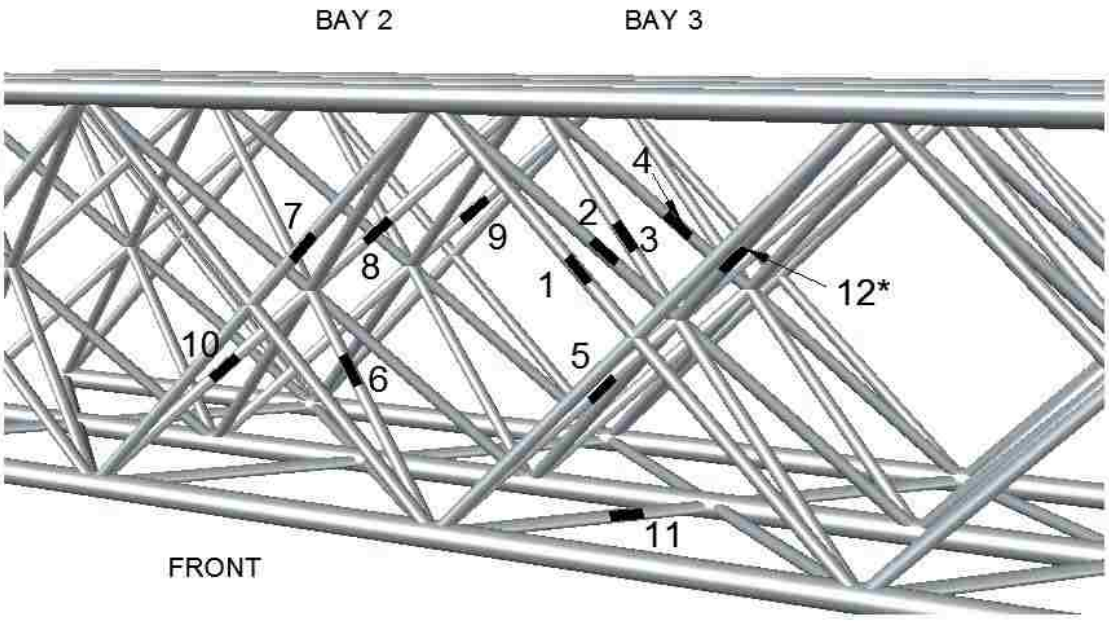

Figure 2-7: Inner Diagonal and Outer Diagonal Strain Gage Locations for Test 2 & 3

The numbering of the strain gages is utilized in the discussion of the results. Strain gage 12 for Test 2 and 3 is starred because this strain gage was only present in Test 3.

2.4.2 String Potentiometers

String potentiometers were used in Test 2 and 3 to accurately account for the displacement of the neoprene pads and calculate the beam's center displacement. Three string potentiometers were mounted to each side of the base beam and a rod epoxied inside the three middle bays of the specimens (Figure 2-12 and Figure 2-13). These measured the displacement on both sides of each base plate and both sides of the center of the beam. The sides were averaged and each base plate's displacement, due to the neoprene, was removed from the center displacement to get the beam's absolute center displacement. This is depicted in Figure 2-8.

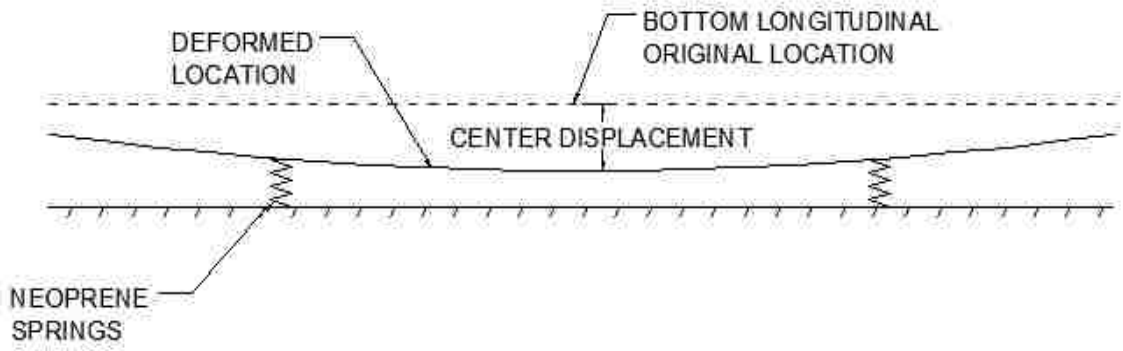

Figure 2-8: Diagram of Beams Bottom Displacement with Neoprene Springs

The displacement of the top of the beam was observed to be different than the displacement of the bottom of the beam. This can be partially attributed to the upper inner diagonals rotating at the rigid center joint. The top neoprene displacement was not measured and was assumed to be similar to the displacement of the two lower neoprene pads. To calculate the displacement of the top longitudinal members, spring displacements of all of the neoprene pads was removed from the machine displacement. Figure 2-9 displays a diagram of the springs during testing and Equations 5-9 derive the total spring displacements. The neoprene springs underneath the beam displaced in parallel which displaced in series with the upper neoprene spring. This resulted in removing 2/3 of the displacement of the neoprene pads from the machine displacement to get the top center displacement.

BOTTOM SPRINGS: Springs in Parallel

$$K_b = k + k \tag{5}$$

$$K_b = 2k \tag{6}$$

WHOLE SYSTEM: Springs in Series

$$\frac{1}{K_t} = \frac{1}{K_b} + \frac{1}{k} \tag{7}$$

$$\frac{1}{K_t} = \frac{1}{2k} + \frac{1}{k} = \frac{3}{2k} \quad \text{Sub Eq. (6) into Eq. (7)} \tag{8}$$

$$K_t = \frac{2k}{3} \tag{9}$$

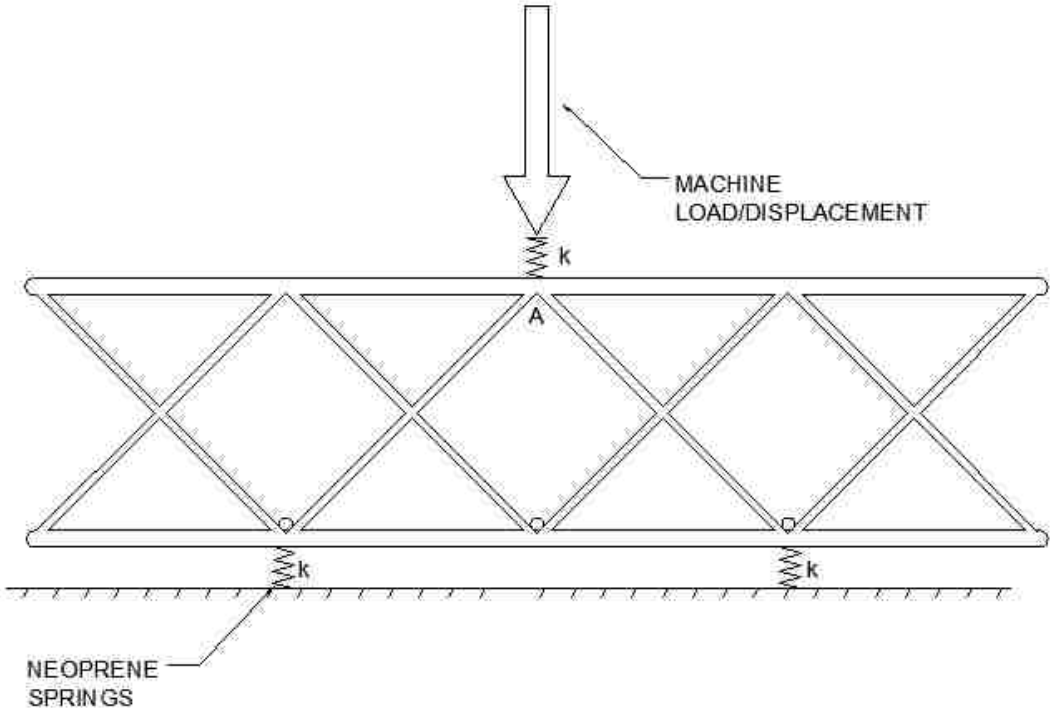

Figure 2-9: Diagram of Spring Displacements

2.5 **Testing**

All the specimens were tested on an MTS machine. The first specimen was tested in four-point bending to induce a pure bending moment in the center section of the beam. Placing the base plates on the edge of the specimen, however, allowed rotation as the base plates slipped out

from under the specimen. This induced local bending stresses in the members producing a premature failure. Therefore, the next two specimens were testing in three-point bending, which enabled the base plates to have a full bay on each end to decrease the rotation of the plates. Both test setups and fixtures are described since all the test data is included in the results.

For all tests, notched base plates with a roller between them were used to interface the beams. This created a statically determinate path for the load. Since each of the primary nodes interfacing the plates were slightly different heights, shims were inserted to ensure even distribution of the load between nodes. Additionally, stiff neoprene was placed between the shims and the nodes to distribute the load around the curved surface. A swivel head was used to distribute load from the machine to the test fixture. Lastly, the test fixture was propped up on a beam to create room for the base plates during the first test and to attach the string potentiometers in the last two tests.

2.5.1 Four-Point Bending Tests

Two steel blocks and rollers were welded to a channel which was used to apply the load at 12 in. (304.8 mm) apart during the four-point bending test. The rollers on the channel interfaced with the base plates on the beam. A small I-beam was placed inside the channel to distribute the load. The front (A) and side (B) views of the test fixture for four-point bending can be viewed in Figure 2-10. The picture in Figure 2-11 shows the actual four-point test setup.

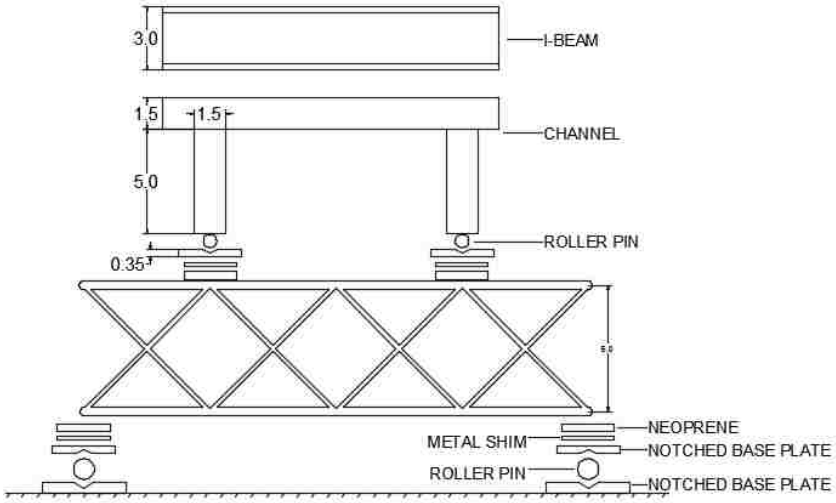

(A)

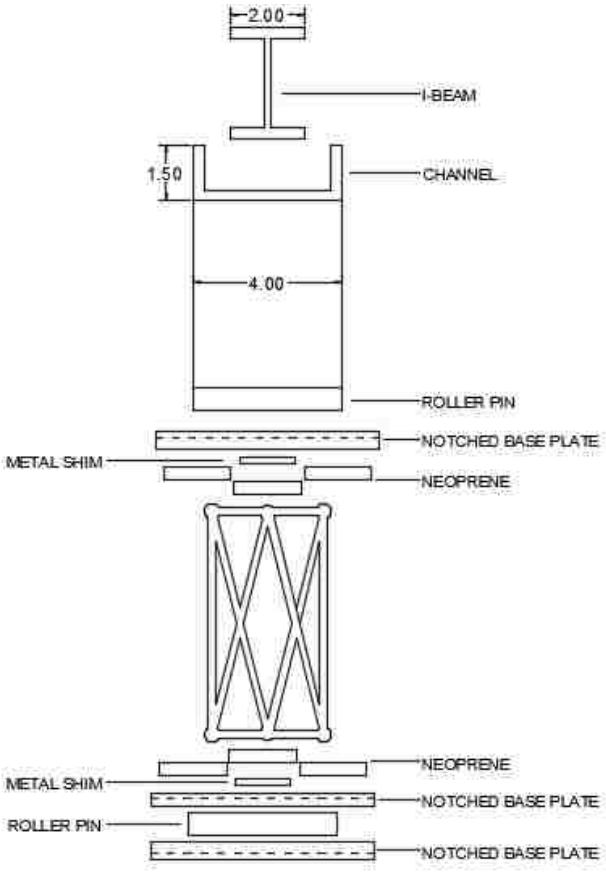

(B)

Figure 2-10: Four-Point Bending Test Setup: A) Front View; and, B) Side View

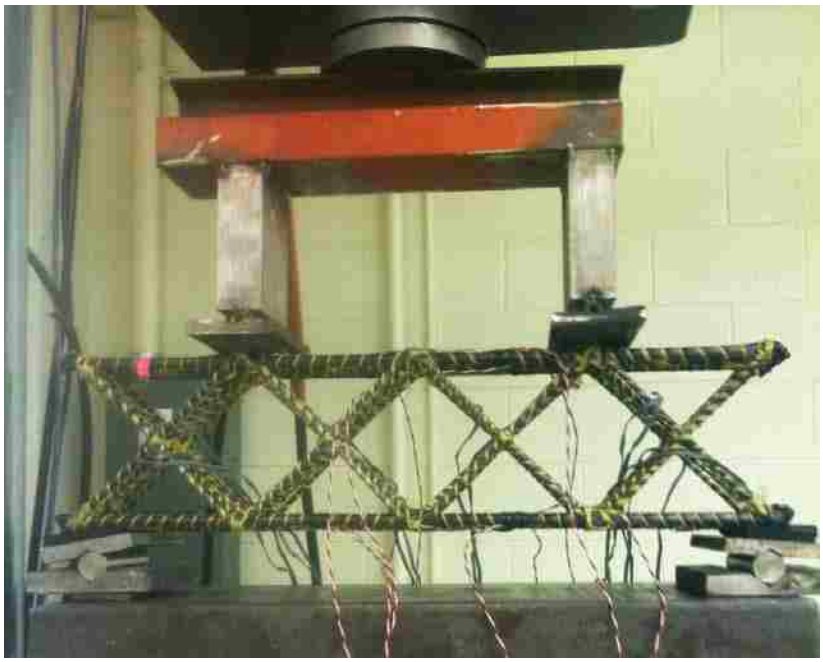

Figure 2-11: Picture of Four-Point Bending Test Setup

2.5.2 Three-Point Bending Tests

For the three-point bending tests, the channel piece and I-beam were replaced by a single base plate and roller that interfaced with the swivel head. The bottom base plates were also each moved in a bay width so that the base plates were 12 in. (305 mm) apart. Metal rods and string potentiometers were epoxied to the inside bottom of the bays where the three loading points were located. These were used in data acquisition and are discussed further in the Data Acquisition section (2.5). The rest of the fixture remained the same. A diagram of the test set up can be viewed in Figure 2-12. Figure 2-13 displays a picture of the actual three-point bending test setup.

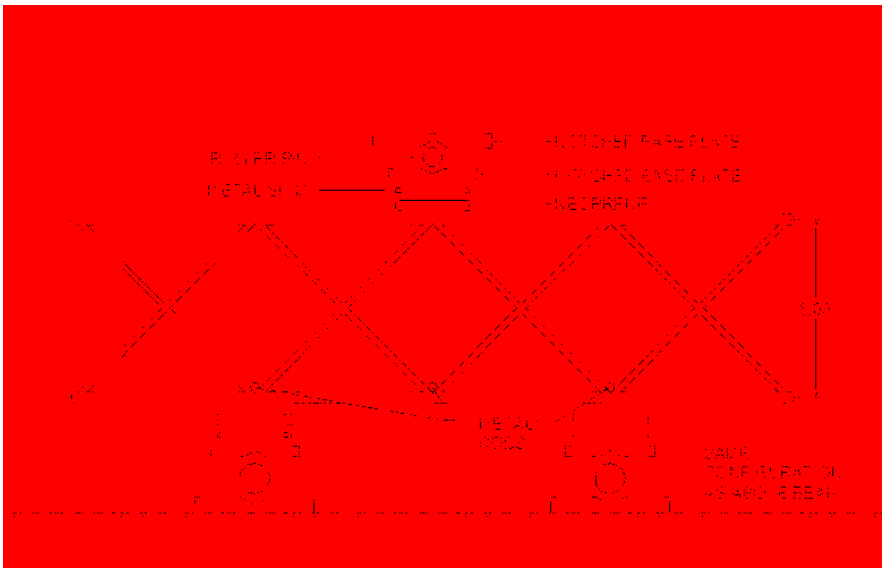

(A)

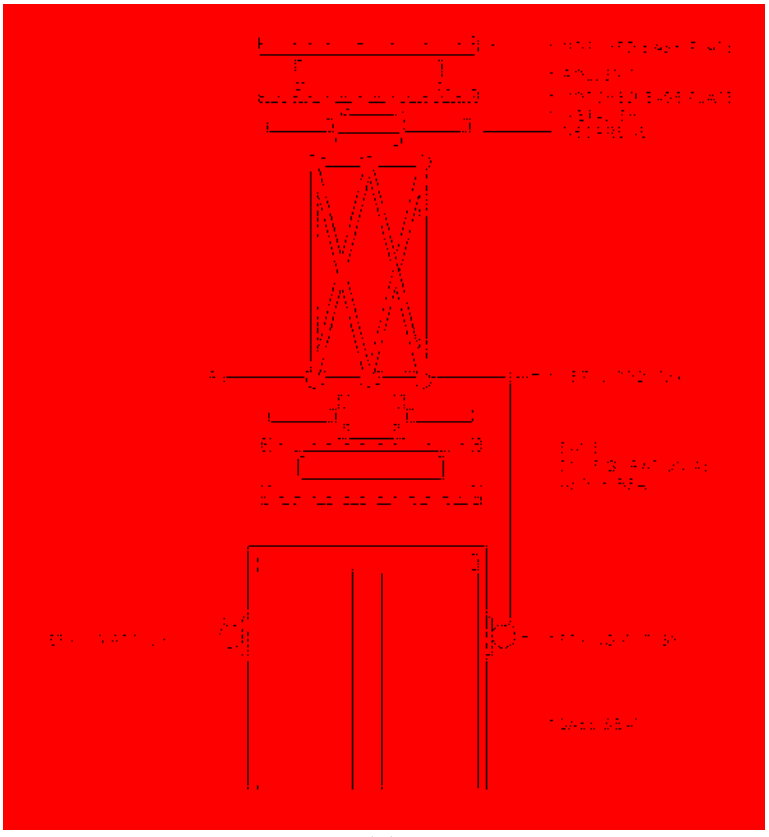

(B)

Figure 2-12: Three-Point Bending Test Setup: A) Front View; and, B) Side View

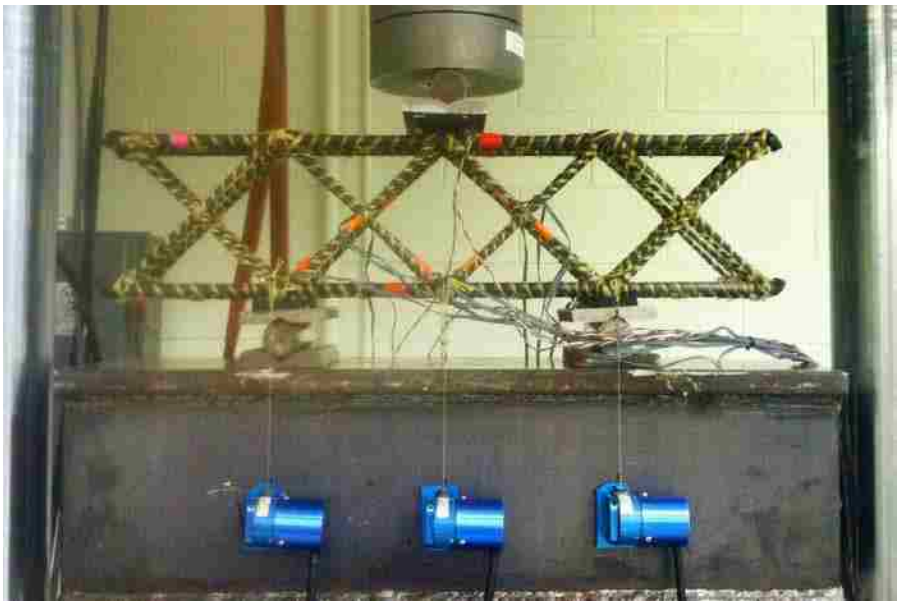

Figure 2-13: Picture of Three-Point Bending Test Setup

2.6 Data Reduction and Statistical Analysis

Test data was imported into Microsoft Excel to be analyzed. Extraneous data before and after loading was removed from the data. The remaining data was consolidated using eight partitions at the same strain step to allow easy averaging. The reduced data was plotted against the real data to ensure proper reduction.

Chauvenet's criterion was used to determine if any individual member test specimens qualified as outliers and should be excluded from the averages. This statically conservative criterion uses an envelope of 1/2n where n is a specified ratio dependent on the number of samples (1.38 and 1.54 for 3 and 4 samples respectively, and so on.). The mean value and standard deviation using all data points are compared to each individual sample point to determine if the data point should be included. The final mean value and standard deviation are computed without the dubious points [27].

3 ISOBEAM TEST RESULTS

This chapter presents the results for the load and displacement of the beams as well as the strain gage data for each member type. The machine displacement is compared to the top and bottom displacements of the beams in tests 2A, 2B and 3. The strain gage measurements are plotted against the compression beam load. The results are plotted with an average curve. The average maximum is shown with the ranges of standard deviation in each direction. Where the standard deviation is large, resulting in a skewed average curve, the average curve is extended with a dashed line to the maximum average. The maximum beam load when either the strain gage or beam failed, whichever occurred first, is shown in the table with the maximum strain at those loads.

3.1 Loading and Displacement Results

The results for the overall loading of the IsoBeam specimens are presented for each test. The displacements of all tests are compared. The measured bottom center displacement of the beams is compared to the derived top center displacement.

3.1.1 IsoBeam Loading Results

The load versus machine displacement plots are shown in Figure 3-1. The average maximum load was 4.11 kips (18.3 kN) with a standard deviation of 0.747 kips (3.32 kN) as

presented in Table 3-1. Also presented, the average deflection at maximum load was 0.595 in. (15.1 mm) with a standard deviation of 0.0338 in. (0.857 mm).

Table 3-1: Maximum Load and Deflection for All Tests

Test	Bending Test Method	Max Load		Deflection at Max Load	
		[kip	(kN)]	[in	(mm)]
1A	4-Point	3.71	16.5	0.622	15.8
1B	4-Point	3.69	16.4	0.556	14.1
2A	3-Point	3.36	14.9	0.582	14.8
2B	3-Point	4.71	20.9	0.578	14.7
3	3-Point	5.10	22.7	0.638	16.2
	Average	4.11	18.3	0.595	15.1
	Std. Dev.	0.747	3.32	0.0338	0.857
	[%]	18.2		5.67	

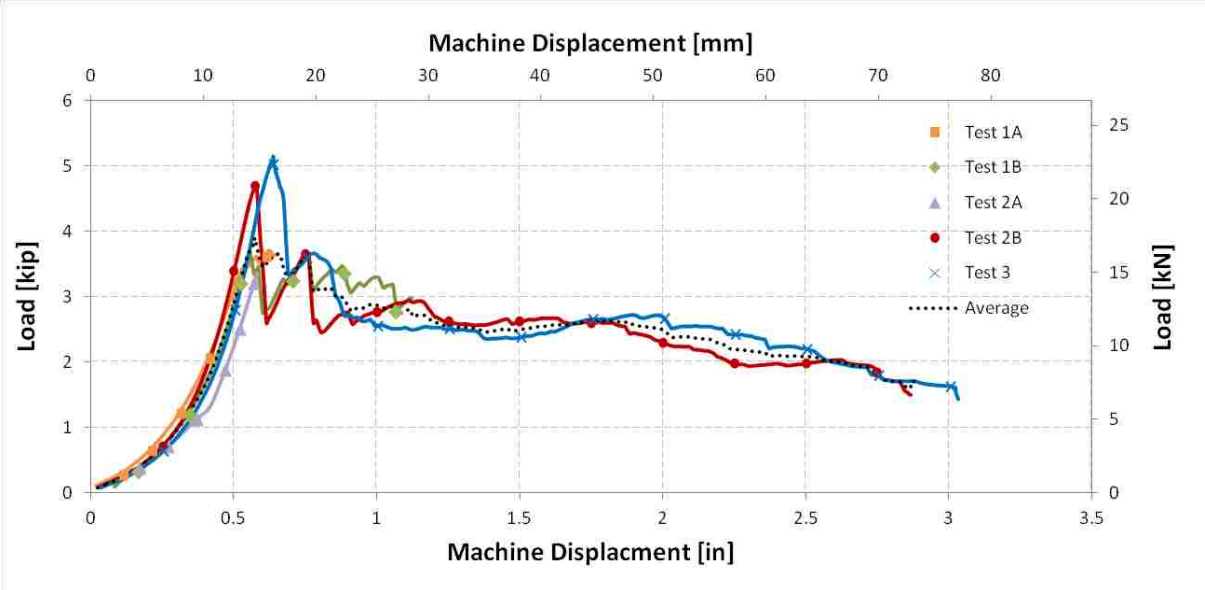

Figure 3-1: Load vs. Machine Displacement Plots for all Tests

3.1.2 IsoBeam Displacement Results

The machine displacement is compared to the top and bottom displacement in Table 3-2 for Test 2A, 2B and 3. The average maximum machine deflection was 0.599 in. (15.2 mm) while the average maximum top deflection was 0.243 in. (6.18 mm). The average maximum bottom deflection was 0.021 in. (0.542 mm). The top and bottom center displacements are compared in Figure 3-2 and Figure 3-3. Figure 3-4 displays the comparison of the deflection of Test 3 for machine, top and bottom. Similar results for deflection were seen for Tests 2A and 2B.

Table 3-2: Deflection Results for Test 2A, 2B and 3

Test	Machine Deflection at Max Load		Top Deflection at Max Load		Bottom Deflection at Max Load	
	[in	(mm)]	[in	(mm)]	[in	(mm)]
2A	0.582	14.8	0.235	6.0	0.016	0.4
2B	0.578	14.7	0.415	10.5	0.021	0.5
3	0.638	16.2	0.475	12.1	0.027	0.7
Average	0.599	15.2	0.375	9.53	0.021	0.542
Std. Dev.	0.0335	0.852	0.125	3.172	0.006	0.140
[%]	5.6		33.3		25.8	

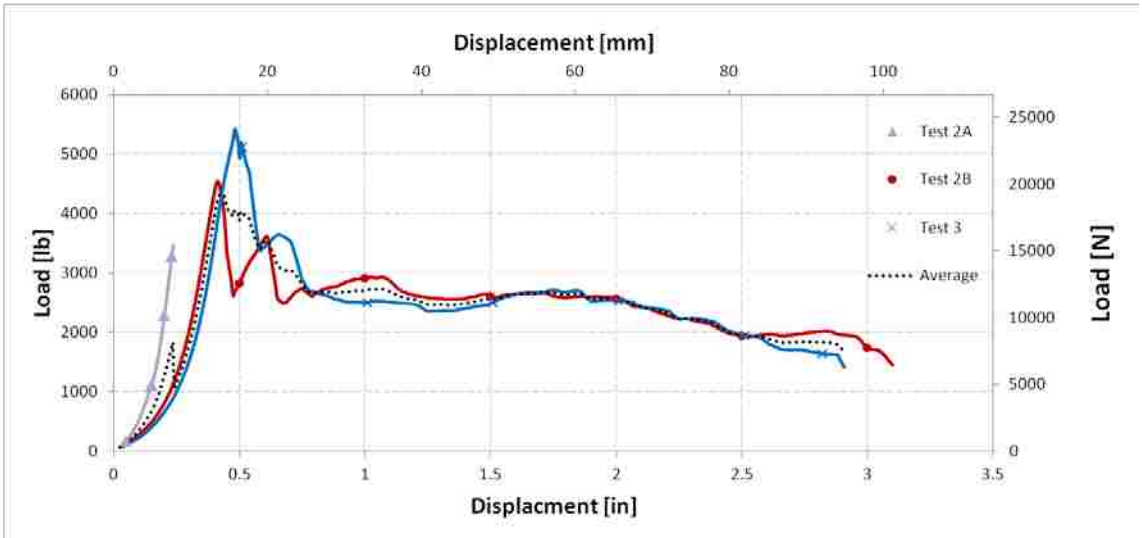

Figure 3-2: Load vs. Top Center Displacement Plots for Test 2A, 2B and 3

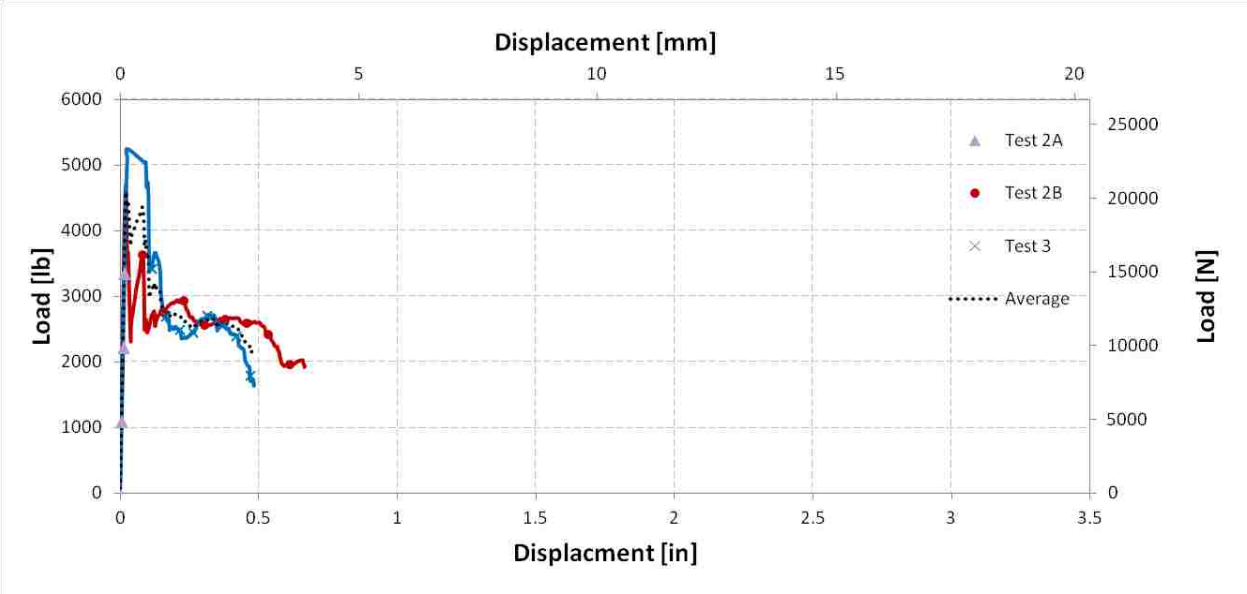

Figure 3-3: Load vs. Bottom Center Displacement Plots for Test 2A, 2B and 3

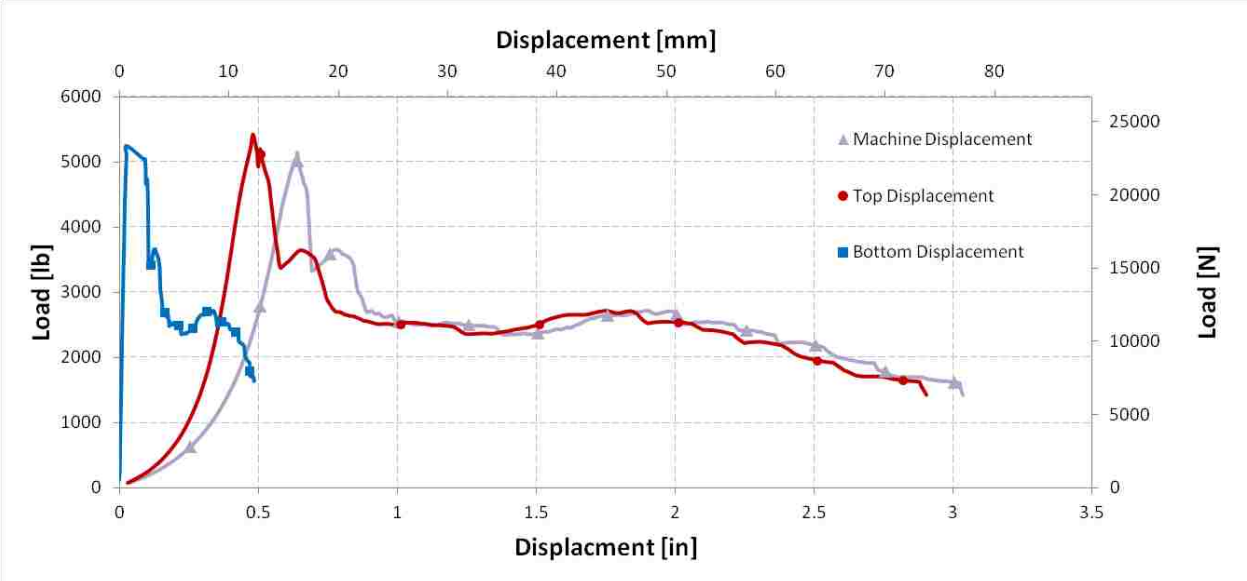

Figure 3-4: Displacements for Test 3

3.2 Specimen 1

This section contains the results for the strain gages of each type of member for Specimen 1, including Test 1A and Test 1B.

3.2.1 All Members

The results for all Test 1A strain gages are presented in the beam load verse strain plot shown in Figure 3-5 summarized in Table 3-3. The average beam load at gage/beam failure is 3,607 lbs (16.2 kN) with a standard deviation of 239 lbs (1.07 kN) and the corresponding average maximum strain is 1.22×10^3 με with a standard deviation of 1.07×10^3 με.

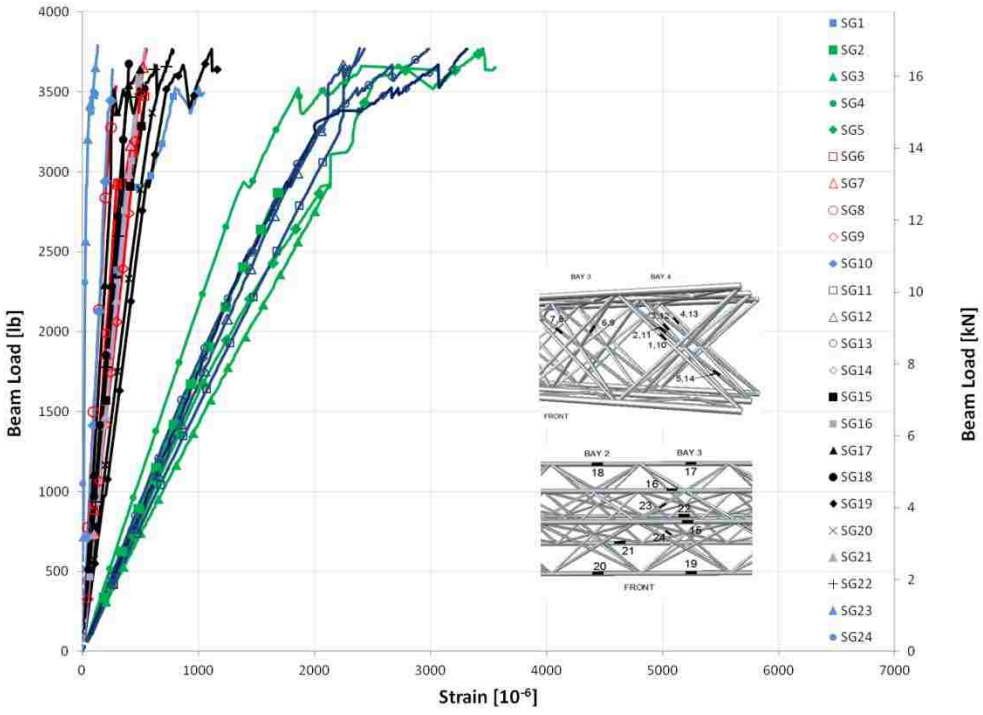

Figure 3-5: Load-Strain Plot for all Test 1A Members

Table 3-3: Summary Table for Test 1A Strain Gages

Strain Gage	Maximum Strain at Gage/Beam Failure [με]	Beam Load at Gage/Beam Failure [lb (kN)]	
1	998	3,533	15.8
2	1,690	2,886	12.9
3	2,134	2,926	13.1
4	2,404	3,662	16.4
5	3,456	3,770	16.9
6	556	3,529	15.8
7	550	3,771	16.9
8	289	3,533	15.8
9	472	3,512	15.7
10	261	3,641	16.3
11	2,430	3,770	16.9
12	2,390	3,775	16.9
13	2,984	3,768	16.9
14	3,310	3,767	16.9
15	550	3,534	15.8
16	474	3,538	15.9
17	514	3,674	16.5
18	405	3,675	16.5
19	1,116	3,767	16.9
20	654	3,527	15.8
21	538	3,775	16.9
22	772	3,767	16.9
23	132	3,791	17.0
24	160	3,678	16.5
Average	1,218	3,607	16.2
Std. Dev.	1,074	239	1.07
[%]	88.2	6.64	

The results for all Test 1B strain gages are summarized in Table 3-4 and presented in the beam load verse strain shown in Figure 3-6. The average beam load at gage/beam failure is 3,761 lbs (16.9 kN) with a standard deviation of 72.7 lbs (0.326 kN) and the corresponding average maximum strain is 1.01x103 με with a standard deviation of 0.850x103 με.

Table 3-4: Summary Table for Test 1B Strain Gages

Strain Gage	Maximum Strain at Gage/Beam Failure [με]	Beam Load at Gage/Beam Failure [lb (kN)]	
1	516	3,783	17.0
2	904	3,803	17.0
3	1,186	3,785	17.0
4	2,092	3,783	17.0
5	1,708	3,783	17.0
6	478	3,774	16.9
7	666	3,783	17.0
8	180	3,799	17.0
9	348	3,783	17.0
10	206	3,840	17.2
11	2,230	3,725	16.7
12	2,142	3,772	16.9
13	3,128	3,783	17.0
14	2,596	3,783	17.0
15	220	3,445	15.4
16	470	3,718	16.7
17	512	3,786	17.0
18	240	3,783	17.0
19	1,076	3,783	17.0
20	598	3,752	16.8
21	652	3,743	16.8
22	1,126	3,783	17.0
23	228	3,783	17.0
24	764	3,718	16.7
Average	1,011	3,761	16.9
Std. Dev.	850	72.7	0.326
[%]	84.1	1.93	

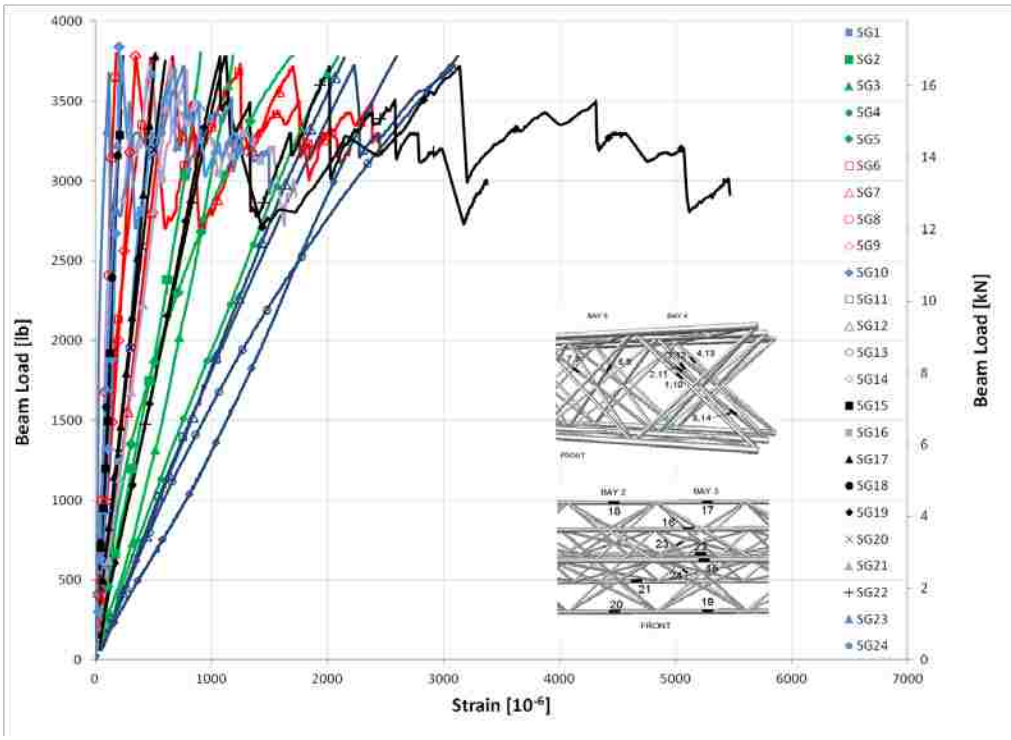

Figure 3-6: Load-Strain Plot for all Test 1B Members

3.2.2 Inner Diagonal Members

The results for Test 1A Outer Bay Inner Diagonal strain gages are summarized in Table 3-5 and presented in the beam load verse strain plot shown in Figure 3-7. The average beam load at gage/beam failure is 3,541 lbs (15.9 kN) with a standard deviation of 394 lbs (1.76 kN) and the corresponding average maximum strain is 2.60x103 με with a standard deviation of 0.602x103 με.

The results for Test 1A Middle Inner Diagonal strain gages are summarized in Table 3-6 and presented in the beam load verse strain plot shown in Figure 3-7. The average beam load at gage/beam failure is 3,586 lbs (16.1 kN) with a standard deviation of 124 lbs (0.555 kN) and the corresponding average maximum strain is 0.467x103 με with a standard deviation of 0.125x103 με.

Table 3-5: Summary Table for Test 1A Outer Bay Inner Diagonal Strain Gages

Strain Gage	Maximum Strain at Gage/Beam Failure [με]	Beam Load at Gage/Beam Failure [lb (kN)]	
2	1,690	2,886	12.9
3	2,134	2,926	13.1
4	2,404	3,662	16.4
5	3,456	3,770	16.9
11	2,430	3,770	16.9
12	2,390	3,775	16.9
13	2,984	3,768	16.9
14	3,310	3,767	16.9
Average	2,600	3,541	15.9
Std. Dev.	602	394	1.76
[%]	23.2	11.1	

Table 3-6: Summary Table for Test 1A Middle Inner Diagonal Strain Gages

Strain Gage	Maximum Strain at Gage/Beam Failure [με]	Beam Load at Gage/Beam Failure [lb (kN)]	
6	556	3,529	15.8
7	550	3,771	16.9
8	289	3,533	15.8
9	472	3,512	15.7
Average	467	3,586	16.1
Std. Dev.	125	124	0.555
[%]	26.7	3.45	

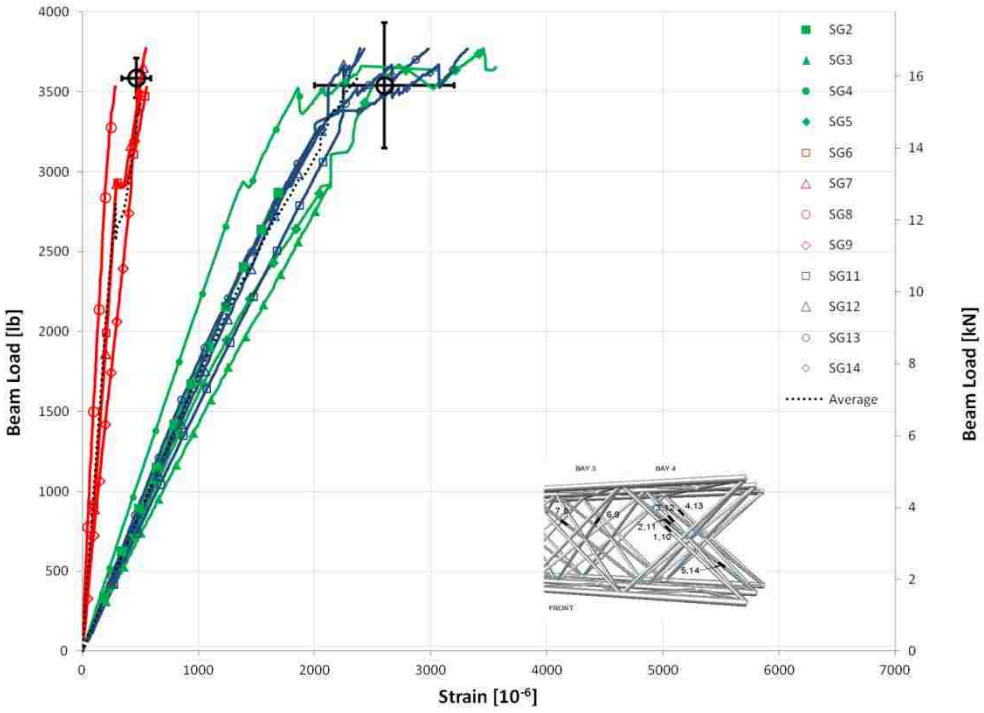

Figure 3-7: Load-Strain Plot for Test 1A Inner Diagonal Members

The results for Test 1B Outer Bay Inner Diagonal strain gages are summarized in Table 3-7 and presented in the beam load verse strain plot shown in Figure 3-8. The average beam load at gage/beam failure is 3,777 lbs (16.9 kN) with a standard deviation of 22.8 lbs (0.102 kN) and the corresponding average maximum strain is 2.00×10^3 με with a standard deviation of 0.723×10^3 με.

Table 3-7: Summary Table for Test 1B Outer Bay Inner Diagonal Strain Gages

Strain Gage	Maximum Strain at Gage/Beam Failure [με]	Beam Load at Gage/Beam Failure [lb (kN)]	
2	904.0	3,803	17.0
3	1,186	3,785	17.0
4	2,092	3,783	17.0
5	1,708	3,783	17.0
11	2,230	3,725	16.7
12	2,142	3,772	16.9
13	3,128	3,783	17.0
14	2,596	3,783	17.0
Average	1,998	3,777	16.9
Std. Dev.	723	22.8	0.102
[%]	36.2	0.604	

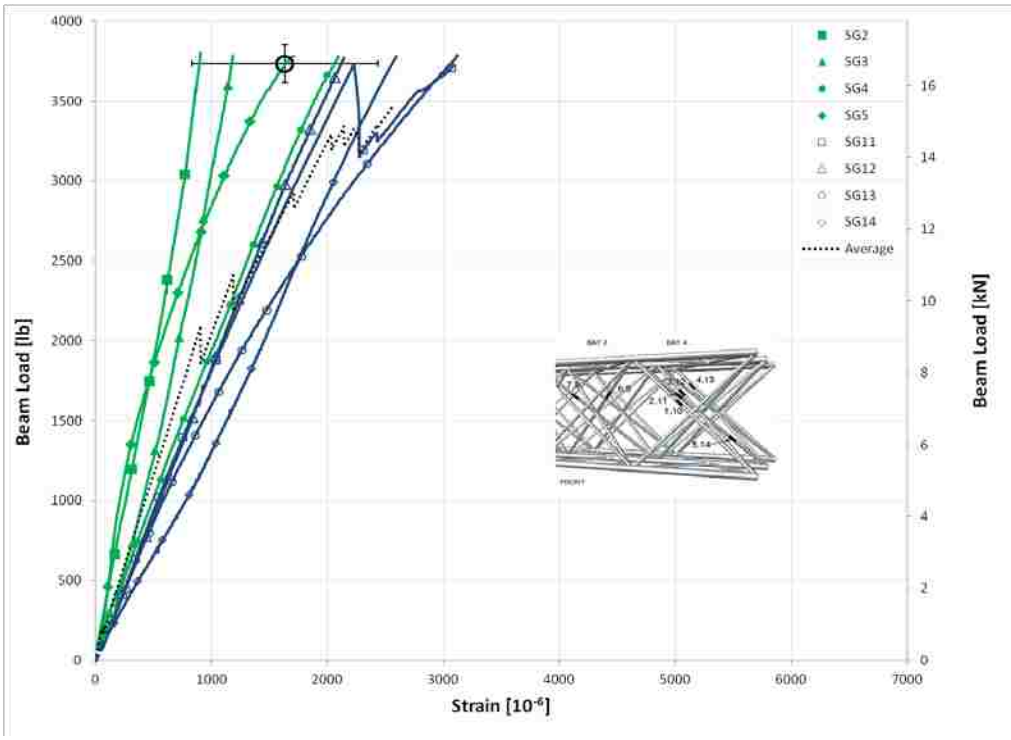

Figure 3-8: Load-Strain Plot for Test 1B Outer Bays Inner Diagonal Members

The results for Test 1B Middle Inner Diagonal strain gages are presented in the beam load verse strain plot shown in Figure 3-9 and summarized in Table 3-8. The average beam load at gage/beam failure is 3,785 lbs (17.0 kN) with a standard deviation of 10.3 lbs (0.046 kN) and the corresponding average maximum strain is 0.418x103 με with a standard deviation of 0.205x103 με.

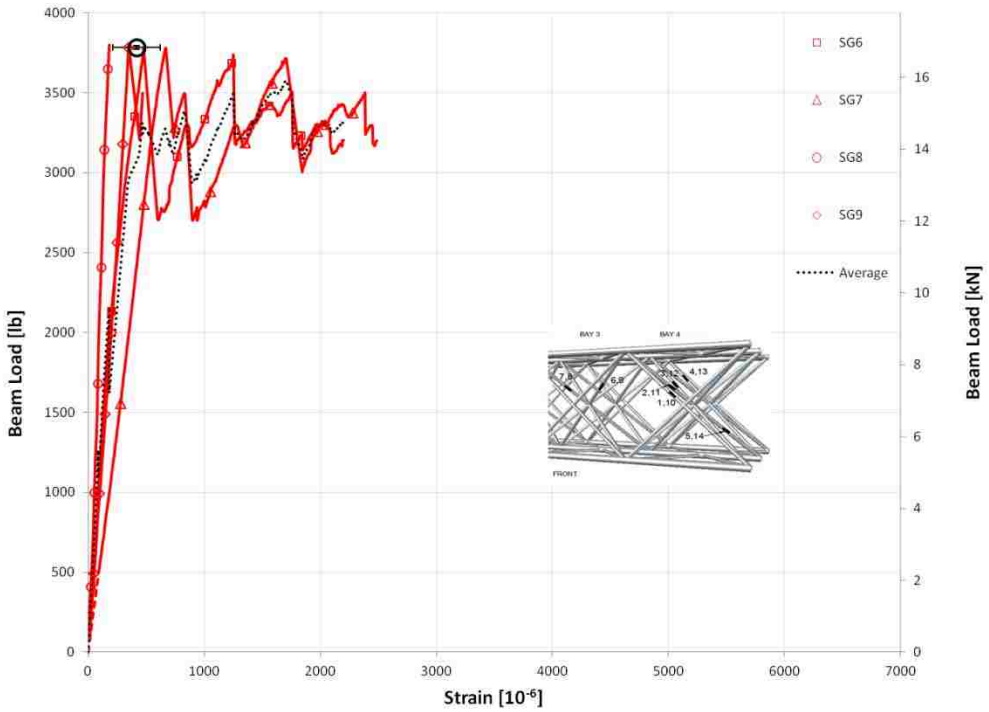

Figure 3-9: Load-Strain Plot for Test 1B Middle Bays Inner Diagonal Members

Table 3-8: Summary Table for Test 1B Middle Inner Diagonal Strain Gages

Strain Gage	Maximum Strain at Gage/Beam Failure [με]	Beam Load at Gage/Beam Failure [lb (kN)]	
6	478	3,774	16.9
7	666	3,783	17.0
8	180	3,799	17.0
9	348	3,783	17.0
Average	418	3,785	17.0
Std. Dev.	205	10.3	0.046
[%]	49.2	0.273	

3.2.3 Outer Diagonal Members

The results for Test 1A Outer Diagonal strain gages are summarized in Table 3-9 and presented in the beam load verse strain plot shown in Figure 3-10. The average ultimate beam load at gage/beam failure is 3,661 lbs (16.4 kN) with a standard deviation of 107 lbs (0.478 kN) and the corresponding average maximum strain is $0.388x10^3$ με with a standard deviation of $0.411x10^3$ με.

The results for Test 1B Outer Diagonal strain gages are summarized in Table 3-10 and presented in the beam load verse strain plot shown in Figure 3-11. The average beam load at gage/beam failure is 3,781 lbs (16.9 kN) with a standard deviation of 50.0 lbs (0.224 kN) and the corresponding average maximum strain is $0.429x10^3$ με with a standard deviation of $0.265x10^3$ με.

Table 3-9: Summary Table for Test 1A Outer Diagonal Strain Gages

Strain Gage	Maximum Strain at Gage/Beam Failure [με]	Beam Load at Gage/Beam Failure [lb (kN)]	
1	998	3,533	15.8
10	261	3,641	16.3
23	132	3,791	17.0
24	160	3,678	16.5
Average	388	3,661	16.4
Std. Dev.	411	107	0.478
[%]	106	2.91	

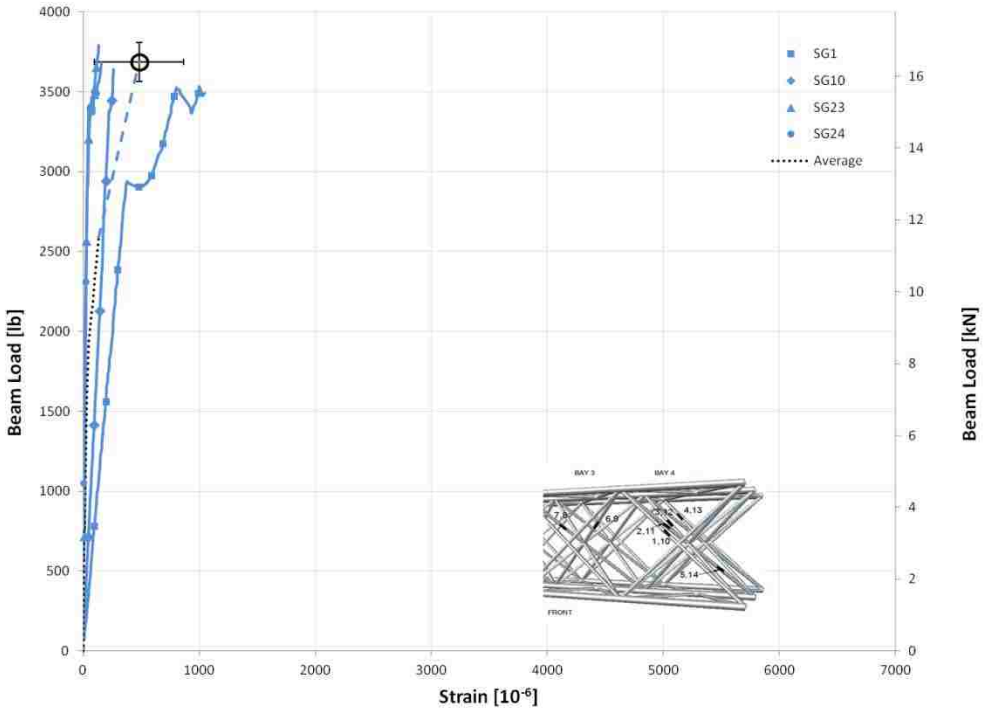

Figure 3-10: Load-Strain Plot for Test 1A Outer Diagonal Members

Table 3-10: Summary Table for Test 1B Outer Diagonal Strain Gages

Strain Gage	Maximum Strain at Gage/Beam Failure [με]	Beam Load at Gage/Beam Failure [lb (kN)]	
1	516	3,783	17.0
10	206	3,840	17.2
23	228	3,783	17.0
24	764	3,718	16.7
Average	429	3,781	16.9
Std. Dev.	265	50.0	0.224
[%]	61.7	1.32	

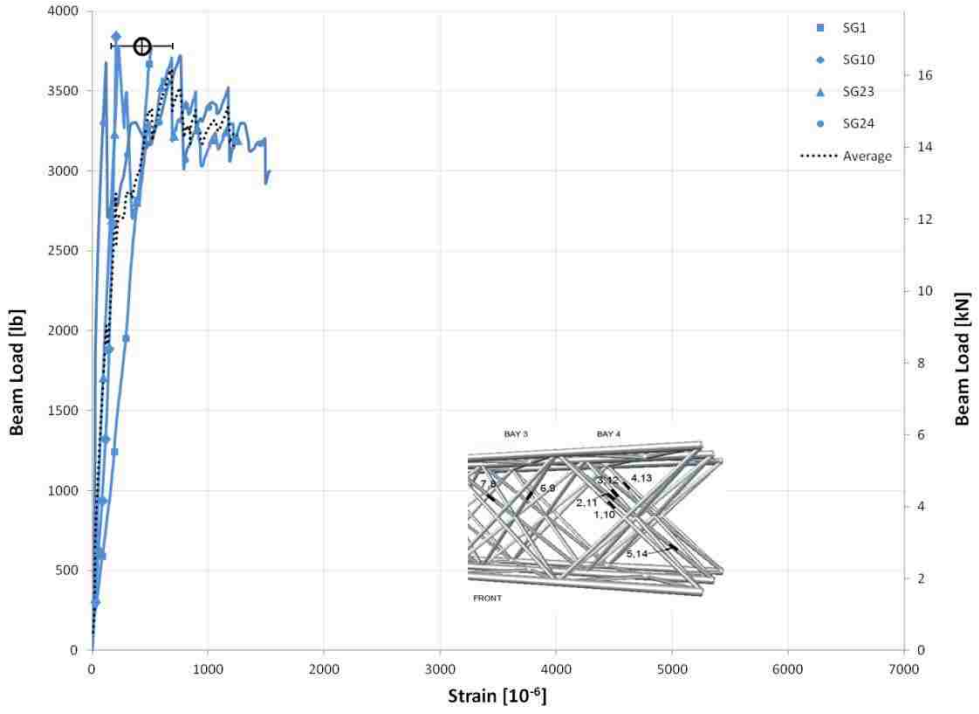

Figure 3-11: Load-Strain Plot for Test 1B Outer Diagonal Members

3.2.4 Longitudinal Members

The results for Test 1A longitudinal strain gages are summarized in Table 3-11 and presented in the beam load verse strain plot shown in Figure 3-12. The average beam load at gage/beam failure is 3,657 lbs (16.4 kN) with a standard deviation of 101 lbs (0.494 kN) and the corresponding average maximum strain is 0.628×10^3 με with a standard deviation of 0.227×10^3 με.

The results for Test 1B longitudinal strain gages are summarized in Table 3-12 and presented in the beam load verse strain plot shown in Figure 3-13. The maximum average and range of standard deviation is also plotted. The average beam load at gage/beam failure is 3,724 lbs (16.7 kN) with a standard deviation of 115 lbs (0.518 kN) and the corresponding average maximum strain is 0.612×10^3 με with a standard deviation of 0.339×10^3 με.

Table 3-11: Summary Table for Test 1A Longitudinal Strain Gages

Strain Gage	Maximum Strain at Gage/Beam Failure [με]	Beam Load at Gage/Beam Failure [lb (kN)]	
15	550	3,534	15.8
16	474	3,538	15.9
17	514	3,674	16.5
18	405	3,675	16.5
19	1,116	3,767	16.9
20	654	3,527	15.8
21	538	3,775	16.9
22	772	3,767	16.9
Average	628	3,657	16.4
Std. Dev.	227	110	0.494
[%]	36.1	3.01	

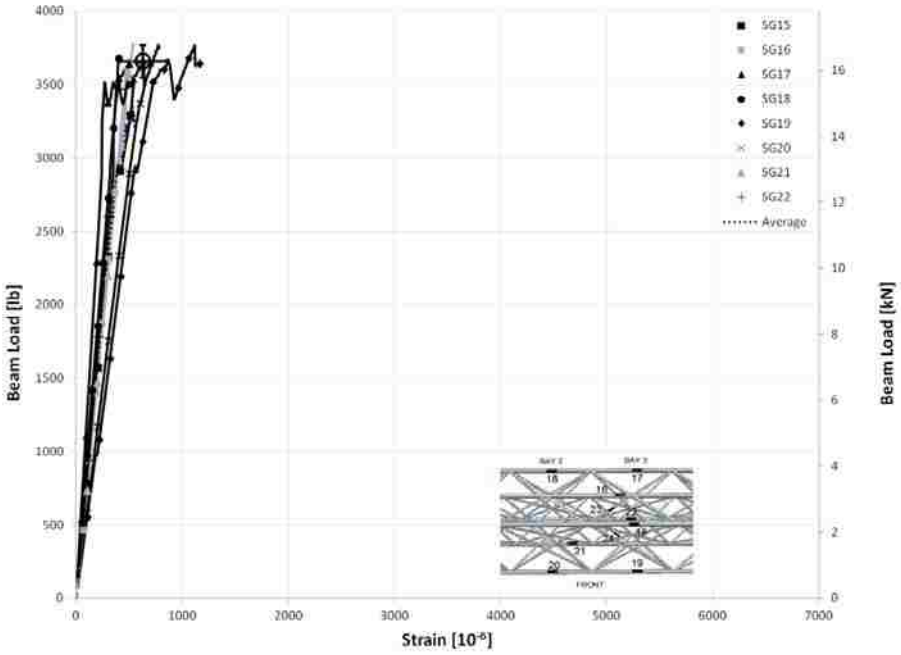

Figure 3-12: Load-Strain Plot for Test 1A Longitudinal Members

Table 3-12: Summary Table for Test 1B
Longitudinal Strain Gages

Strain Gage	Maximum Strain at Gage/Beam Failure [με]	Beam Load at Gage/Beam Failure [lb (kN)]	
15	220	3,445	15.4
16	470	3,718	16.7
17	512	3,786	17.0
18	240	3,783	17.0
19	1,076	3,783	17.0
20	598	3,752	16.8
21	652	3,743	16.8
22	1,126	3,783	17.0
Average	612	3,724	16.7
Std. Dev.	339	115	0.518
[%]	55.4	3.10	

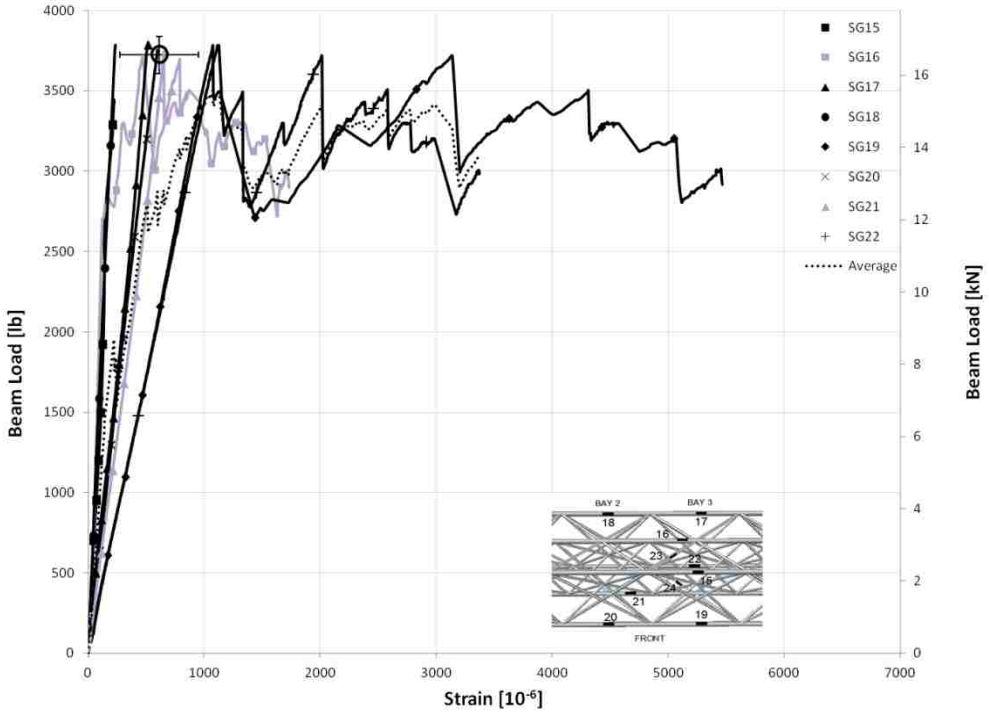

Figure 3-13: Load-Strain Plot for Test 1B Longitudinal Members

3.3 Specimen 2

This section contains the results for the strain gages of each type of member for Specimen 2, including Test 2A and Test 2B.

3.3.1 All Members

The results for all Test 2A strain gages are summarized in Table 3-13 and presented in the beam load verse strain plot shown in Figure 3-14. The average beam load at gage/beam failure is 3,247 lbs (14.6 kN) with a standard deviation of 384 lbs (1.72 kN) and the corresponding average maximum strain is 0.837×10^3 με with a standard deviation of 0.764×10^3 με.

Table 3-13: Summary Table for Test 2A Strain Gages

Strain Gage	Maximum Strain at Gage/Beam Failure [με]	Beam Load at Gage/Beam Failure [lb (kN)]	
1	588	3,361	15.1
2	2,354	3,351	15.0
3	1,790	3,358	15.1
4	2,388	3,360	15.1
5	374	3,364	15.1
6	132	3,365	15.1
7	180	1,870	8.38
8	448	3,362	15.1
9	844	3,354	15.0
10	498	3,350	15.0
11	302	3,178	14.2
15	146	3,366	15.1
16	1,272	3,368	15.1
17	760	3,357	15.0
18	478	3,337	15.0
Average	837	3,247	14.6
Std. Dev.	764	384	1.72
[%]	91.3	11.8	

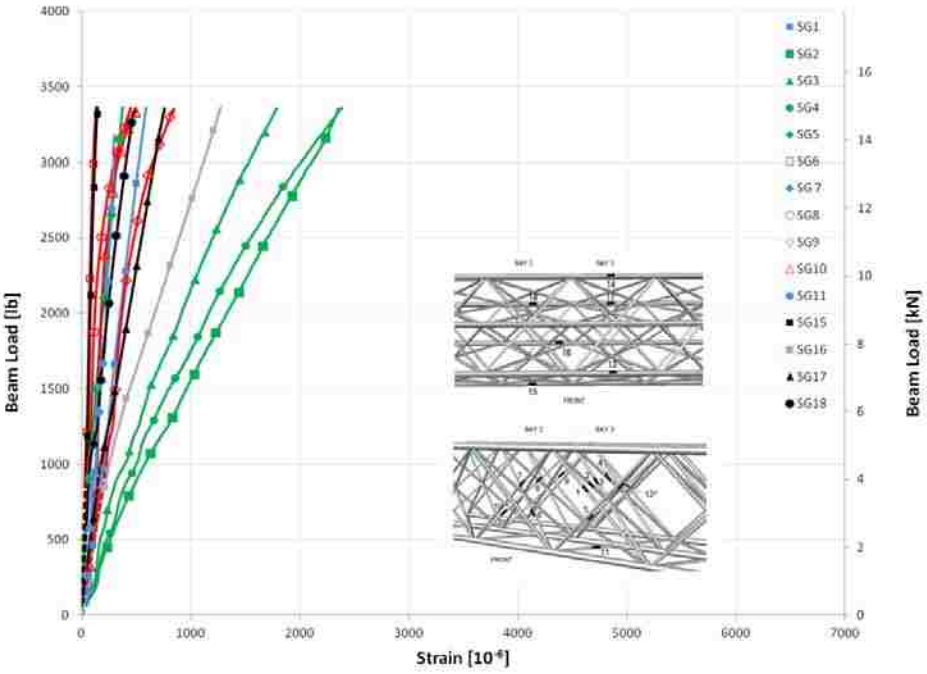

Figure 3-14: Load-Strain Plot for Test 2A Members

The results for all Test 2B strain gages are summarized in Table 3-14 and presented in the beam load verse strain plot shown in Figure 3-15. The average beam load at gage/beam failure is 4,433 lbs (19.9 kN) with a standard deviation of 562 lbs (2.52 kN) and the corresponding average maximum strain is $1.04x10^3$ με with a standard deviation of $1.09x10^3$ με.

Table 3-14: Summary Table for Test 2B Strain Gages

Strain Gage	Maximum Strain at Gage/Beam Failure [με]	Beam Load at Gage/Beam Failure [lb (kN)]	
1	1,058	4,688	21.0
2	2,894	4,762	21.3
3	888	4,724	21.2
4	3,014	4,721	21.2
5	360	4,762	21.3
6	60.0	3,782	17.0
7	360	4,752	21.3
8	500	3,412	15.3
9	394	3,025	13.6
10	3,322	4,763	21.3
11	228	4,662	20.9
15	408	4,657	20.9
16	1,096	4,755	21.3
17	676	4,729	21.2
18	394	4,299	19.3
Average	1,043	4,433	19.9
Std. Dev.	1,094	562	2.52
[%]	105	12.7	

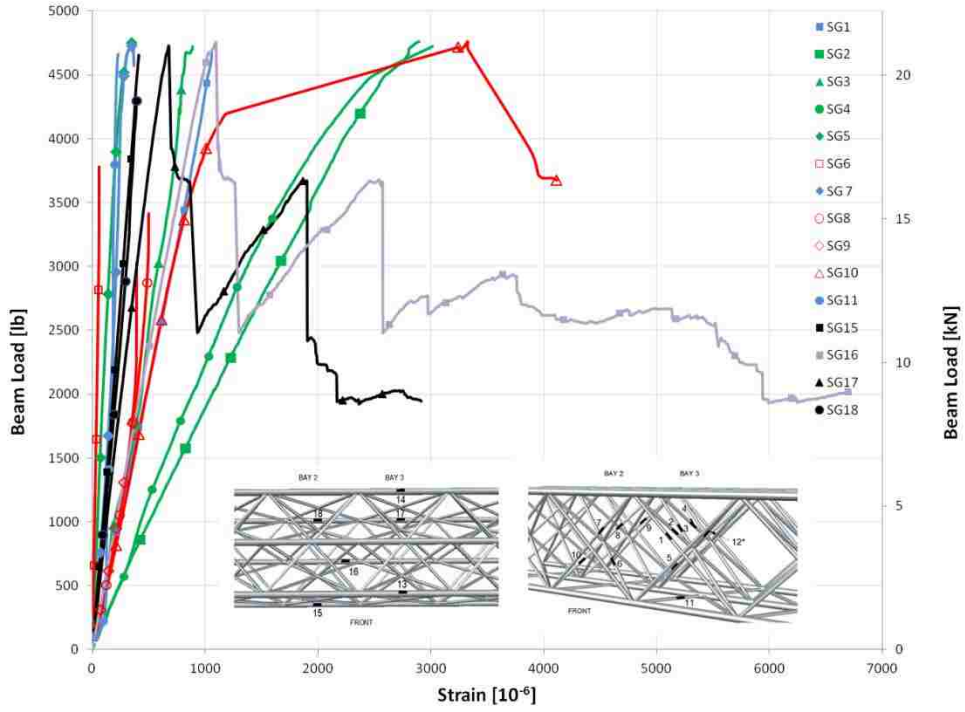

Figure 3-15: Load-Strain Plot for Test 2B Members

3.3.2 Inner Diagonal Members

The results for Test 2A Bay 3 Inner Diagonal strain gages are presented in the beam load verse strain plot shown in Figure 3-16 and summarized in Table 3-15. The average beam load at gage/beam failure is 3,358 lbs (15.1 kN) with a standard deviation of 5.48 lbs (0.0246 kN) and the corresponding average maximum strain is 1.73×10^3 με with a standard deviation of 0.942×10^3 με.

The results for Test 2A Bay 2 Inner Diagonal strain gages are presented in the beam load verse strain plot shown in Figure 3-16 and summarized in Table 3-16. The average beam load at gage/beam failure is 3,358 lbs (15.1 kN) with a standard deviation of 6.96 lbs (0.031 kN) and the corresponding average maximum strain is 0.481×10^3 με with a standard deviation of 0.292×10^3 με.

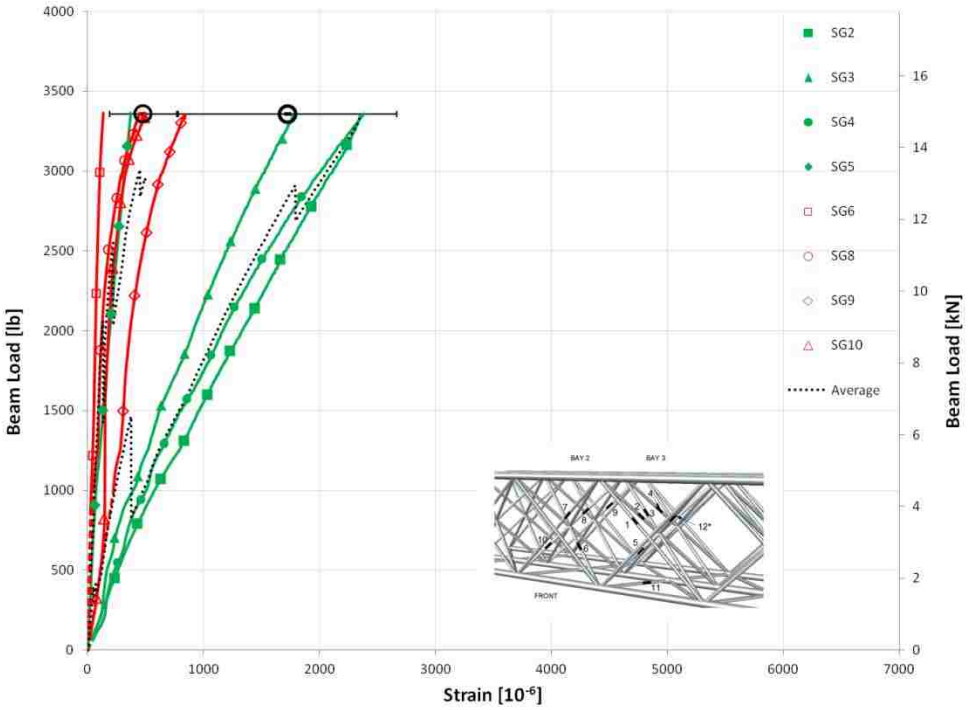

Figure 3-16: Load-Strain Plot For Test 2A Inner Diagonal Members

Table 3-15: Summary Table for Test 2A Bay 3 Inner Diagonal Strain Gages

Strain Gage	Maximum Strain at Gage/Beam Failure [με]	Beam Load at Gage/Beam Failure [lb (kN)]	
2	2,354	3,351	15.0
3	1,790	3,358	15.1
4	2,388	3,360	15.1
5	374	3,364	15.1
Average	1,727	3,358	15.1
Std. Dev.	942	5.48	0.025
[%]	54.6	0.163	

Table 3-16: Summary Table for Test 2A Bay 2 Inner Diagonal Strain Gages

Strain Gage	Maximum Strain at Gage/Beam Failure [με]	Beam Load at Gage/Beam Failure [lb (kN)]	
6	132	3,365	15.1
8	448	3,362	15.1
9	844	3,354	15.0
10	498	3,350	15.0
Average	481	3,358	15.1
Std. Dev.	292	6.96	0.031
[%]	60.7	0.207	

The results for Test 2B Bay 3 Inner Diagonal strain gages are summarized in Table 3-17 and presented in the beam load verse strain plot shown in Figure 3-17. The average beam load at gage/beam failure is 4,742 lbs (21.3 kN) with a standard deviation of 22.8 lbs (0.102 kN) and the corresponding average maximum strain is $1.79x10^3$ με with a standard deviation of $1.36x10^3$ με.

Table 3-17: Summary Table for Test 2B Bay 3 Inner Diagonal Strain Gages

Strain Gage	Maximum Strain at Gage/Beam Failure [με]	Beam Load at Gage/Beam Failure [lb (kN)]	
2	2,894	4,762	21.3
3	888	4,724	21.2
4	3,014	4,721	21.2
5	360	4,762	21.3
Average	1,789	4,742	21.3
Std. Dev.	1,363	22.8	0.102
[%]	76.2	0.480	

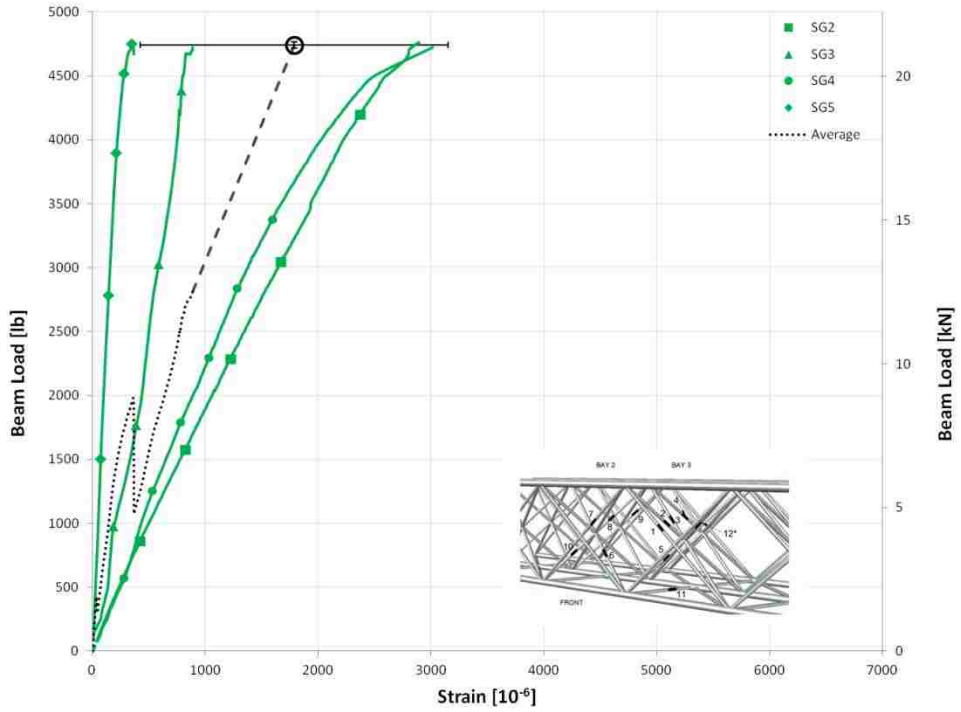

Figure 3-17: Load-Strain Plot For Test 2B Bay 3 Inner Diagonal Members

The results for Test 2B Bay 2 Inner Diagonal strain gages are summarized in Table 3-18 and presented in the beam load verse strain plot shown in Figure 3-18. The average beam load at gage/beam failure is 3,746 lbs (16.8 kN) with a standard deviation of 745 lbs (3.34 kN) and the corresponding average maximum strain is 1.07×10^3 με with a standard deviation of 1.51×10^3 με.

Table 3-18: Summary Table for Test 2B Bay 2 Inner Diagonal Strain Gages

Strain Gage	Maximum Strain at Gage/Beam Failure [με]	Beam Load at Gage/Beam Failure [lb (kN)]	
6	60.0	3,782	17.0
8	500	3,412	15.3
9	394	3,025	13.6
10	3,322	4,763	21.3
Average	1,069	3,746	16.8
Std. Dev.	1,514	745	3.34
[%]	142		19.9

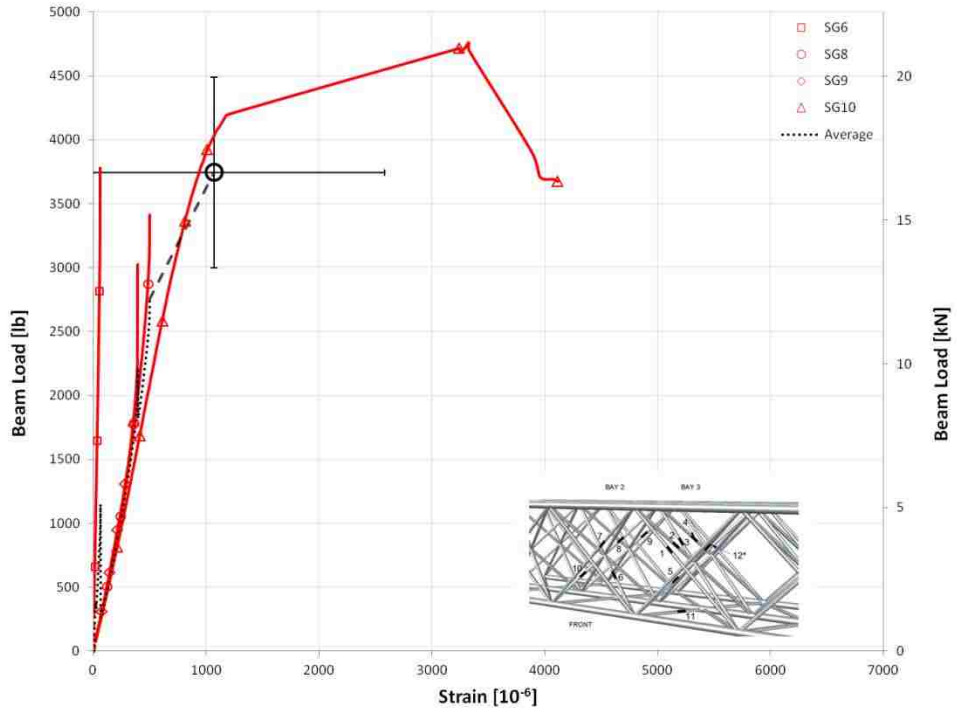

Figure 3-18: Load-Strain Plot For Test 2B Bay 2 Inner Diagonal Members

3.3.3 Outer Diagonal Members

The results for Test 2A Outer Diagonal strain gages are summarized in Table 3-19 and presented in the beam load verse strain plot shown in Figure 3-19. The average beam load at gage/beam failure is 2,803 lbs (12.6 kN) with a standard deviation of 813 lbs (3.64 kN) and the corresponding average maximum strain is 0.357×10^3 με with a standard deviation of 0.209×10^3 με.

The results for Test 2B Outer Diagonal strain gages are summarized in Table 3-20 and presented in the beam load verse strain plot shown in Figure 3-20. The average beam load at gage/beam failure is 4,700 lbs (21.1 kN) with a standard deviation of 46.3 lbs (0.208 kN) and the corresponding average maximum strain is 0.549×10^3 με with a standard deviation of 0.446×10^3 με.

Table 3-19: Summary Table for Test 2A Outer Diagonal Strain Gages

Strain Gage	Maximum Strain at Gage/Beam Failure [με]	Beam Load at Gage/Beam Failure [lb (kN)]	
1	588	3,361	15.1
7	180	1,870	8.38
11	302	3,178	14.2
Average	357	2,803	12.6
Std. Dev.	209	813	3.64
[%]	58.7	29.0	

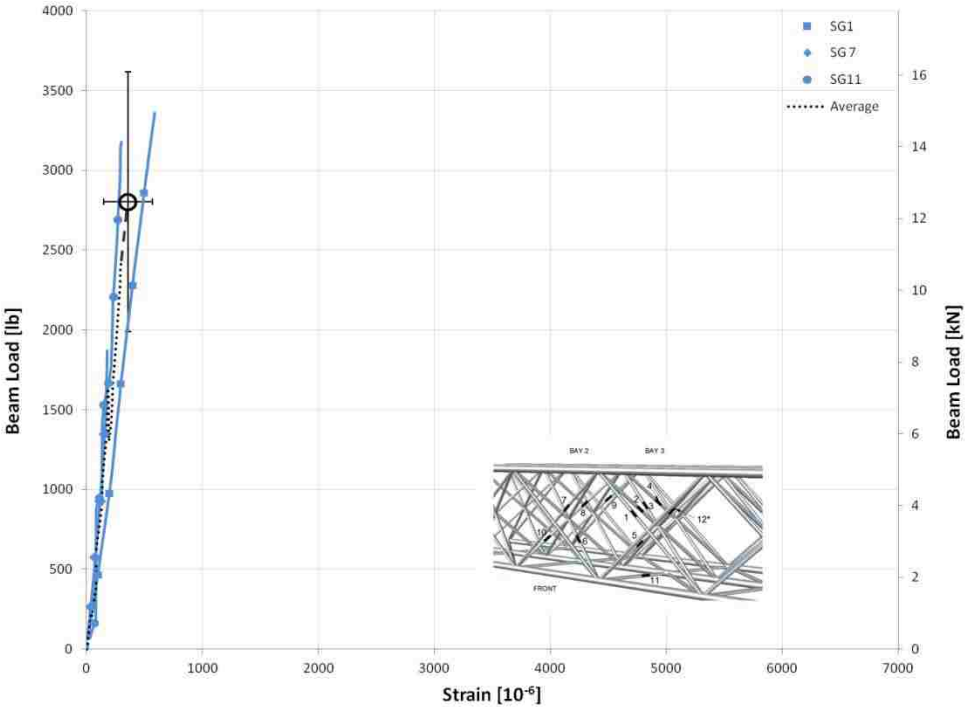

Figure 3-19: Load-Strain Plot For Test 2A Outer Diagonal Members

Table 3-20: Summary Table for Test 2B Outer Diagonal Strain Gages

Strain Gage	Maximum Strain at Gage/Beam Failure [με]	Beam Load at Gage/Beam Failure [lb (kN)]	
1	1,058	4,688	21.0
7	360	4,752	21.3
11	228	4,662	20.9
Average	549	4,700	21.1
Std. Dev.	446	46.3	0.208
[%]	81.3	0.985	

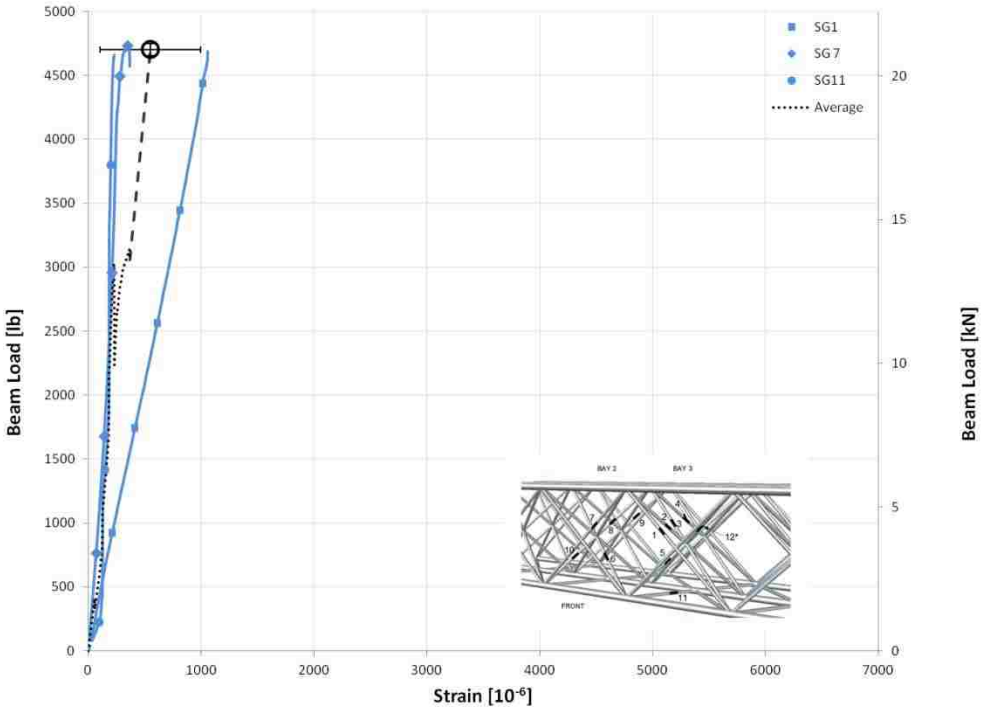

Figure 3-20: Load-Strain Plot For Test 2B Outer Diagonal Members

3.3.4 Longitudinal Members

The results for Test 2A longitudinal strain gages are summarized in Table 3-21 and presented in the beam load verse strain plot shown in Figure 3-21. The average beam load at gage/beam failure is 3,357 lbs (15.0 kN) with a standard deviation of 14.1 lbs (0.063 kN) and the corresponding average maximum strain is 0.664×10^3 με with a standard deviation of 0.477×10^3 με.

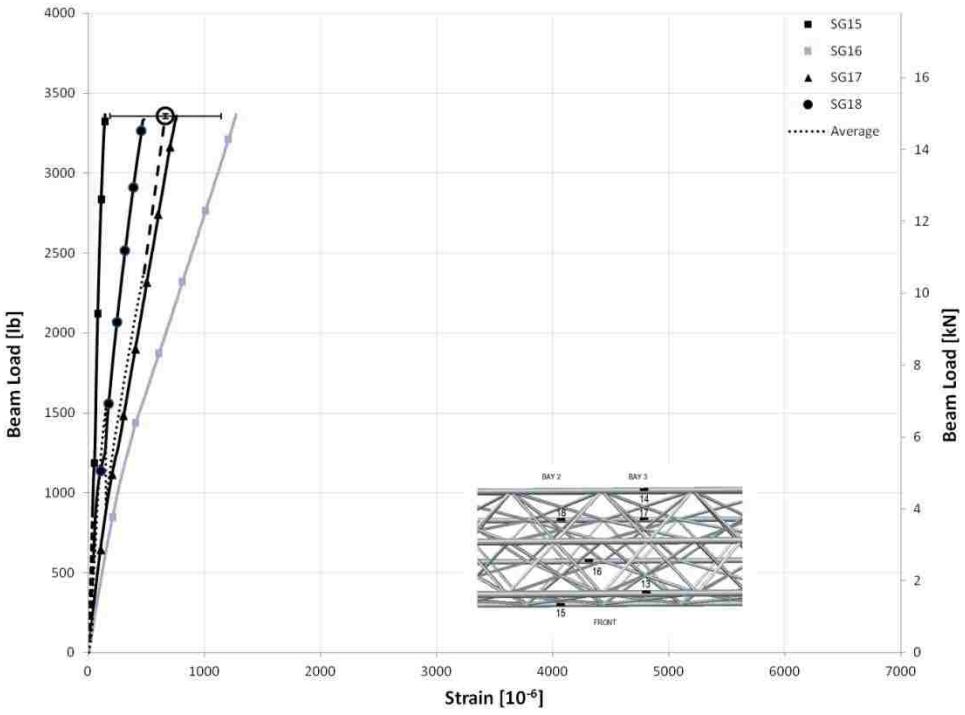

Figure 3-21: Load-Strain Plot For Test 2A Longitudinal Members

Table 3-21: Summary Table for Test 2A Longitudinal Strain Gages

Strain Gage	Maximum Strain at Gage/Beam Failure [με]	Beam Load at Gage/Beam Failure [lb (kN)]	
15	146	3,366	15.1
16	1,272	3,368	15.1
17	760	3,357	15.0
18	478	3,337	15.0
Average	664	3,357	15.0
Std. Dev.	477	14.1	0.063
[%]	71.8	0.421	

The results for Test 2B longitudinal strain gages are summarized in Table 3-22 and presented in the beam load verse strain plot shown in Figure 3-22. The maximum average and range of standard deviation is also plotted. The average beam load at gage/beam failure is 4,610 lbs (20.7 kN) with a standard deviation of 212 lbs (0.948 kN) and the corresponding average maximum strain is 0.644×10^3 με with a standard deviation of 0.328×10^3 με.

Table 3-22: Summary Table for Test 2B Longitudinal Strain Gages

Strain Gage	Maximum Strain at Gage/Beam Failure [με]	Beam Load at Gage/Beam Failure [lb (kN)]	
15	408	4,657	20.9
16	1,096	4,755	21.3
17	676	4,729	21.2
18	394	4,299	19.3
Average	644	4,610	20.7
Std. Dev.	328	212	0.948
[%]	51.0	4.59	

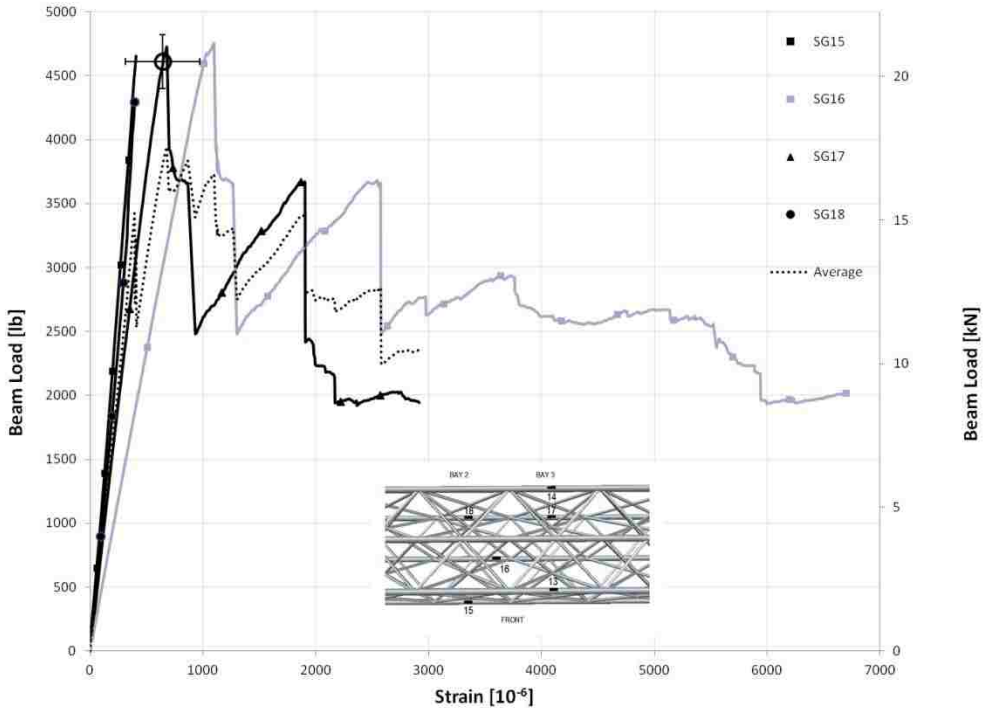

Figure 3-22: Load-Strain Plot For Test 2B Longitudinal Members

3.4 **Specimen 3**

This section contains the results for the strain gages of each type of member for Specimen 3.

3.4.1 All Members

The results for all Test 3 strain gages are summarized in Table 3-23 and presented in the beam load verse strain plot shown in Figure 3-23. The average beam load at gage/beam failure is 4,737 lbs (21.2 kN) with a standard deviation of 466 lbs (2.09 kN) and the corresponding average maximum strain is 1.68×10^3 με with a standard deviation of 1.69×10^3 με.

Table 3-23: Summary Table for Test 3 Strain Gages

Strain Gage	Maximum Strain at Gage/Beam Failure [με]	Beam Load at Gage/Beam Failure [lb (kN)]	
1	738	5,066	22.7
2	1,948	4,538	20.3
3	4,828	5,085	22.8
4	5,526	4,906	22.0
5	812	5,016	22.5
6	664	4,947	22.2
7	248	4,837	21.7
8	2,020	4,670	20.9
9	2,938	3,940	17.7
10	3,604	4,906	22.0
11	10.70	4,858	21.8
12	1,080	4,917	22.0
15	236	3,393	15.2
16	954	5,035	22.6
17	740	5,148	23.1
18	588	4,522	20.3
Average	1,683	4,737	21.2
Std. Dev.	1,688	466	2.09
[%]	100	9.83	

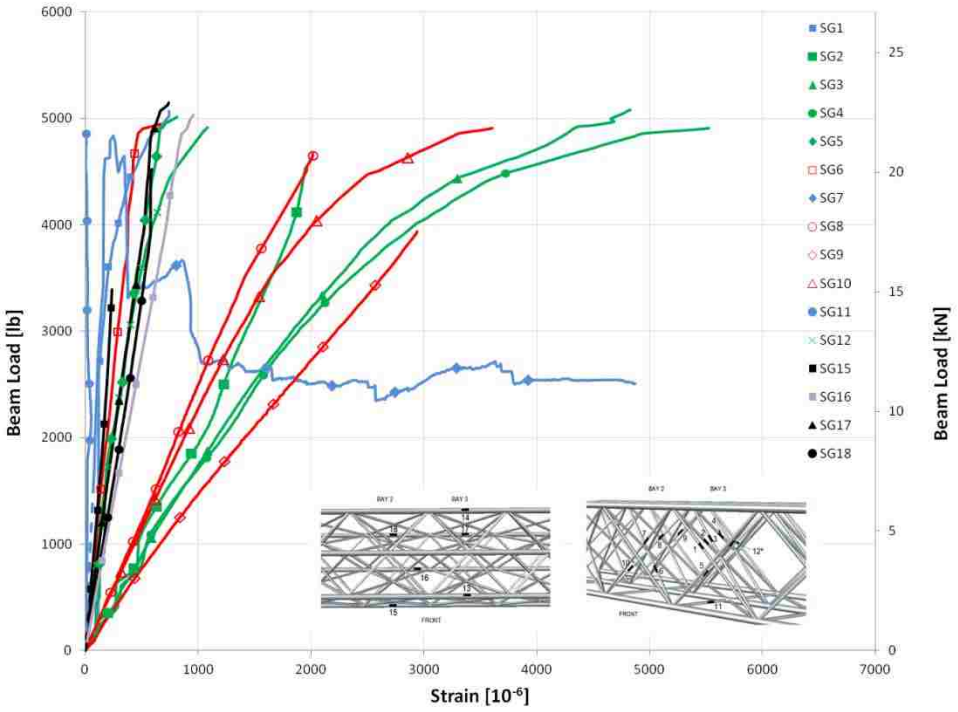

Figure 3-23: Load-Strain Plot For Test 3 Members

3.4.2 Inner Diagonal Members

The results for Test 3 Bay 3 Inner Diagonal strain gages are summarized in Table 3-24 and presented in the beam load verse strain plot shown in Figure 3-24. The average beam load at gage/beam failure is 4,892 lbs (21.9 kN) with a standard deviation of 212 lbs (0.948 kN) and the corresponding average maximum strain is 2.84×10^3 με with a standard deviation of 2.19×10^3 με.

Table 3-24: Summary Table for Test 3 Bay 3 Inner Diagonal Strain Gages

Strain Gage	Maximum Strain at Gage/Beam Failure [με]	Beam Load at Gage/Beam Failure [lb (kN)]	
2	1,948	4,538	20.3
3	4,828	5,085	22.8
4	5,526	4,906	22.0
5	812	5,016	22.5
12	1,080	4,917	22.0
Average	2,839	4,892	21.9
Std. Dev.	2,189	212	0.948
[%]	77.1	4.32	

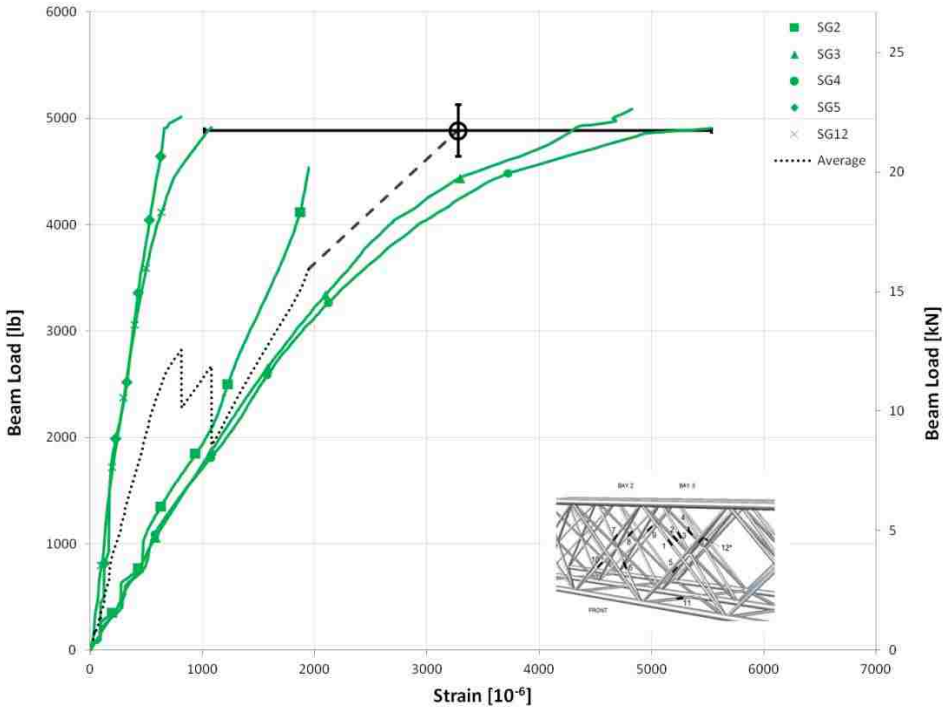

Figure 3-24: Load-Strain Plot For Test 3 Bay 3 Inner Diagonal Members

The results for Test 3 Bay 2 Inner Diagonal strain gages are summarized in Table 3-25and presented in the beam load verse strain plot shown in Figure 3-25. The average beam

load at gage/beam failure is 4,616 lbs (20.7 kN) with a standard deviation of 467 lbs (2.09 kN) and the corresponding average maximum strain is 2.31x103 με with a standard deviation of 1.27x103 με.

Table 3-25: Summary Table for Test 3 Bay 2 Inner Diagonal Strain Gages

Strain Gage	Maximum Strain at Gage/Beam Failure [με]	Beam Load at Gage/Beam Failure [lb (kN)]	
6	664	4,947	22.2
8	2,020	4,670	20.9
9	2,938	3,940	17.7
10	3,604	4,906	22.0
Average	2,307	4,616	20.7
Std. Dev.	1,273	467	2.09
[%]	55.2	10.1	

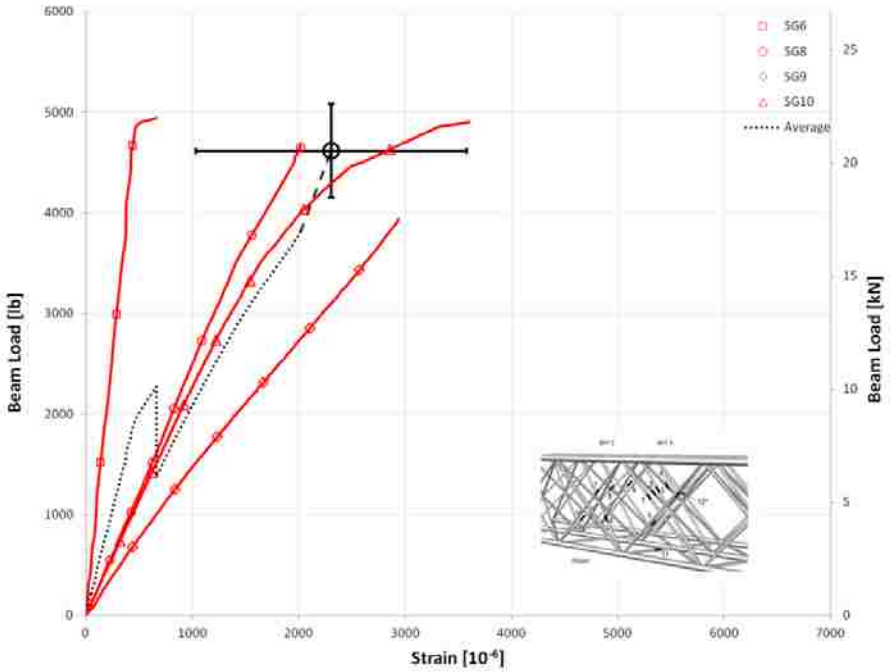

Figure 3-25: Load-Strain Plot For Test 3 Bay 2 Inner Diagonal Members

3.4.3 Outer Diagonal Members

The results for Test 3 Bay 3 Inner Diagonal strain gages are presented in the beam load verse strain plot shown in Figure 3-26 and summarized in Table 3-26. The beam load at gage/beam failure is 4,921 lbs (22.1 kN) with a standard deviation of 126 lbs (0.566 kN) and the corresponding average maximum strain is 0.332×10^3 με with a standard deviation of 0.371×10^3 με.

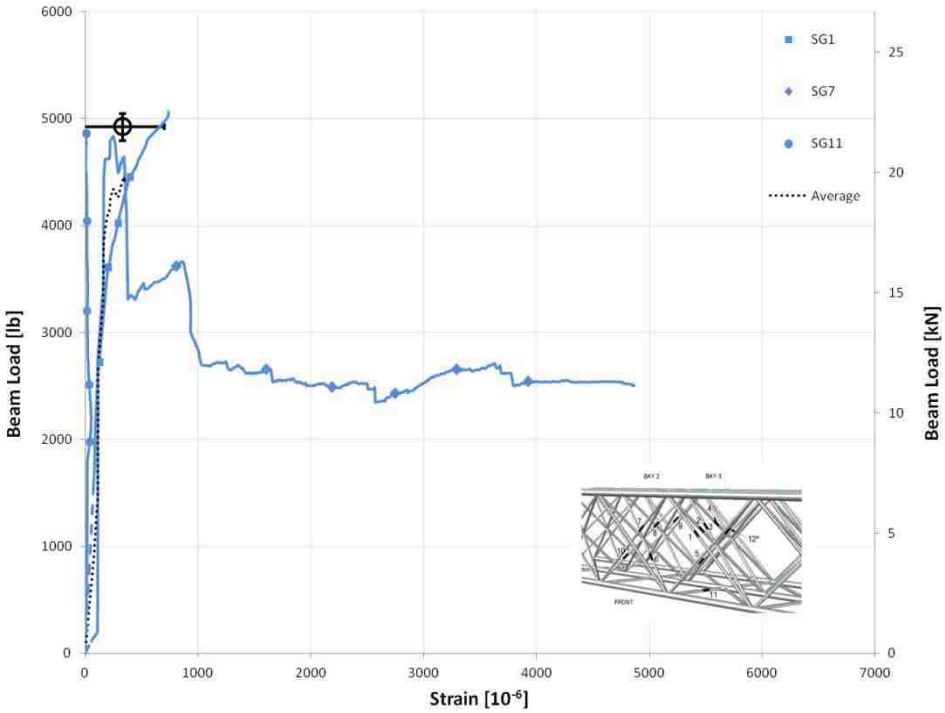

Figure 3-26: Load-Strain Plot For Test 3 Outer Diagonal Members

Table 3-26: Summary Table for Test 3 Outer Diagonal Strain Gages

Strain Gage	Maximum Strain at Gage/Beam Failure [με]	Beam Load at Gage/Beam Failure [lb (kN)]	
1	738	5,066	22.7
7	248	4,837	21.7
11	10.7	4,858	21.8
Average	332	4,921	22.1
Std. Dev.	371	126	0.566
[%]	112	2.57	

3.4.4 Longitudinal Members

The results for Test 3 Bay 3 Longitudinal strain gages are summarized in Table 3-27 and presented in the beam load verse strain plot shown in Figure 3-27. The maximum average and range of standard deviation is also plotted. The average beam load at gage/beam failure is 4,525 lbs (20.3 kN) with a standard deviation of 802 lbs (3.59 kN) and the corresponding average maximum strain is 0.630×10^3 με with a standard deviation of 0.302×10^3 με.

Table 3-27: Summary Table for Test 3 Bay 3 Longitudinal Strain Gages

Strain Gage	Maximum Strain at Gage/Beam Failure [με]	Beam Load at Gage/Beam Failure [lb (kN)]	
15	236	3,393	15.2
16	954	5,035	22.6
17	740	5,148	23.1
18	588	4,522	20.3
Average	630	4,525	20.3
Std. Dev.	302	802	3.59
[%]	48.0	17.7	

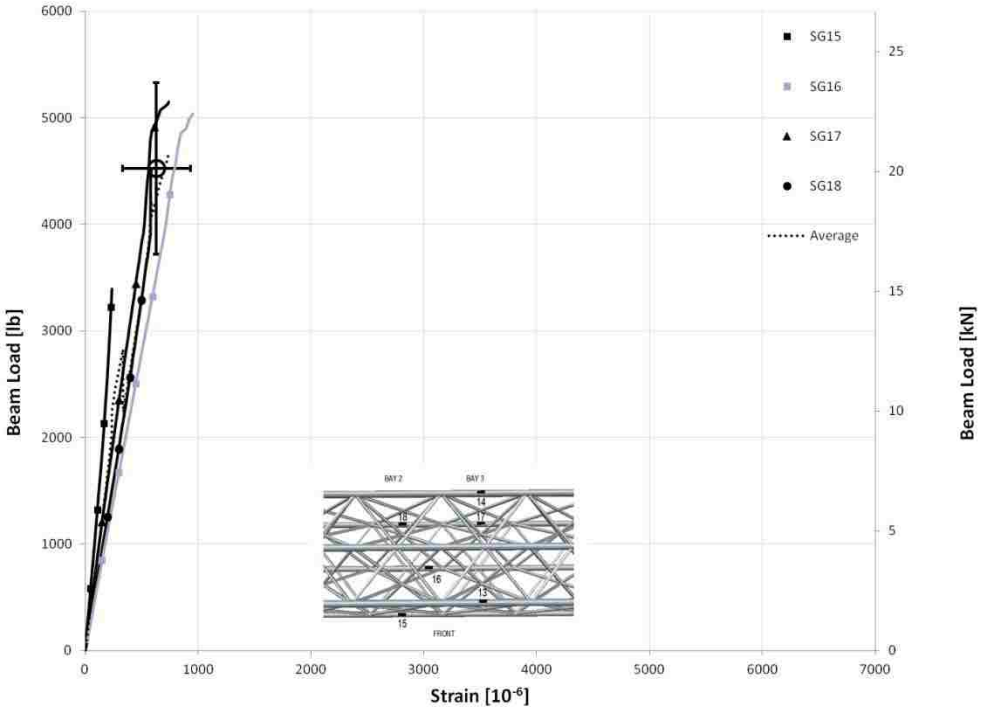

Figure 3-27: Load-Strain Plot For Test 3 Longitudinal Members

4 MEMBER COMPRESSION TESTING EXPERIMENTAL APPROACH

This chapter contains a description of the specimen preparation, microscopic analysis and testing procedures for the individual members tested in compression.

4.1 Unsupported Length

Longitudinal and inner diagonal members were removed post-mortem from each beam using a Dremel tool and cut to length using a Leco CM-10 cutting jig with a diamond tip blade (Figure 4-1A). Two sets of a longitudinal and inner diagonal member were removed from each specimen for a total of six of each type of member. The first set was removed from the top, left, rear of Bay 1 of each specimen. The second set was removed from the top, right, front of Bay 4 of each specimen. The members were taken from outer, unloaded bays of the beams. Since members were being removed from the IsoBeam specimens, the length was determined by the length of each member between bays. The members were removed as close to the nodes as possible to allow the longest possible member. The longitudinal members were cut to 3.0 in. (76 mm) in length with 1.5 in. (38 mm) for bonding into the end caps. The diagonal members were cut to 2.5 in. (63.3 mm) also with 1.5 in. (38 mm) for end cap bonding. Both final unsupported lengths between caps were less than the calculated buckling lengths which are 4.5 in. and 8.9 in. for the inner diagonal and longitudinal members, respectively. These members were polished

with a Leco Spectrum 2000 using a fixture created by Allen [17] (Figure 4-1B) to ensure proper vertical alignment. A detailed description of the sanding process is contained in Appendix C.

(A) (B)

Figure 4-1: Member Preparation Machinery: A) Leco Saw; and, B) Leco Sander

4.2 Label Notation

The members are numbered first by the type of member (D or L, for diagonal or longitudinal, respectively), and second by which IsoBeam specimen they were removed from. Lastly, a -1 or -2 is added since two of each member was removed from each IsoBeam. An example of this notation is D2-1, where D denotes a diagonal member, 2 denotes IsoBeam specimen 2 and -1 represents the first set of members removed from that specimen.

4.3 Microscope Measurements

Microscopic measurements of the end sections for cross-sectional area and voids were generated using a Leco Olympus SZX12 microscope while the fiber volume fraction was

measured using pictures taken on the Leco Olympus GX51. Pax-it software was used to analyze both sets of pictures. The pictures and complete data for the cross-sectional area, voids, and fiber volume fraction analysis can be viewed in Appendix C.

4.3.1 Cross-Sectional Area

Pictures of each end of the members were taken with the Leco Olympus SZX12 microscope at 7X. The cross-sectional area of each member was measured by drawing a region of interest (ROI) around the carbon core of the material. This was also the area used for evaluating the void content and void percentages of the ROI. The average cross-sectional area of both ends was used as the final area of each member. The complete list of cross-sectional areas of each member are listed in Appendix C.1.

4.3.2 Void Content

After defining the ROI around the cross-section, the voids were changed to a bright green color and the area of the green measured using the Pax-it software (Figure 4-2). This can be seen for each member in Appendix C pictures and results.

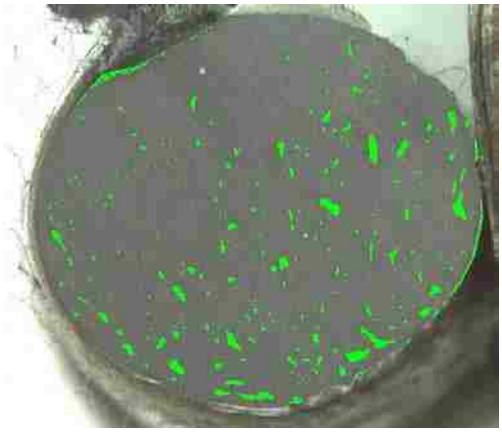

Figure 4-2: Void Content Measurements using Pax-It Software

4.3.3 Fiber Volume Fraction

The fiber volume fraction was measured using pictures taken on the Leco Olympus GX51 at 50X. At this high level of zoom, the microscope was very sensitive to movement and the plumbness of the member. Since the Leco Olympus GX51 is an inverted microscope, the specimen hanging above the lens was complicated to level. Thus, only the area in focus was able to be measured accurately as seen in Figure 4-3. The pictures of the fiber volume fraction of all the members are contained in Appendix C.

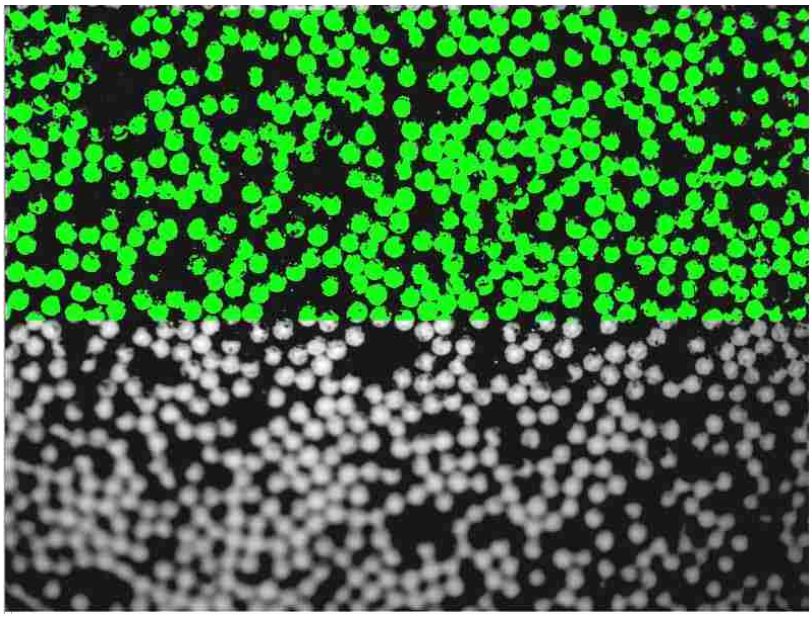

Figure 4-3: Measurement Area for Fiber Volume Fraction

4.4 Bonding in End Caps

The members were capped using special housing designed to align the members. Loctite 5-minute epoxy was used to bond the members into the caps which were bolted to the bottom section to ensure the members were vertically aligned with the flat surface. The end caps and flat bottom surface helped to prevent splaying of the ends of each specimen.

4.5 **Test Procedures**

The members were tested using a 20 kip (80 kN) Instron Model 1321 using the same method detailed in Allen [17], Embley [19] and Sika [20]. The end caps were aligned and gripped with 0.46-0.75 in. (11.68-19.05 mm) wedge grips. Figure 4-4 displays the test fixture. The members were tested at a rate of 0.05 in/min (1.27 mm/min). The strain data was recorded with strain gages similar to those used on the IsoBeam specimens.

The member tests provided material data for our beam specimens that were easily comparable to members created in past research. The results are summarized in the Chapter 5, Member Compression Test Results.

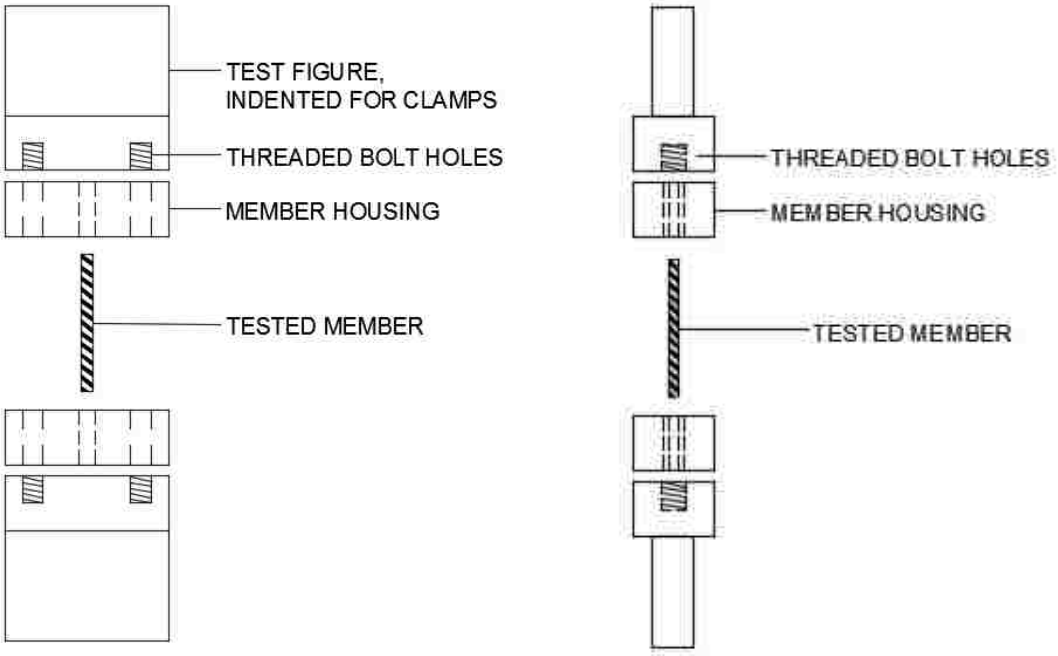

Figure 4-4: Member Compression Test Fixture

5 MEMBER COMPRESSION TEST RESULTS

This chapter summarizes the results of the member compression tests. This includes combined results as well as results separated by member type and by beam specimen number.

5.1 All Member Test Results

The average properties for each member type are summarized in Table 5-1 and presented in the stress-strain plot shown in Figure 5-1. The average compression stress is 86.9 ksi (599 MPa) with a standard deviation of 34.5 ksi (238 MPa). The average strain at ultimate strength is 5.31×10^3 με with a standard deviation of 2.71×10^3 με. The average Young's modulus is 17.8×10^6 psi (122 GPa) with a standard deviation of 4.24×10^6 psi (29.2 GPa).

Table 5-1: Summary Table of Average Properties by Member Type

Member Type	Cross-Sectional Area		Compression Young's Modulus		Strain at Ultimate Compression Stress	Ultimate Compression Stress	
	[in^2	(mm^2)]	[10^6 psi	(GPa)]	[10^3 με]	[ksi	(MPa)]
Longitudinal	0.121	77.8	20.8	143	3,392	62.5	431
Diagonal	0.0272	17.6	14.8	102	7,229	111	767
Average			17.8	122	5,310	86.9	599
Std. Dev.			4.24	29.2	2,714	34.5	238
[%]			23.9		51.1	39.7	

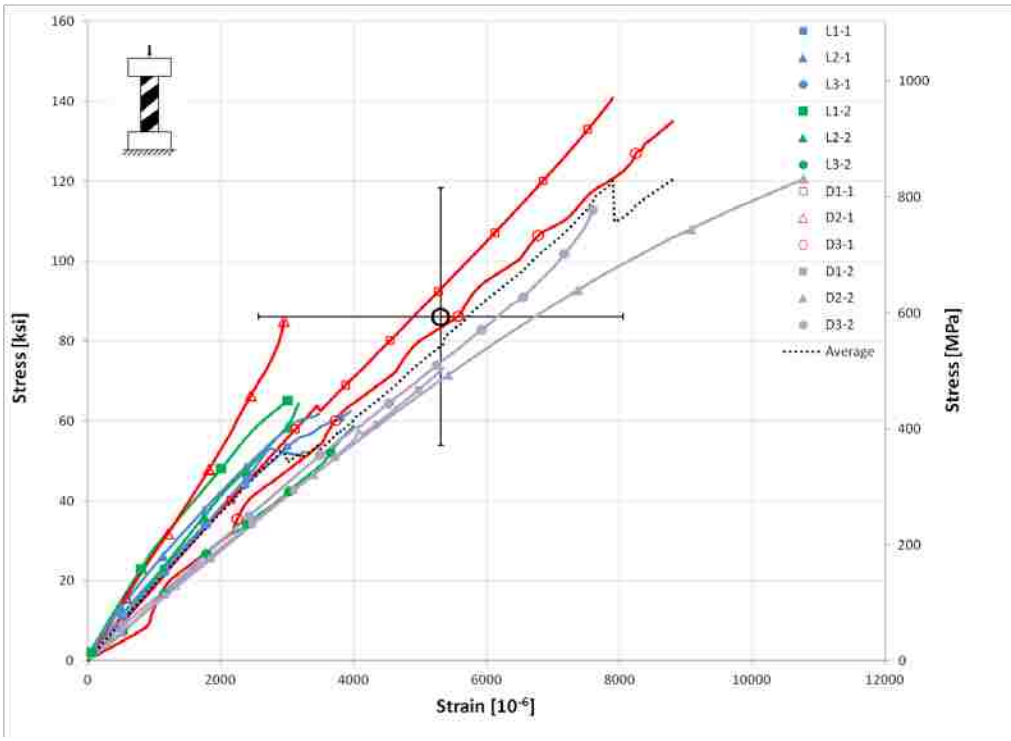

Figure 5-1: Stress-Strain Plot for All Members

5.2 Longitudinal Member Test Results

The results for the longitudinal members are summarized in Table 5-2 and presented in the stress-strain plot shown in Figure 5-2. The average alternate compression stress is 62.5 ksi (431 MPa) with a standard deviation of 2.56 ksi (17.6 MPa). The average strain at ultimate strength is 3.39×10^3 με with a standard deviation of 0.510×10^3 με. The average Young's modulus is 20.8×10^6 psi (143 GPa) with a standard deviation of 4.21×10^6 psi (29.0 GPa).

Table 5-2: Summary Table for Longitudinal Members

Specimen ID	Cross-Sectional Area		Compression Young's Modulus		Strain at Ultimate Compression Stress	Ultimate Compression Stress	
	[in^2	(mm^2)]	[10^6 psi	(GPa)]	[με]	[ksi	(MPa)]
L1-1	0.123	79.3	18.8	130	3,950	62.4	431
L2-1	0.119	76.9	22.8	157	3,475	61.7	426
L3-1	0.120	77.7	19.1	132	2,750	53.2*	367*
L1-2	0.119	76.9	27.6	190	3,000	65.1	449
L2-2	0.118	76.0	21.0	145	3,175	64.4	444
L3-2	0.124	79.7	15.2	105	4,000	58.6	404
Average	0.121	77.8	20.8	143	3,392	62.5	431
Std. Dev.	0.002	1.48	4.21	29.0	510	2.56	17.6
[%]	1.91		20.3		15.0	4.09	

*Property eliminated using Chauvenet's criterion, values not included in average or standard deviation

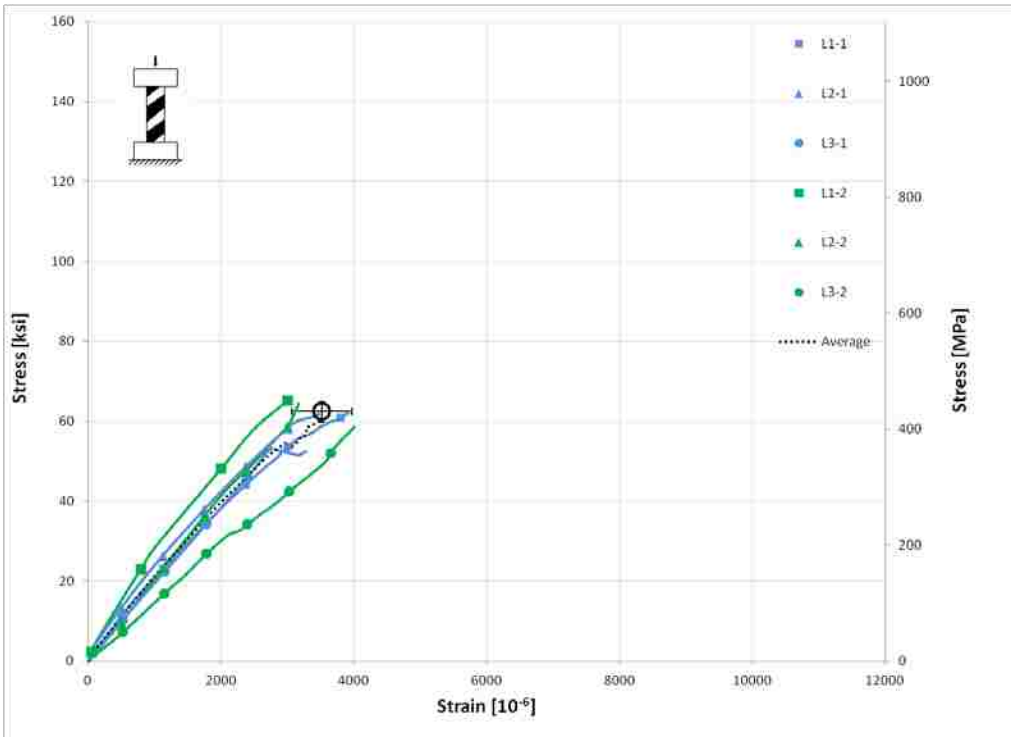

Figure 5-2: Stress-Strain Plot for Longitudinal Members

5.3 **Diagonal Member Test Results**

The results for the diagonal members are summarized in Table 5-3 and presented in the stress-strain plot shown in Figure 5-3. The average compression stress is 111 ksi (767 MPa) with a standard deviation of 27.1 ksi (187 MPa). The average strain at ultimate strength is 7.23×10^3 με with a standard deviation of 2.74×10^3 με. The average Young's modulus is 14.8×10^6 psi (102 GPa) with a standard deviation of 1.65×10^6 psi (11.4 GPa).

Table 5-3: Summary Table for Diagonal Members

Specimen ID	Cross-Sectional Area		Compression Young's Modulus		Strain at Ultimate Compression Stress	Ultimate Compression Stress	
	[in^2	(mm^2)]	[10^6 psi	(GPa)]	[με]	[ksi	(MPa)]
D1-1	0.026	16.7	17.4	120	7,900	141	971
D2-1	0.024	15.7	26.2*	181*	2,950	85.0	586
D3-1	0.023	15.1	15.3	105	8,800	135	931
D1-2	0.032	20.7	13.6	93.8	5,350	73.2	505
D2-2	0.027	17.1	13.4	92.4	10,775	121	832
D3-2	0.031	20.1	14.1	97.2	7,600	113	778
Average	0.027	17.6	14.8	102	7,229	111	767
Std. Dev.	0.004	2.33	1.65	11.4	2,738	27.1	187
[%]	13.3		11.2		37.9	24.3	

*Property eliminated using Chauvenet's criterion, values not included in average or standard deviation

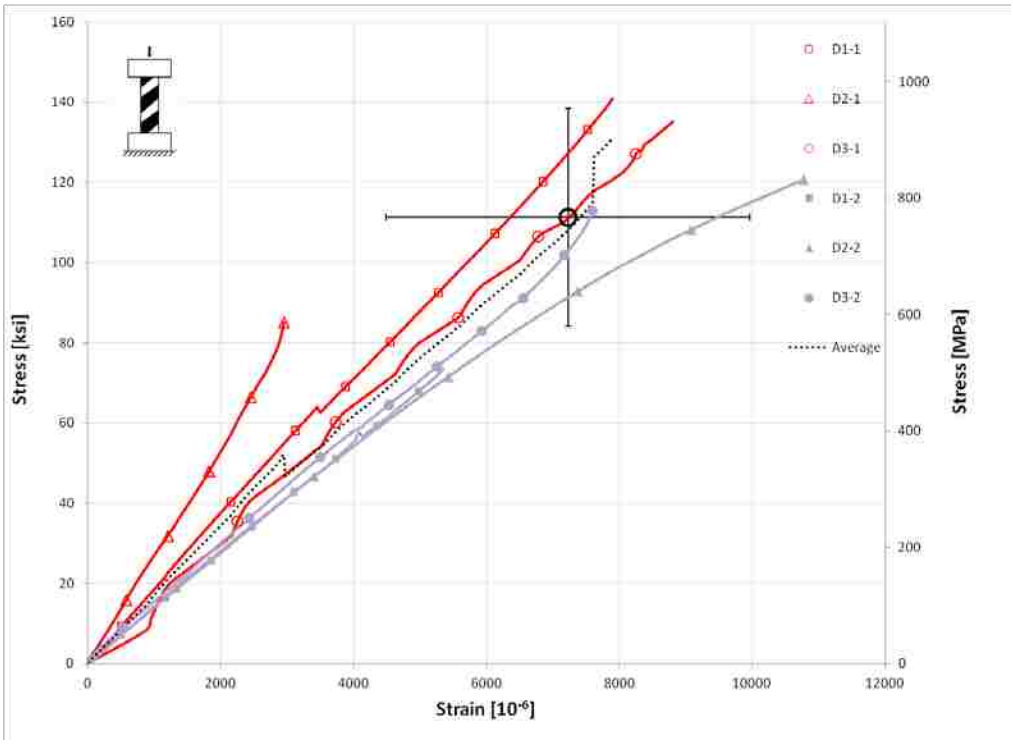

Figure 5-3: Stress-Strain Plot for Diagonal Members

6 FINITE ELEMENT MODEL ANALYSIS

A finite element model of the IsoBeam was created to provide a prediction of the failure and validation of results. The finite element model (Figure 6-1) was generated using Abaqus CAE finite element analysis program. The model was a 4-bay IsoBeam consisting of 160 members. The IsoBeam was analyzed under three-point bending to facilitate comparison to Test 3 of the experiment results. The axial load, maximum strain and Tsai-Wu failure criteria were recorded. The properties, loading and analysis of the finite element model are detailed in this chapter. The results are discussed and will be compared to the experimental results.

Figure 6-1: Rendered Picture of Finite Element Model

6.1 Description of Finite Element Model

6.1.1 Geometry and Properties

The geometry of the model was an IsoBeam with a height of 6 in. (152.4 mm), width of 3 in. (76.2 mm), and a bay length of 6 in. (152.4 mm). The model had four bays for a total length of 2 ft (0.61 m). This was the same size as the experimental specimens. The geometry was created by drawing wire members between nodes. The members were created as B31 beam elements which are three dimensional, linear beam elements between two nodes with six degrees of freedom: three translational and three rotational. The longitudinal members had a radius of 0.2 in. (5.08 mm) and the diagonal members had a radius of 0.1 in. (2.54 mm).

The material properties (Table 6-1) were obtained by adjusting the values provided by an AGATE technical data sheet for T700 unidirectional tape [23] multiplied by a correction factor. TCR Composite T700/UF3369 technical data sheet [22] for the material used provided limited properties so a ratio of the TCR properties to the AGATE properties was multiplied by the AGATE properties to provide all the values needed for analysis. Equations 10 & 11 below average the tensile and compressive properties in the primary direction for both the stiffness and strength properties. The respective ratio was applied to the stiffness and strength properties on the AGATE data sheet. Material properties provided by Sika in past research were also utilized [20]. Similarly, the failure properties were taken from the same sources (Table 6-2).

$$R = \frac{(E_1^t + E_1^c)_{TCR}}{(E_1^t + E_1^c)_{AGATE}} \tag{10}$$

$$S = \frac{(F_1^t + F_1^c)_{TCR}}{(F_1^t + F_1^c)_{AGATE}} \tag{11}$$

Table 6-1: Finite Element Model Material Properties

Material Property	Msi (GPa)	Source
E_1	22 (152)	[20]
E_2	1.48 (10.2)	[23]*
E_3	1.48 (10.2)	[23]*
G_{12}	0.68 (4.7)	[23]*
G_{13}	0.68 (4.7)	[23]*
G_{23}	0.46 (3.2)	[23]*
v_{12}	0.341	[23]*
v_{13}	0.341	[23]*
v_{23}	0.6	Similar Material

*Adjusted using correction factor

Table 6-2: Finite Element Model Failure Properties

Failure Property	ksi (MPa)	Source
0° Tensile Strength	345 (2280)	[23]*
0° Compressive Strength	139 (958)	[20]
90° Tensile Strength	7.8 (54)	[23]*
90° Compressive Strength	32 (221)	[23]*
Shear Strength	25 (172)	[23]*

*Adjusted using correction factor

The Tsai-Wu failure criterion was used to determine failure in the members. The Tsai-Wu failure criteria accounts for composites having a different tensile and compression strength. This failure criterion is based on a curve-fitting aspect rather than a physical phenomenon. Failure of the finite element model was determined to be when the first member reached a Tsai-Wu value of 1 or in other words, failure. While the IsoBeam would be able to sustain more load after failure of the first member, the peak strength of the model easily compared to the maximum strength of the experimental IsoBeam specimen test results.

6.1.2 Loading and Analysis

The model was loaded with three point loads applied at the three top center nodes. This loading is similar to the loading in Test 3. The bottom nodes between Bays 1 and 2 as well as between Bays 3 and 4 were all constrained in the y-direction (vertical direction). The middle nodes of these sets were further constrained: one as a pin and the other as a roller. The loading and boundary conditions can be seen in Figure 6-2.

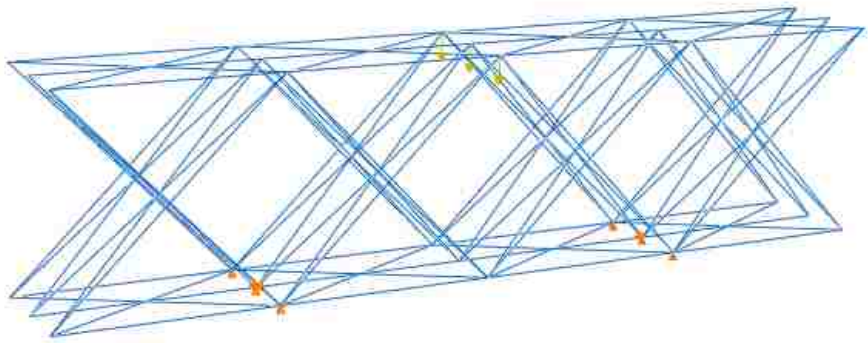

Figure 6-2: Finite Element Model Loading and Boundary Conditions

The model was determined to have converged when the strain changed by less than 1.0% after doubling the number of elements. The model mesh converged with a global element size of 2 in. (50.8 mm) which created two elements per diagonal member and three per longitudinal members. Figure 6-3 displays the mesh elements and nodes.

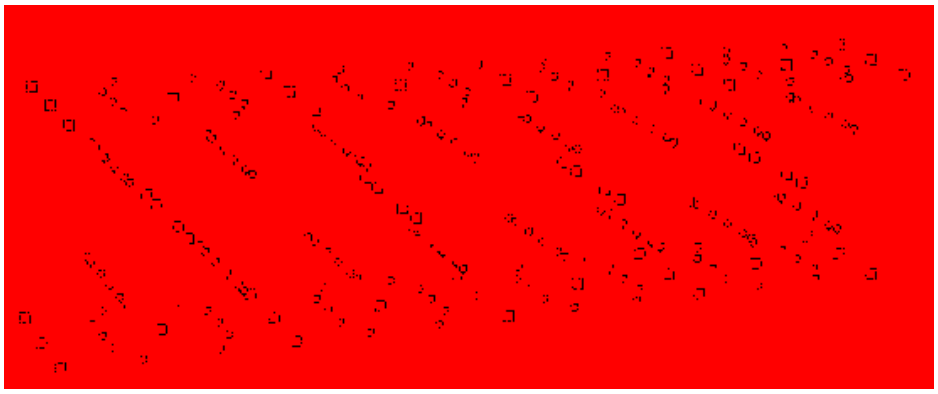

Figure 6-3: Finite Element Model Mesh

6.2 Preliminary Analysis for Validation

A preliminary analysis of the load distribution of the members was done to predict the results of the analytical and experimental data. A total load P was applied at the top nodes/members of an IsoBeam bay which were cut to create a simple 2-dimensional force body diagram as seen in Figure 6-4. Assuming even distribution of the load, each side would take half of the load P. The stiffness of each side consists of the stiffness of 2 vertical outer diagonals and 4 inner diagonals. Since the stiffness of the outer diagonals is different than the inner diagonals, the load is not evenly distributed between the six members.

The relative stiffness of each member type was found using Equations 12-14 which results in a ratio of the length of the members since the members have essentially the same area and modulus of elasticity. The angle of the outer verse inner diagonal members was approximated to be the same for the distribution of the load.

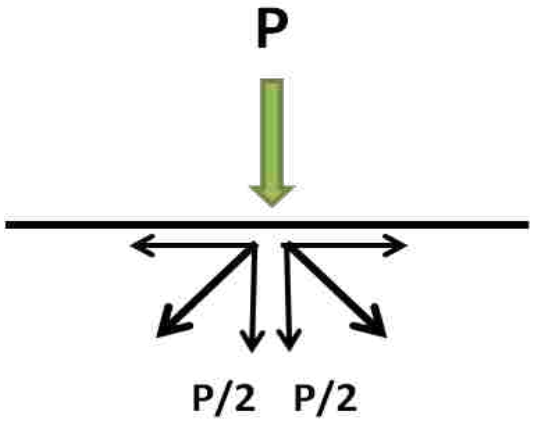

Figure 6-4: Force Body Diagram of IsoBeam Members

$$K = 2k_O + 4k_I \tag{12}$$

$$k = \frac{EA}{L} \tag{13}$$

$$\frac{k_I}{k_O} = \frac{\frac{EA}{L_I}}{\frac{EA}{L_O}} = \frac{L_O}{L_I} \approx 2 \tag{14}$$

The length of the inner diagonal is taken as the length from the upper node to the center node since the center node is effectively rigid due to the constraints applied by adjoining members in all three directions. The length of the vertical outer diagonal is taken as the length from the upper node to the lower node since the center node does not constrain the member in all three directions. Thus, the lengths from the IsoBeam specimens of this research are 4.31 in. (109 mm) and 8.49 in. (216 mm) for the inner and vertical outer diagonals, respectively. This results in a ratio of about 2:1 stiffness of the inner diagonals compared to that of the vertical outer diagonals. Using this ratio, each inner diagonal takes 9.97% of the load while the vertical outer diagonals only take 5.06% each.

6.3 **Results**

Failure of the first member was reached at a total load of 34 kips (151 kN) applied to the IsoBeam. Table 6-3 summaries the analytical results for the failure member and compares the results to the expected results. Member FTL3-OD or the front, top, left outer diagonal in Bay 3 (Element 207) was the first to fail with a Tsai-Wu value of 1.00. It failed with an axial compression load of 4,260 lbs (19.4 kN) and a maximum strain of 6,084 με. The load distribution of the IsoBeam can be seen in Figure 6-5 where negative results denote compression loading.

Table 6-3: Comparison of Analytical Results to Expected Results

	Analytical Results	Expected Results	Difference [%]
Axial Load [lbs (kN)]	4260 (18.9)	4370 (19.4)	2.52
Maximum Strain (με)	6,084	6,230	2.34
Tsai-Wu	1.000	-	-

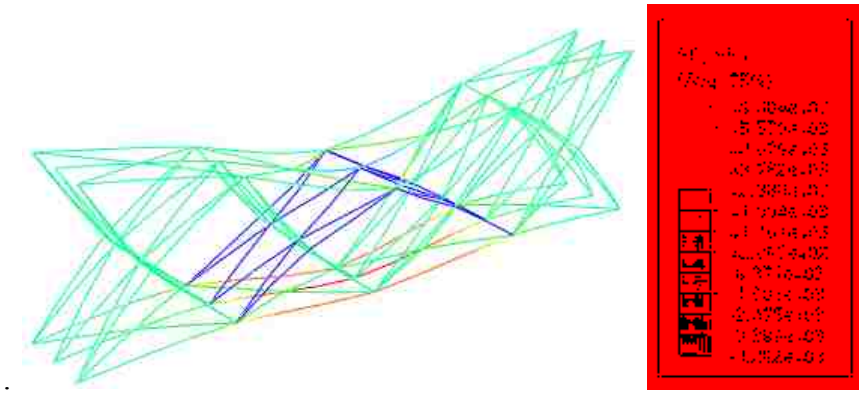

Figure 6-5: Axial Load Diagram of Finite Element Analysis Results

The model was validated by quick calculations using the material properties and comparing the analytical results to the experimental results discussed in Chapter 7. By dividing the compressive strength of 139 ksi (958 MPa) by the stiffness of 22.3 Msi (152 GPa), the expected strain at failure is 6,230 με. This value is only 2.34% different than the failure of the member in the analysis. The expected failure axial load was calculated by multiplying the area of the member by the compressive strength which results in an axial load of 4,370 lbs (19.4 kN) for diagonal members. This value is also comparable to the model's axial load failure.

The distribution of strain can be viewed in Figure 6-6 and the Tsai-Wu value results in Figure 6-7.

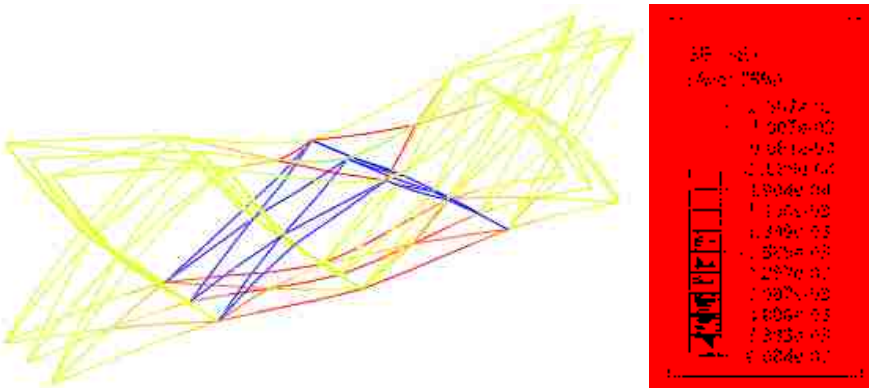

Figure 6-6: Strain Diagram of Finite Element Analysis Results

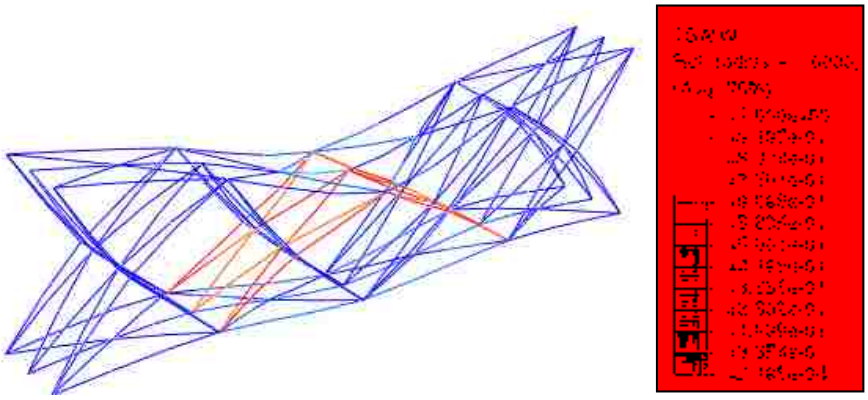

Figure 6-7: Tsai-Wu Diagram of Finite Element Analysis Results

The results for the members with the highest Tsai-Wu values for each member type at the beam failure load are presented in Table 6-4. The longitudinal and horizontal outer diagonal members took a lower load and experienced a lower strain value. This was expected since there is not much bending in the short beam, similar to the results seen in the experimental tests. They also have much lower Tsai-Wu values than the other two types of members.

Table 6-4: Results for Maximum Tsai-Wu Values for Each Member Type at Beam Failure Load

Member Type	Member Strain [με]	Member Axial Load [lbs (kN)]		Tsai-Wu
Inner Diagonal	-5,779	-4,049	-18.0	0.94
V. Outer Diagonal	-6,084	-4,262	-19.0	1.00
H. Outer Diagonal	2,050	1,436	6.39	0.15
Longitudinal	-651	-1,825	-8.12	0.22
Average	-2,616	-2,175	-9.67	0.58
Std. Dev.	3,986	2,648	11.8	0.45
[%]	152	122		78.1

The outer and inner diagonal members took the largest portion of the load, which was expected from the validation analysis previously discussed. Contrary to the validation, the outer diagonals take an equal percentage of the load as the inner diagonals. The linear finite element analysis does not include a buckling analysis. Thus, the outer diagonals do not buckle out of plane in the analysis results as seen in the experimental results. To further investigate the distribution of the load and capacity of the IsoBeam, a bucking analysis finite element analysis should be performed to accurately model the buckling of the outer diagonals.

Table 6-5 contains a comparison of these results with the validation calculations. They are not similar as previously discussed. To further investigate the relationship of the inner and

vertical outer diagonals, Table 6-6 contains the average results for the vertical outer and inner diagonals in the load path at the beam failure load. The vertical outer diagonals take an average of 12.5% of the load while the inner diagonals take an average of 11.4%. The Tsai-Wu value is higher on average for the vertical outer diagonals than the inner diagonals. During experimental tests, the vertical outer diagonals also failed prior to the inner diagonals, but the failure involved buckling out of plane which was not seen in the linear finite element analysis.

Table 6-5: Comparison of Load Distribution between Inner and Vertical Outer Diagonals

	Analytical % of Load	Expected % of Load
Vertical Outer Diagonal	12.5	5.06
Inner Diagonal	11.4	9.97

Table 6-6: Average Results for Inner and Vertical Outer Diagonals in Load Path at Beam Failure Load

Member Type	Average Member Strain [με]	Average Member Axial Load [lbs]	% of Total Beam Load [%]	Average Tsai-Wu
Inner Diagonal Avg.	-5,582	-3,911	11.5	0.897
Outer Diagonal Avg.	-6,084	-4,262	12.5	0.975
Average	-5,833	-4,086	12.0	0.936
Std. Dev.	355	248	0.73	0.055
[%]	6.08	6.08	6.08	5.89

7 DISCUSSION OF RESULTS

The parameters investigated in this section include discussion of the moment and shear properties, validation of test methods, characterization of the IsoBeam, assessment of manufacturing quality, identification of load paths in the IsoBeam and comparison of the analytical and experimental data. The average results for the strain gages are also presented and discussed for the IsoBeam specimens. Discussion regarding failure strength focuses on Tests 1B, 2B and 3 since Tests 1A and 2A did not reach failure.

7.1 Moment and Shear Properties

The moment versus machine displacement plots are shown in Figure 7-1. The average maximum moment was 12.3 kip-in (1.39 kN-m) with a standard deviation of 2.24 kip-in (0.25 kN-m) as presented in Table 7-1. The energy absorbed by the beam after failure was quantified by calculating the toughness or the area under the moment vs. deflection curve. The average toughness of the beams was 20.0 kip-in^2 (57.3 N-m^2) with a standard deviation of 1.0 kip-in^2 (2.8 N-m^2). The toughness of Test 1B is lower than the others because the test was ended soon after failure rather than allowing the beam to be tested to 25% of peak load like the other two tests. For this reason, it is not included in the average toughness calculation.

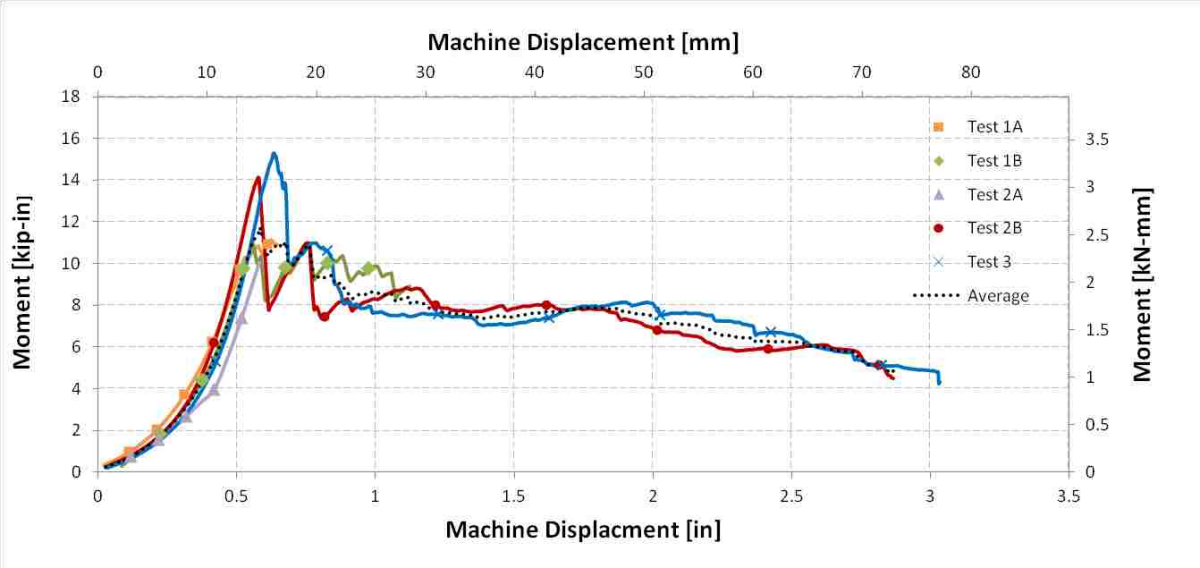

Figure 7-1: Moment vs. Machine Displacement Plots for all Tests

Table 7-1: Moment Results for All Tests

Test	Bending Test Method	Max Moment		Deflection at Max Moment		Toughness	
		[kip-in	(kN-mm)]	[in	(mm)]	[kip-in^2	(N-m^2)]
1A	4-Point	11.1	1.26	0.622	15.8	-	-
1B	4-Point	11.1	1.25	0.556	14.1	7.36*	21.1*
2A	3-Point	10.1	1.14	0.582	14.8	-	-
2B	3-Point	14.1	1.60	0.578	14.7	19.3	55.3
3	3-Point	15.3	1.73	0.638	16.2	20.7	59.3
	Average	12.3	1.39	0.595	15.1	20.0	57.3
	Std. Dev.	2.24	0.25	0.0338	0.857	1.0	2.8
	[%]	18.2		5.67		4.87	

*Not included in average because test was terminated after failure

The shear versus machine displacement plots are shown in Figure 7-2. The average maximum load was 2.06 kips (9.15 kN) with a standard deviation of 0.347 kips (1.66 kN) as presented in Table 7-2.

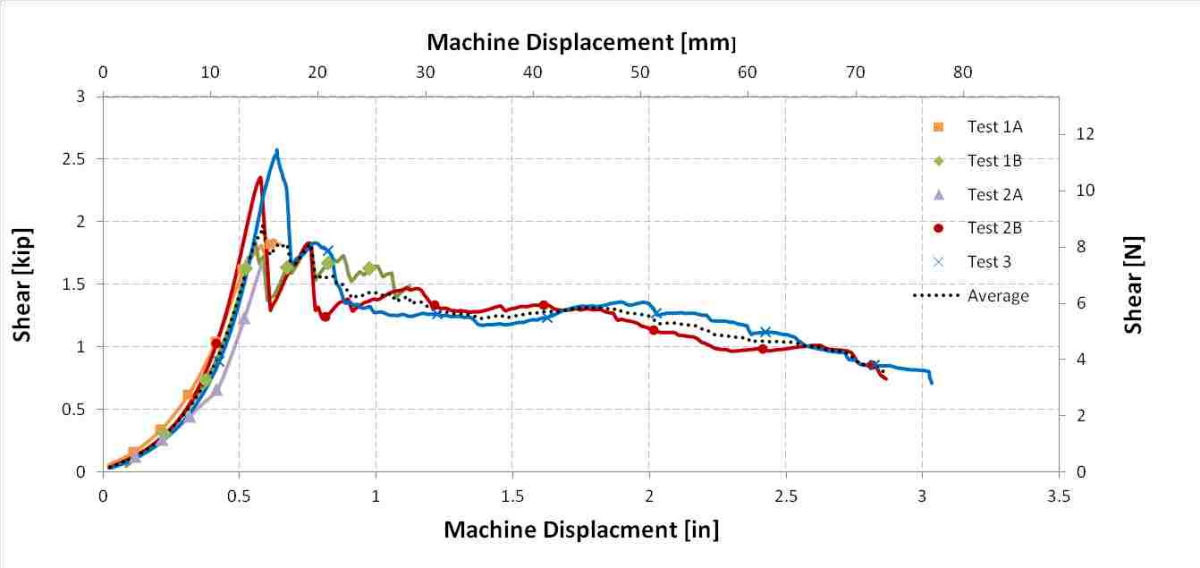

Figure 7-2: Shear vs. Machine Displacement Plots for all Tests

Table 7-2: Shear Results for All Tests

Test	Bending Test Method	Max Shear		Deflection at Max Shear	
		[kip	(kN)]	[in	(mm)]
1A	4-Point	1.86	8.3	0.622	15.8
1B	4-Point	1.85	8.2	0.556	14.1
2A	3-Point	1.68	7.5	0.582	14.8
2B	3-Point	2.35	10.5	0.578	14.7
3	3-Point	2.55	11.3	0.638	16.2
	Average	2.06	9.15	0.595	15.1
	Std. Dev.	0.374	1.66	0.0338	0.857
	[%]	18.2		5.67	

Table 7-3, which is a summary of the failure loads for the IsoBeams tested to failure, also shows an increase in maximum load from Specimen 1 to 3. The maximum load increase for each IsoBeam specimen test shows a steady improvement in manufacturing quality. Table 7-4 displays the results of Test 2B and 3 since these two tests were the most carefully controlled

tests. These averages are most representative of the actual capacity of the IsoBeam specimens in this research.

Table 7-3: Summary of IsoBeam Specimen Tested to Failure

Test	Deflection at Max		Max Moment		Max Shear		Max Load	
	[in	(mm)]	[kip-in	(kN-m)]	[kip	(kN)]	[kip	(kN)]
1B	0.556	14.1	11.1	1.25	1.85	8.21	3.69	16.4
2B	0.578	14.7	28.2	3.19	2.35	10.5	4.71	20.9
3	0.638	16.2	30.6	3.46	2.55	11.3	5.10	22.7
Average	0.591	15.0	23.3	2.63	2.25	10.01	4.50	20.0
Std. Dev.	0.0424	1.08	10.66	1.20	0.363	1.62	0.726	3.23
[%]	7.19		45.7		16.1		16.1	

Table 7-4: Summary of Test 2B and 3 IsoBeam Specimen Results

Test	Deflection at Max		Max Moment		Max Shear		Max Load	
	[in	(mm)]	[kip-in	(kN-m)]	[kip	(kN)]	[kip	(kN)]
2B	0.578	14.7	14.1	1.60	2.35	10.5	4.71	20.9
3	0.638	16.2	15.3	1.73	2.55	11.3	5.10	22.7
Average	0.608	15.4	14.7	1.66	2.45	10.90	4.90	21.8
Std. Dev.	0.0424	1.08	0.83	0.09	0.138	0.61	0.275	1.23
[%]	6.98		5.6		5.6		5.6	

7.2 **Development of Valid Test Methods**

The first specimen was tested in four-point bending as noted previously. The base plates were located on the outer most nodes, allowing them to rotate, inducing local bending moments into the individual members and leading to early failure. For this reason, the last two specimens were tested in three-point bending which provided an unloaded bay on either side of the base

plates. These tests produced more desirable/expect results. String potentiometers were also used to measure the bottom deflection of the beam for Specimens 2 and 3.

As previously discussed, there were two phases in the tests for both Specimens 1 and 2. During the initial phase of each of these tests, as the load increased, undesired secondary loads were induced in the members. During the test of Specimen 1, the base plates at each end rotated as they started to slip out from under the specimen. This occurred because the base plates were positioned at the end of the specimen with no bay on the other side to restrict these large rotations. As the plates rotated, they came in contact with other members, causing the members at the bottom of the two end bays to break prematurely. It was concluded that at least one bay should be placed on each side of the base plates or the last bays reinforced to restrict this rotation.

Specimen 2 shifted during initial testing due to unconstrained lateral translation enabled by the rollers. The top base plate rotated into the members inducing secondary loads similar to those in the first specimen. The test was halted, however, before substantial damage occurred unlike the first specimen test. This is evident since Test 2B reached a higher load than Test 2A whereas Test 1B failed before reaching the peak load of Test 1A. The entire test data, including data from tests which were ended early, is plotted to show the similar load-displacement behavior in each case, shown previously in Figure 7-1 and Figure 7-2.

The string potentiometers accurately measured the deflection of the bottom of the beam, but since there was no significant bending in the beam, the bottom center deflection was small. Conversely, the top center deflection of the beam was considerable due to load damage in the diagonal members. Based on these observations, it is recommended that both the bottom center

and top center deflection be measured for more accurate analysis of the behavior of the IsoBeam under shear and bending loads.

7.3 IsoBeam Characteristics

This section describes the structural performance characteristics exhibited by the IsoBeam specimens during testing. The strength of the IsoBeam is examined as well as the ductility and deflection.

7.3.1 Strength

Test 3 was the most carefully controlled test and yielded the highest capacity at 5.10 kips (22.7 kN). Test 2B had a similar strength of 4.71kips (20.9 kN) with an average between Test 2B and 3, the most carefully controlled tests, of 4.90 kips (21.8 kN). The lower strength of Test 1B of 3.69 kips (16.4 kN) is attributed to the significant damage caused during Test 1A. Similarly, the slight damage obtained during Test 2A may be the cause of the slightly lower strength of Test 2B. Figure 7-3 shows Test 3 after the load decreased to 25% of the peak load.

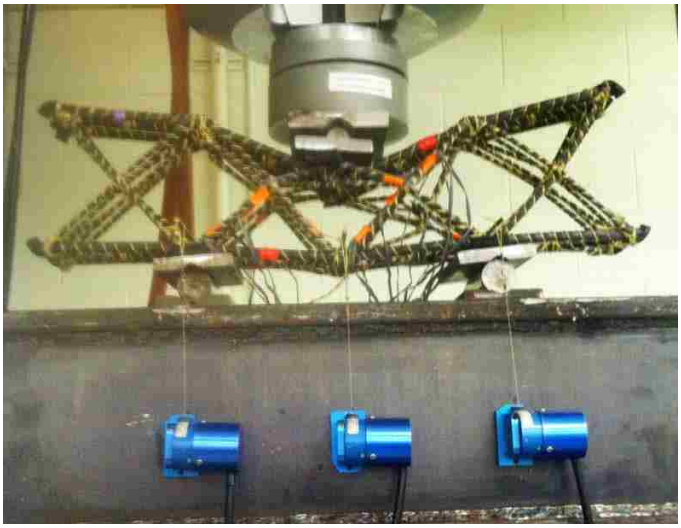

Figure 7-3: IsoBeam Specimen at 25% of Peak Loading

Figure 7-4 is a bar graph comparing all the maximum load results for the IsoBeam specimens. It is apparent from the figure that Tests 2A, 1A and 1B produced similar results while Tests 2B and 3 produced higher results. Since Tests 2B and 3 were the most carefully controlled tests, they more closely represent the expected strengths for IsoBeam specimens in this research.

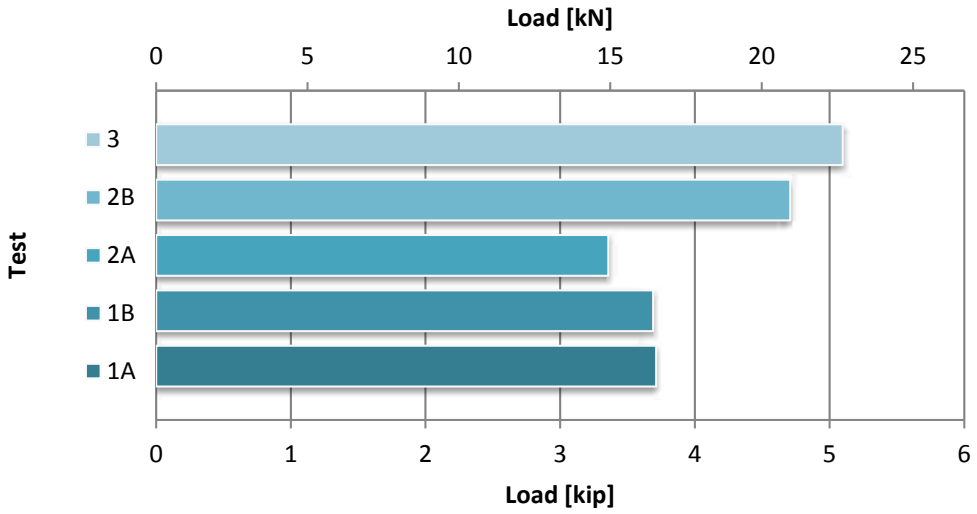

Figure 7-4: Bar Graph of Maximum Load for IsoBeam Specimens

The strength of the IsoBeam specimens, including Tests 2B and 3, is less than the desired strength. This is attributed to the inadequate manufacturing quality, as discussed in the subsequent section (7.4).

7.3.2 Ductility

A noticeable trait is the ability of the specimens to continue to support load after damage. This ductility is mostly observed for Test 2B and Test 3. Test 1B was ended before this behavior was recorded. After reaching a peak load and sustaining damage, both specimens exhibited a pattern of a large decrease in load followed by a subsequent increase until around

50% of the maximum strength where the load leveled off and then, slowly decreased. The tests were stopped and the specimens unloaded when this residual strength dropped to about 25% of the peak load. This was done since no catastrophic failure was expected, but rather a continuation of the gradual load decline. The specimens were able to absorb a lot of energy and after unloading, returned to a nearly un-deformed state (Figure 7-5). The energy absorbed during each test is quantified by the toughness presented in Table 7-1.

Figure 7-5: IsoBeam Specimen 3 After Unloading

The observed ductility and toughness are favorable characteristics of the IsoBeam, demonstrating the beam's ability to continue to sustain load after maximum capacity and not catastrophically fail. This trait is sought after in many applications, particularly in aerospace applications.

7.3.3 Deflection

The bottom center deflection of the IsoBeam was measured using string potentiometers as previously discussed. The load was expected to transfer throughout the beam with a uniform deflection across each plane of the beam (i.e., top plane vs. bottom plane). Contrary to this, the members rotated at the center nodes creating a larger deflection in the top half of the beam than in the bottom half of the beam. The top center deflection was calculated as previously discussed to compare the bottom and top center deflection.

The bottom center deflection was smaller than the top center deflection for all tests measured (Test 2A, 2B and 3). This also shows that the bottom center section of the beam was taking a smaller portion of the load. This is further discussed below while comparing the strain of the individual beam members.

Crushing of the diagonal members exhibited in these tests also indicates that the test was dominated by shear in the members between the load path and the base plates. This effect would be reduced by adding more bays between the points of loading and the base plates. Additional bays would also allow the beam to exhibit more of a moment-dominated behavior with a more typical beam deflection response.

7.4 Manufacturing Quality

The strength of the IsoBeam as manufactured is considerably below the expected value. This low strength is attributed to the hand-manufacturing process employed to create a complex, non-windable structure with large diameter members. The required constant tension to ensure that the members are straight during fabrication and subsequent consolidation of the assembled members was not adequately applied due to the complex geometry. Removing, sanding and examining members under a microscope shows large voids that greatly decrease the individual

member strength, as well as the overall strength of the IsoBeam structure. The following sub-section summarizes the impact of manufacturing quality on individual members' properties and compares the results to past research results on similar members.

7.4.1 Member Compression Properties

LONGITUDINAL VS. DIAGONAL MEMBERS

The longitudinal members contained 92 tows while the diagonal members contained 21 tows. The nominal factor of area is 4 times larger for the longitudinals, but the actual factor for the individual members measured is 4.45 times larger area for the longitudinals. This is due to the larger void content of the longitudinal members. The diagonal members had higher average compression strength and elongation to failure than the longitudinal members, while the longitudinal members had a higher average modulus of elasticity.

The longitudinal members exhibited a standard deviation of 4.09% for compression strength and 15.0% for maximum strain. The standard deviation for the compression strain is larger than the 8-10% variance expected in composites, and the compression stress variance is lower. The diagonal members had a much larger standard deviation for the compression strength and maximum strain of 24.3% and 37.9%, respectively. The diagonals also had a larger range of disparity in void percentage which may have resulted in the wider variation in compression strengths of the members discussed in the following sub-section (7.4.2).

The longitudinal and diagonal members exhibited an average compression modulus of 20.8×10^6 psi (143 GPa) and 14.8×10^6 psi (102 GPa), respectively. A bar graph of the average compression modules by member type for each specimen in Table 7-5 displays the higher

modulus for the longitudinal members. The diagonal members from Specimen 2 have a similar compression modulus as the longitudinal members.

Table 7-5: Bar Graph of Average Member Compression Young's Modulus for Each Specimen

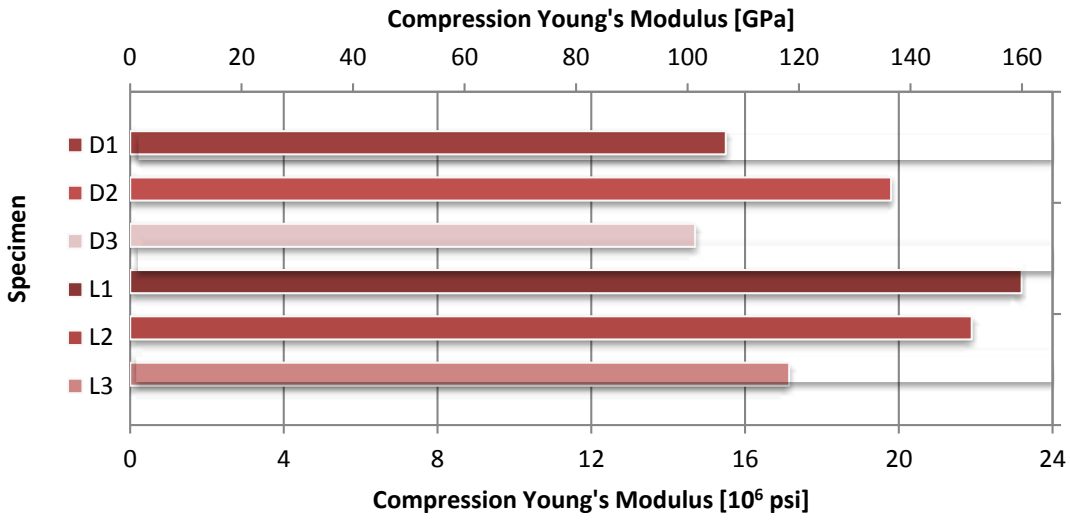

Additionally, the longitudinal and diagonal members exhibited an average strain at ultimate compression stress of 3.39×10^3 με and 7.23×10^3 με, respectively. Table 7-6 displays the much higher strain at ultimate compression stress and Table 7-7 the higher ultimate compression stress for the diagonal members. Since all members were made from the same material, the results of these two properties should be similar. Furthermore, the great percentage of voids in the longitudinal members should results in the longitudinal members having a lower modulus of elasticity than the diagonal members.

Table 7-6: Bar Graph of Average Member Strain at Ultimate Compression Stress for Each Specimen

Table 7-7: Bar Graph of Average Member Ultimate Compression Stress for Each Specimen

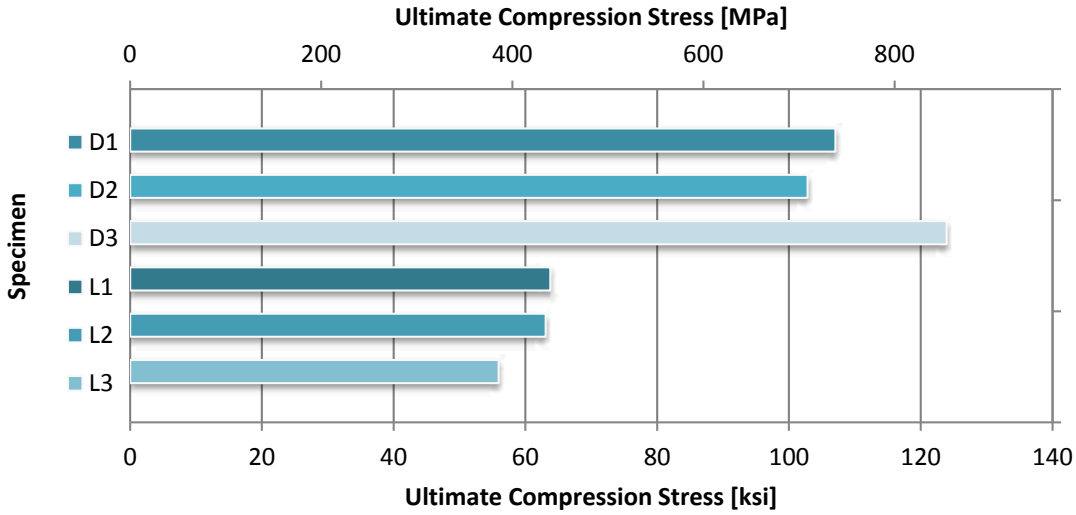

SPECIMEN MEMBER PROPERTIES

Specimens 1 and 2 members have similar averages for compression strength and maximum strain of the members, but the Specimen 3 members have a considerably higher

compression strength and maximum strain as seen in Table 7-8. The increase in properties for Specimen 3 members suggests that the manufacturing quality was higher for this specimen.

Table 7-8: Summary of Compression Properties of Members by Beam Specimen

Specimen		Compression Young's Modulus		Strain at Ultimate Compression Stress	Ultimate Compression Stress	
		[10^6 psi	(GPa)]	[με]	[ksi	(MPa)]
1	L	23.2	160	3475	63.8	440
	D	15.5	107	6625	107	738
	Average	19.4	133	5050	85.4	589
2	L	21.9	151	3325	63.1	435
	D	19.8	137	6863	103	709
	Average	20.9	144	5094	83.0	572
3	L	17.2	118	3375	55.9	386
	D	14.7	101	8200	124	854
	Average	15.9	110	5788	89.9	620
Average		18.7	129	5310	86.1	593.7
Std. Dev.		3.47	23.95	2170	28.6	197.15
[%]		18.6		40.9	33.2	

One of the members from each beam exhibited higher strength, meaning the overall quality of the beams is insufficient because of the variable quality between individual members that results in the lower overall beam strength. Once an individual member breaks, the IsoBeam is able to continue to take load by distributing the load to other members in the highly redundant system, but an inadequate member results in the other members taking a higher load and produces a lower overall performance of the IsoBeam.

7.4.2 Voids

The lower strength of the longitudinal members compared to the diagonal members is mostly due to the higher void percentage in the longitudinals. The member area, void area and percentages are summarized in Table 7-9 and Table 7-10. The average void percentage is 6.4% for longitudinal members, whereas the average is only 4.3% for diagonal members. The longitudinal members are two times as large in diameter and contain more than three times the number of tows than the diagonal members. Thus, longitudinal members require higher and more consistent force to consolidate. On the other hand, the complex geometry of the IsoBeam complicates the manufacturing of the inner diagonal members while the longitudinal members are relatively unaffected.

The diagonal member removed from IsoBeam 3 had the lowest void percentage at 0.92%. Of the members examined for voids, the diagonal member from IsoBeam 3 had the highest maximum strain of $8.8x10^3$ με, as well as the second highest compression strength of 135 ksi (931 MPa). The trend of low voids and high compression strength/strain is similar for the diagonal member from IsoBeam 1. Conversely, the member removed from Specimen 3 had the lowest fiber volume fraction.

Table 7-9: Area and Void Content Results for the Diagonal Members

Specimen		Area [10^3 in^2 (mm^2)]		Void Area [10^3 in^2 (mm^2)]		%
1	Top	27.3	17.6	0.84	0.54	3.1
	Bottom	24.3	15.7	1.9	1.2	7.8
2	Top	23.8	15.4	1.4	0.91	5.9
	Bottom	24.4	15.7	1.8	1.1	7.2
3	Top	23.3	15.0	0.21	0.14	0.92
	Bottom	23.5	15.2	0.22	0.14	0.92
	Average	24.4	15.8	1.1	0.68	4.3
	Std. Dev.	1.48	0.958	0.75	0.48	3.1
	[%]	6.07		71		72

Table 7-10: Area and Void Content Results for the Longitudinal Members

Specimen		Area [10^3 in^2 (mm^2)]		Void Area [10^3 in^2 (mm^2)]		%
1	Top	126	81.1	11	7.1	8.7
	Bottom	115	74.2	4.3	2.8	3.8
2	Top	114	73.7	7.4	4.8	6.5
	Bottom	112	72.0	7.9	5.1	7.1
3	Top	118	76.2	9.8	6.3	8.3
	Bottom	114	73.6	4.4	2.9	3.9
	Average	116	75.1	7.5	4.8	6.4
	Std. Dev.	4.99	3.22	2.7	1.7	2.1
	[%]	4.28		36		33

7.4.3 Fiber Volume Fraction

The average fiber volume fraction for all members was 38% as seen in Appendix C.3. The standard deviation of the fiber volume fraction percentage is only 10.5%, which is on the high end for composites. The fiber volume as calculated using the fiber diameter and number of tows is compared to the average measured values in Table 7-11.

Table 7-11: Calculated and Measured Fiber Volume Fraction

Member Type	Calculated Fiber Volume Fraction [%]	Measured Fiber Volume Fraction [%]	Difference [%]
Longitudinal	54.5	40.3	14.2
Diagonal	49.4	35.4	14.0

In both cases, 14% of the fibers are uncounted for. The disparity between the calculated values and the measure can be attributed to several factors. During fabrication, the tows frayed which resulted in fewer fibers in each tow and subsequently the member. Fraying increased as the material aged which is consistent with the decreasing fiber volume content from Specimen 1

to Specimen 3. Also, the voids in the member may produce stress concentrations that allow fiber to break off. This would result in the appearance of voids in the fiber where there is actually just a broken fiber. Lastly, due to limited focal length, the microscope may not be able to pick up all of the fibers if they aren't on the same plane. This is evident in the fiber content photographs where only half of a fiber is seen in the picture and analysis software. Since it is unable to detect half of several fibers, there is the possibility that the microscope is also not detecting full fibers.

The low fiber volume fraction results in an overall lower strength, but the fiber volume fraction of each member doesn't have high enough variation to cause a variation in strength properties. This is seen for the diagonal member from Test 3, which has the lowest fiber volume fraction but some of the highest compression strength and maximum strain values. The trend that the fiber volume fraction does not correlate with the overall strength of the member is observed for all members tested.

While voids and a low fiber volume fraction lower the strength of members that fail in compression, these properties may actually increase the local moment of inertia in the members which is favorable in buckling situations. The members in this research were designed and expected to fail in compression, thus high voids and low fiber volume fractions were unfavorable.

7.4.4 Past Research Comparison

Sika also tested carbon members wrapped with a half spiral sleeve of aramid in compression. His results produced an average compression strength and stiffness of 139 ksi (958 MPa) and 22.3 Msi (147 GPa), respectively [20, 21]. Sika's members had an average strain of 7,180 με. As noted in Table 5-1, the average strength of 86.9 ksi (599 MPa) and average strain of

5,310 με are considerably lower than the averages from Sika with only members D1-1, D2-2 and D3-1 producing strength results in the range of the members that Sika tested.

This lower strength is attributed to inadequate tension and consolidation, resulting in high void percentages. Also, another contributing factor is that the material donated for this research was out of specification with a low resin content while the material Sika used was within specification and had an overall better quality. Lastly, Sika created simple, unidirectional members on a braiding machine under proper tension rather than creating them by hand on a complex geometry, as in the current research.

7.5 Average Member Strain in IsoBeam

The average strain by member type for each test is presented below to allow discussion of the strength of each member type and load distribution.

7.5.1 Test 1 Averages

The average results for Test 1A strain gages are summarized in Table 7-12 and presented in the beam load verse strain plot shown in Figure 7-6. The average results for Test 1B strain gages are summarized in Table 7-13 and presented in the beam load verse strain plot shown in Figure 7-7.

Table 7-12: Summary Table for Average Test 1A Strain Gages

Member Type	Maximum Strain at Gage/Beam Failure			Beam Load at Gage/Beam Failure			
	[με]	Std. Dev.	[%]	[lbs	(kN)]	Std. Dev.	[%]
Outer Bay Inner Diagonals	2,600	602	23.2	3,541	16	394	11.1
Middle Bay Inner Diagonals	467	125	26.7	3,586	16	124	3.45
Outer Diagonals	388	411	106	3,661	16	107	2.91
Longitudinals	628	227	36.1	3,657	16	110	3.01
Average	1,021	341	48.0	3,611	16.2	184	5.1
Std. Dev.	1,058	211	39.0	58.2	0.261	140	4.0
[%]	104	61.8	81.3	1.6		76.4	78.1

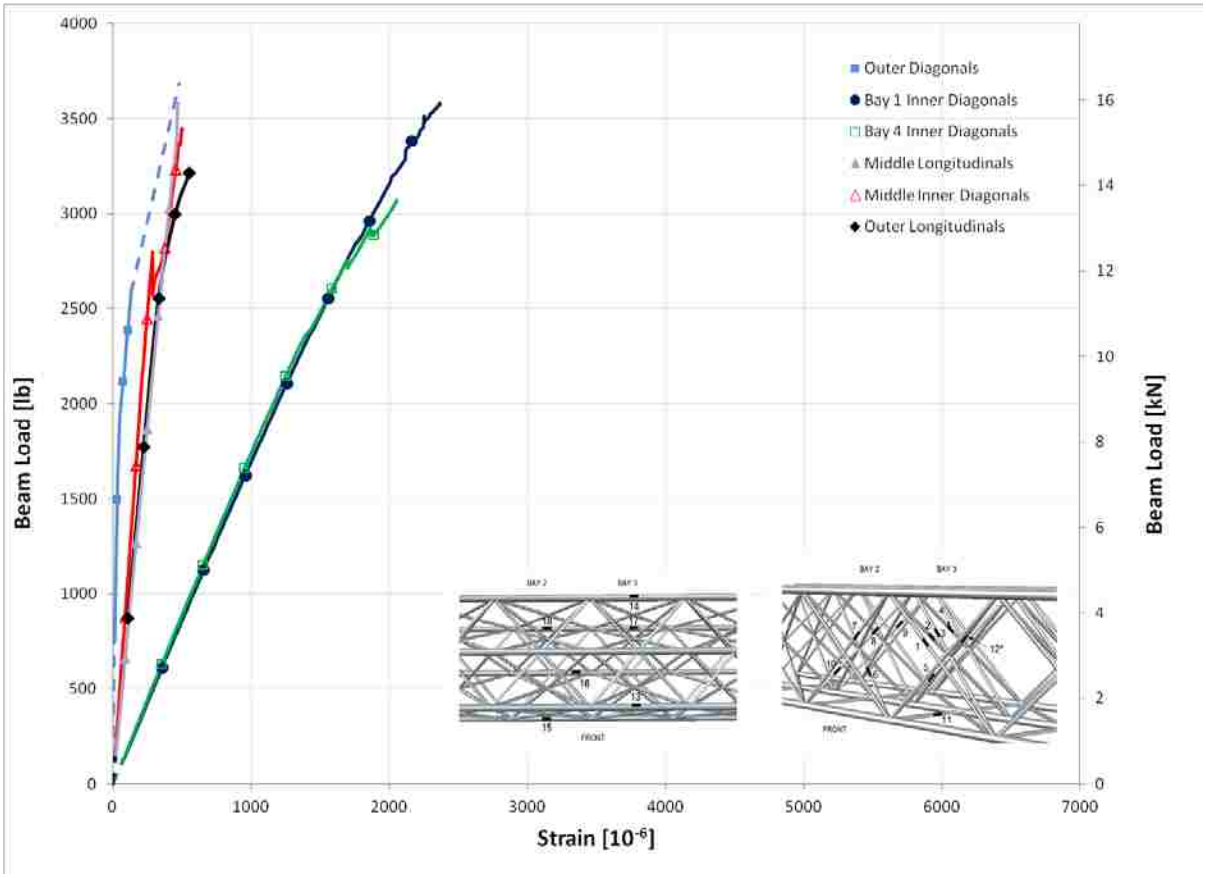

Figure 7-6: Average Load vs. Strain Plot for Test 1A Members

Table 7-13: Summary Table for Average Test 1B Strain Gages

Member Type	Maximum Strain at Gage/Beam Failure			Beam Load at Gage/Beam Failure			
	[με]	Std. Dev.	[%]	[lbs	(kN)]	Std. Dev.	[%]
Outer Bay Inner Diagonals	1,998	723	36.2	3,777	16.9	22.8	0.60
Middle Bay Inner Diagonals	418	205	49.2	3,785	17.0	10.3	0.273
Outer Diagonals	429	265	61.7	3,781	16.9	50.0	1.32
Longitudinals	612	339	55.4	3,724	16.7	115	3.10
Average	864	383	50.6	3,767	16.9	49.7	1.32
Std. Dev.	761	233	10.9	28.6	0.128	46.9	1.26
[%]	88.1	60.9	21.6	0.759		94.5	95.3

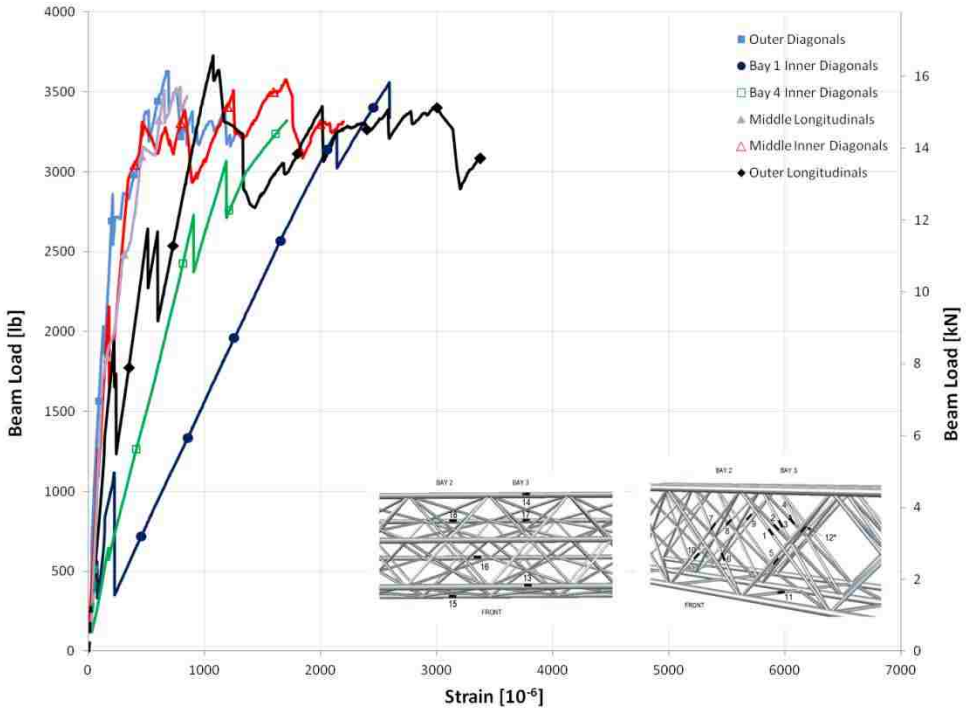

Figure 7-7: Average Load vs. Strain Plot for Test 1B Members

7.5.2 Test 2 Averages

The average results for Test 2A strain gages are summarized in Table 7-14 and presented in the beam load verse strain plot shown in Figure 7-8. The average results for Test 2B strain gages are summarized in Table 7-15 and presented in the beam load verse strain shown in Figure 7-9.

Table 7-14: Summary Table for Average Test 2A Strain Gages

Member Type	Maximum Strain at Gage/Beam Failure			Beam Load at Gage/Beam Failure			
	[με]	Std. Dev.	[%]	[lbs	(kN)]	Std. Dev.	[%]
Bay 2 Inner Diagonals	481	292	60.7	3,358	15.1	6.96	0.207
Bay 3 Inner Diagonals	1,727	942	54.6	3,358	15.1	5.48	0.163
Outer Diagonals	357	209	58.7	2,803	12.6	813	29.0
Longitudinals	664	477	71.8	3,357	15.0	14.1	0.421
Average	807	480	61.4	3,219	14.4	210	7.45
Std. Dev.	626	328	7.35	277	1.24	402	14.4
[%]	77.6	68.3	12.0	8.61		192	193

Table 7-15: Summary Table for Average Test 2B Strain Gages

Member Type	Maximum Strain at Gage/Beam Failure			Beam Load at Gage/Beam Failure			
	[με]	Std. Dev.	[%]	[lbs	(kN)]	Std. Dev.	[%]
Bay 2 Inner Diagonals	1,069	1,514	142	3,746	16.8	745	19.9
Bay 3 Inner Diagonals	1,789	1,363	76.2	4,742	21.3	22.8	0.480
Outer Diagonals	549	446	81.3	4,700	21.1	46.3	0.985
Longitudinals	644	328	51.0	4,610	20.7	212	4.59
Average	1,013	913	87.5	4,450	19.9	256	6.49
Std. Dev.	565	612	38.4	473	2.12	336	9.12
[%]	55.8	67.0	43.9	10.6		131	141

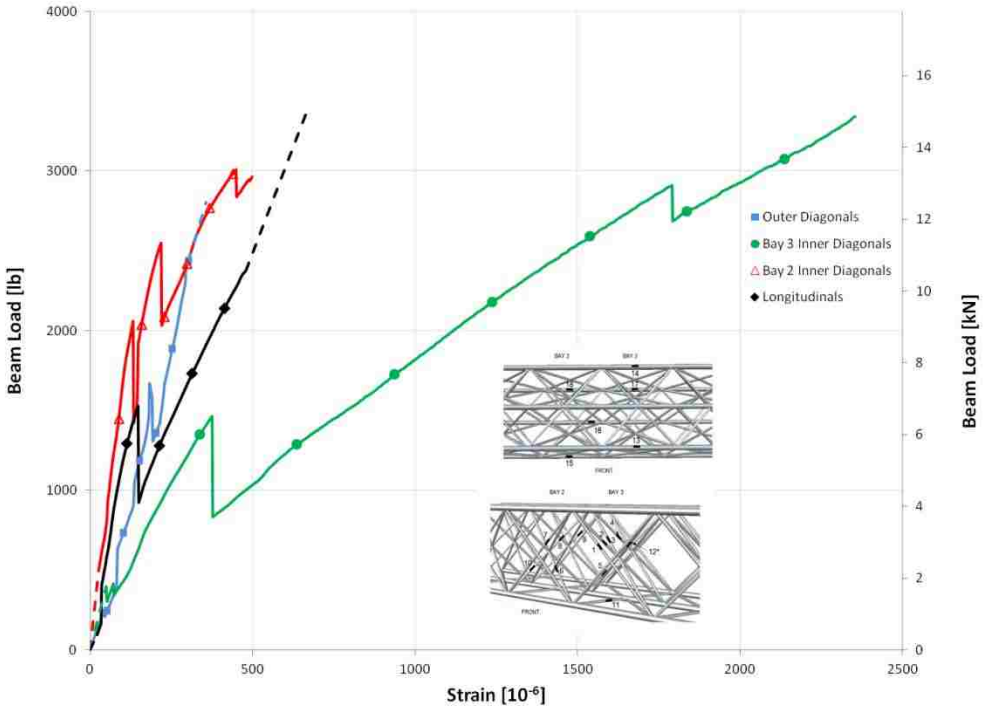

Figure 7-8: Average Load vs. Strain Plot for Test 2A Members

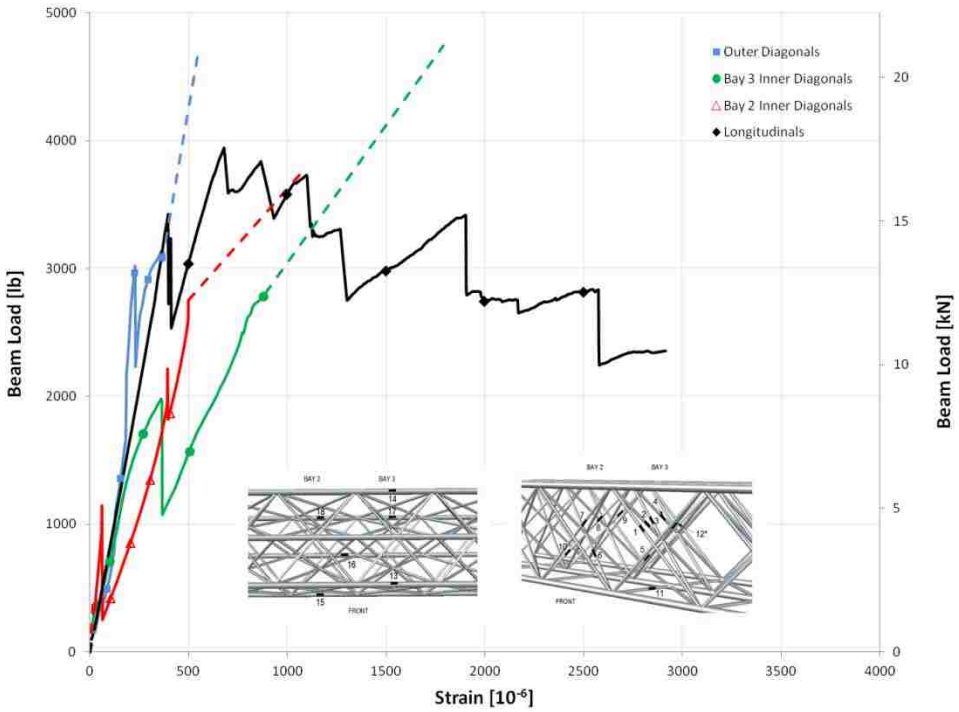

Figure 7-9: Average Load vs. Strain Plot for Test 2B Members

7.5.3 Test 3 Averages

The average results for Test 3 strain gages are summarized in Table 7-16 and presented in the beam load verse strain shown in Figure 7-10.

Table 7-16: Summary Table for Average Test 3 Strain Gages

Member Type	Maximum Strain at Gage/Beam Failure			Beam Load at Gage/Beam Failure			
	[με]	Std. Dev.	[%]	[lbs	(kN)]	Std. Dev.	[%]
Bay 2 Inner Diagonals	2,307	1,273	55.2	4,616	20.7	467	10.1
Bay 3 Inner Diagonals	2,839	2,189	77.1	4,892	21.9	212	4.32
Outer Diagonals	332	371	112	4,921	22.1	126	2.57
Longitudinals	630	302	48.0	4,525	20.3	802	17.7
Average	1,527	1,034	73.0	4,738	21.2	402	8.68
Std. Dev.	1,233	888	28.6	198	0.888	304	6.84
[%]	80.8	85.9	39.2	4.18		75.6	78.7

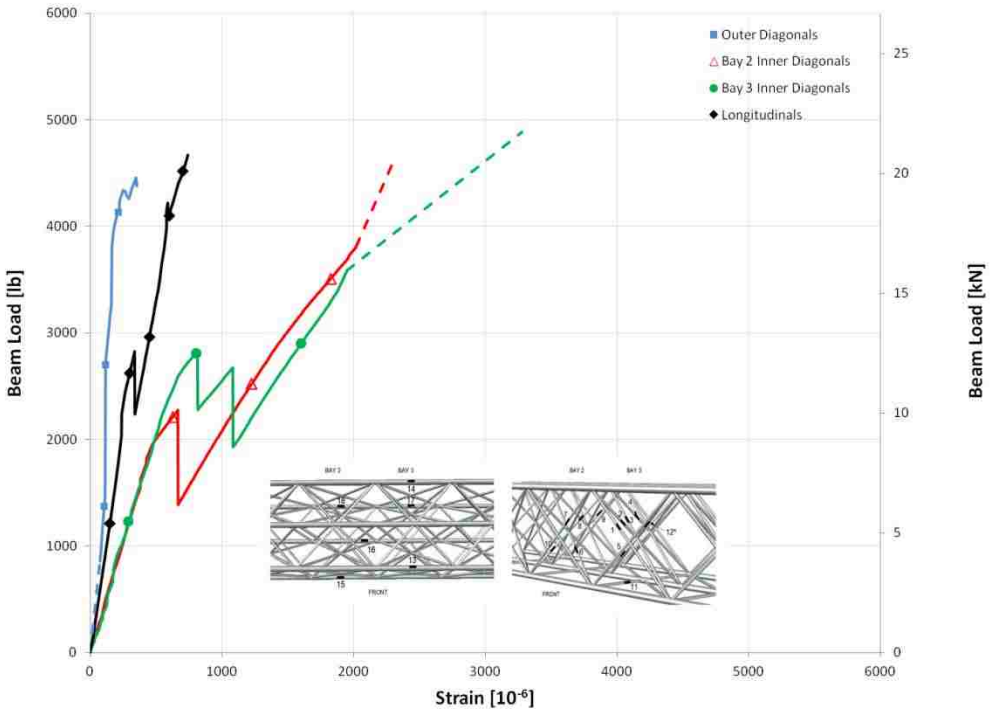

Figure 7-10: Average Load vs. Strain Plot for Test 3 Members

7.5.4 Overall Test Averages

The average maximum strain for the members at failure gage/beam load of Tests 1B, 2B and 3 are compared in Table 7-17. Table 7-18 contains the average maximum strain for the members at failure gage/beam load for only Tests 2B and 3 since these tests are the tests that most represent the capacity of the IsoBeam specimens in this research.

Table 7-17: Average Strain for IsoBeam Specimens Loaded to Failure of Gage/Beam

Test	1B		2B		3		AVG
	[με]	Std. Dev.	[με]	Std. Dev.	[με]	Std. Dev.	[με]
End Bay/Bay 2 Inner Diagonals	1,998	723	1,069	1,514	2307	1273	1,791
Center/Bay 3 Inner Diagonals	418	205	1,789	1,363	2839	2189	1,682
Outer Diagonals	429	265	549	446	332	371	436
Longitudinals	612	339	644	328	630	302	628
Average	864	383	1,013	913	1,527	1034	1,134
Std. Dev.	761	233	565	612	1,233	888	853
[%]	88	60.9	55.8	67.0	80.8	85.9	74.9

Table 7-18: Average Strain for IsoBeam Tests 2B and 3 at Gage/Beam Failure

Test	2B		3		AVG
	[με]	Std. Dev.	[με]	Std. Dev.	[με]
Bay 2 Inner Diagonals	1,069	1,514	2307	1273	1,688
Bay 3 Inner Diagonals	1,789	1,363	2839	2189	2,314
Outer Diagonals	549	446	332	371	440
Longitudinals	644	328	630	302	637
Average	1,013	913	1,527	1034	1,270
Std. Dev.	565	612	1,233	888	899
[%]	55.8	67.0	80.8	85.9	68

7.6 **Load Distribution between Members**

The inner diagonal members experience higher strain than any other type of member. This is consistent in all of the tests except 2A. This shows that a majority of the load is transferred through the beam as compression axial load in the inner diagonal members.

In both Test 1A and 1B (four-point bending), the inner diagonal members in the center bays do not exhibit the same trend as the inner diagonal members in the end bays. The center bay inner diagonal members experienced lower strains similar to the outer diagonal members. The original goal of the bending test was to apply a pure bending moment to the center of the beam, but the lower strain in the inner diagonal members in the center shows that the beams were dominated by shear, since the IsoBeams was too short to be dominated by bending.

In Test 2A, the inner diagonal members in Bay 2 exhibited lower strain than the Bay 3 inner diagonal members. These members also exhibited lower strains than the longitudinal and outer diagonal members, which is contrary to the other tests. This implies that the load was asymmetrically applied but corrected when the beam was unloaded and reloaded for Test 2B, since Test 2B exhibited more typical strains for all inner diagonal members.

For Tests 2A, 2B and 3, the inner diagonal members have large standards of deviation due to several members exhibiting low strain values. The strain gages with lower strains were 5, 6 and 12. Strain gage 12, only present during Test 3, was located on an outer bay. Thus, the member was not in the direct load path and would be expected to have a lower strain. Strain gage 5 and 6 were located in the center bay in the lower half of the beam. The low strain values and low bottom center deflection clearly shows that the load was not fully transferred to these members in bending as intended, another indication of shear dominated behavior. Strain gage 10,

located on a lower inner diagonal directly above the base plat, has a large strain in both Tests 2B and 3 which shows that the load transferred to the other side of the bay and into the base plates.

The longitudinal members in Test 1B and 2B continue to take more strain at lower loads even after failure. Even as the longitudinal members break, they continue to sustain load unlike the diagonal members. As the other member fail, the longitudinal members exhibit higher strain and thus, take a larger portion of the load. Test 3 doesn't exhibit this behavior, most likely due to strain gage failure rather than longitudinal member failure.

7.7 **Finite Element Analysis Comparison**

As previously stated, the maximum load of the finite element analysis was 34 kips (151 kN). This suggests that the experimental results, which reached a maximum of 5.1 kips (22.7 kN), only reached about 15% of the actual capacity of the IsoBeam. The finite element model included only a linear geometric analysis. A buckling analysis was not performed. Thus, the actual maximum load for the IsoBeam is expect to be slightly lower but still substantially larger than the 5.1 kips (22.7 kN) exhibited in the experiments.

To estimate the actual failure load of the IsoBeam, if buckling was accounted for, the load required for the outer diagonals to buckle was calculated and compared to the axial load in the outer diagonal members at the predicted failure for the IsoBeam. A ratio of the buckling load and the axial load of the outer diagonal members was multiplied by the ultimate IsoBeam failure load to scale the failure load to the load when the outer diagonal members are expected to buckle and cause the IsoBeam to fail. The results for several effective column length factors, K are presented in Table 7-19. A K-value of 1 represents a pinned-pinned connection at the joint while a K-value of 4 represents a fully fixed connection. Since the buckling load for a fixed-fixed joint

results in a higher load than the axial load in the analytical member, compression failure will occur prior to buckling so the IsoBeam failure load is taken as the initial 34 kips (151 kN).

Table 7-19: IsoBeam Finite Element Analysis Failure Load Adjusted for Buckling of Members

Effective Column Length Factor, K	Outer Diagonal Axial Buckling Load		Ratio	IsoBeam Failure Load	
	[lbs	(kN)]		[kips	(kN)]
1	1201	5.34	0.28	9.59	42.7
2.5	3004	13.4	0.71	24.0	107
4	4806	21.4	1.13	34*	151

*Compression failure axial load is lower than buckling load and thus, governs failure.

Previous tests have shown that interwoven joints similar to these have a connection type somewhere between pinned and fixed so the table also displays the results for a K-value of 2.5. These calculations suggest that the failure load of a properly manufactured IsoBeam will be between 9.6-24 kips (42-107 kN) with a capacity expected to be around 24.0 kips (107 kN).

The maximum strain in the experiment is compared to the strain predicted by the analysis at the predicted ultimate beam load of 34 kips (151 kN) in Table 7-20. A ratio of 1:1 is desired to demonstrate that the experimental and analytical results are equivalent.

The strains of the inner diagonals match for strain gages 3 & 4 but the strain is higher for the rest of the finite element analysis inner diagonals member in the load path (strain gages 2 and 8-10). The lower strain in the experimental inner diagonals could be attributed to slightly unsymmetrical loading as well as the variable material quality which results in varying stiffnesses of the inner diagonals. Local bending in the experimental members also contributes to the disparity between experimental and analytical strains. Strain gages were only place on one side of the member, and as the member locally bends, the strain reading varies between the top

and bottom plane of bending. Thus, depending on which side of the member the strain gage was placed on, the experimental strain reading may be slightly different.

Table 7-20: Measured and Predicted Strain at Predicted Ultimate Beam Load Comparison

Strain Gage	Member Type	Experimental Strain [με]	Analytical Strain [με]	Ratio	Difference
1	OD	738	-6,084	-0.12	6,822
2	ID	-1,948	-5,386	0.36	3,438
3	ID	-4,828	-5,779	0.84	951
4	ID	-5,526	-5,386	1.03	-140
5	ID	-812	-219	3.70	-593
6	ID	-664	-219	3.03	-445
7	OD	248	-6,084	-0.04	6,332
8	ID	-2,020	-5,779	0.35	3,759
9	ID	-2,938	-5,386	0.55	2,448
10	ID	-3,604	-5,661	0.64	2,057
11	OD	-10.70	128	-0.08	-138
12	ID	-1,080	-127	8.48	-953
15	L	236	1,843	0.13	-1,607
16	L	954	1,651	0.58	-697
17	L	740	1,843	0.40	-1,103
18	L	588	1,843	0.32	-1,255

The strains of the inner diagonals outside the load path are all small with the finite element analysis predicting even less strain in these members (strain gages 5, 6 and 12).

The strains of the longitudinal and horizontal outer diagonals are similarly small (strain gages 11 and 15-18). The finite element analysis predicted about twice as high strains for these members.

The predicted strains in the side outer diagonals (strain gages 7 and 11) do not match the experimental strains. The experiment yielded low strains on the vertical outer diagonals while the finite element analysis predicted higher strains for the vertical outer diagonals than the inner

diagonals. This is inconsistent with the validation discussed in Chapter 6. As previously discussed, the side outer diagonals did not buckle out of plane in the finite element model and a buckling analysis should be performed.

Table 7-21 compares the maximum strain in the experimental members to the strain predicted by the analysis at the maximum experimental beam load of 5.1 kips (22.7 kN). The experimental strains are seen to be much higher than the strain in the analytical members at the same load. This is expected since the experimental members failed earlier than the analytical model predicted because of the insufficient manufacturing quality. The only exception is the outer diagonals which are taking a larger percentage of the load in analytical model than in the experimental tests as previously discussed.

Table 7-21: Measured and Predicted Strain at Measured Ultimate Beam Load Comparison

Strain Gage	Member Type	Experimental Strain [με]	Scale Analytical Strain [με]	Ratio	Difference
1	OD	738	-912	-0.81	1,650
2	ID	-1,948	-807	2.41	-1,141
3	ID	-4,828	-866	5.57	-3,962
4	ID	-5,526	-807	6.84	-4,719
5	ID	-812	-33	24.68	-779
6	ID	-664	-33	20.18	-631
7	OD	248	-912	-0.27	1,160
8	ID	-2,020	-866	2.33	-1,154
9	ID	-2,938	-807	3.64	-2,131
10	ID	-3,604	-849	4.25	-2,755
11	OD	-10.70	19	-0.56	-30
12	ID	-1,080	-19	56.57	-1,061
15	L	236	276	0.85	-40
16	L	954	248	3.85	706
17	L	740	276	2.68	464
18	L	588	276	2.13	312

8 CONCLUSIONS AND RECOMMENDATIONS

This research included the manufacturing and testing of IsoBeam™ structures in shear-dominated short-beam bending. Individual members of the IsoBeam specimens were removed to examine the quality of the material and hand-manufacturing process. The experimental results were compared to predictions from a linear finite element analysis. This section summarizes the observations of this research and describes the conclusions to answer to the research questions. Further research suggestions are provided.

8.1 Observations

8.1.1 Valid Test Methods

1. Load cannot be applied to end bays without reinforcing.
2. The displacements of the top and bottom of the IsoBeam specimen are not equal during shear loading, due to deformation of the cross-section, and both should be measured.

8.1.2 IsoBeam Characteristics

1. Specimens in this research were too short to be dominated by bending and thus, failed in shear.

2. The average maximum strength of the IsoBeam structure was 4.11 kips (18.3 kN), yielding an equivalent shear of 2.06 kips (9.15 kN) and bending moment of 20.2 kip-in (2.29 kN-m).

8.1.3 Manufacturing Quality

1. Spiral sleeves without monitored tension do not provide adequate consolidation.
2. The diagonal members tested in compression had a higher strength of 111 ksi (767 MPa) than the longitudinal compression strength of 62.5 ksi (431 MPa).
3. The average void percentage for diagonal and longitudinal members was 4.3% and 6.4%, respectively.
4. Members from Specimen 3 tested in compression had a higher average strength than members from Specimens 1 and 2.
5. The average fiber volume fraction of all members was 38% with a standard deviation of 10.5%. This is a very low value for fiber volume fraction with a typical spread for composites suggesting overall low quality of material.
6. Similar specimens from past research had both a higher compression strength and maximum strain.

8.1.4 Load Distribution between Members

1. The inner diagonals take more load than the outer diagonals.
2. The longitudinal members do not catastrophically fail and continue to sustain load after damage.

8.1.5 Finite Element Analysis

1. A high-quality IsoBeam of this geometry is predicted to have a strength in the range of 9.6-34 kips (42-151 kN), without considering buckling. Buckling considerations will reduce the maximum predicted load to a value of 24 kips (107 kN).
2. Failure is expected to first occur in the vertical outer diagonals members.

8.2 Conclusions

1. The IsoBeam is a ductile system able to absorb a lot of energy during loading.
2. The IsoBeam is a fail-safe structure that will not fail catastrophically due to system redundancy. The IsoBeam can sustain substantial load after damage.
3. The quality of the hand-woven specimens in this research was not sufficient resulting in a lower overall strength in the IsoBeam than desired. This is attributed to the material quality, complex geometry, hand-manufacturing process and lack of adequate and continuous tension while laying tows and during consolidation.
4. A majority of the load under shear-dominated bending is transferred through the beam as an axial compression load in the inner diagonal member.

The characteristics exhibited by the IsoBeams are favorable characteristics in beams, especially in aerospace applications. The IsoBeam is a damage-tolerant system because of the many members which create redundant load paths. With proper manufacturing and consolidation, the IsoBeam should provide a strong, light-weight, ductile and fail-safe structure to be used in beam applications.

8.3 **Recommendations**

1. Manufacture and test longer IsoBeam specimens.
2. Shrink tape or other methods should be used for consolidation of IsoBeam members due to the complex geometry.
3. Construct a 3-dimentional braiding machine large enough to manufacture IsoBeam specimens.
4. Study an IsoBeam specimen without the Outer Diagonal members to investigate their role.
5. Create a finite element analysis that accounts for buckling of members of the IsoBeam structure.

REFERENCES

[1] Strong, A. B. and Jensen, D., (2002). "The Ultimate Composite Structure," *Composites Fabrication*, pp. 22–27, Aug. 2002.

[2] Jarvis, David, "Development of a Rectangular IsoTruss for Reinforced Concrete Beams," M.S. Thesis, Brigham Young University, Provo, Utah, August 2001.

[3] Kesler, S. (2006). "Consolidation and Interweaving of Composite Members by a Continuous Manufacturing Process," M.S. Thesis, Brigham Young University, Provo, Utah.

[4] Winkel, L. (2001). "Parametric Investigation of IsoTruss™ Geometry Using Linear Finite Element Analysis," M.S. Thesis, Brigham Young University, Provo, Utah.

[5] Scoresby, B. (2003). "Low Velocity Longitudinal and Radial Impact of IsoTruss™ Grid Structures," M.S. Thesis, Brigham Young University, Provo, Utah.

[6] McCune, A. (2001). "Tension and Compression of Carbon/Epoxy IsoTruss™ Grid Structures," M.S. Thesis, Brigham Young University, Provo, Utah.

[7] Su, J., Shenoi, R., Jiang, D., & Sobey, A. (2013). "Multi-parameter optimization of lightweight composite triangular truss structure based on response surface methodology." *Composite Structures*, 97, 107-116. Retrieved from Science Direct.

[8] Durai, D., Venkatesh, S., Varughese, B., Ramanaiah, B., and Dayananda, G., (2010). "Concepts for Truss Based Aerofoil Construction," presented at the ISAMPE National Conference on Composites.

[9] Morozov, E., & Lopatin, A. (2011). "Design and analysis of the composite lattice frame of a spacecraft solar array." *Composite Structures*, 93, 1640-1648.

[10] Ben, G., Suzuki, T., & Sakata, K. (2012). "Optimum Structural Design of CFRP Isogrid Cylindrical Shells," presented at the *15th European Conference on Composite Materials*, June 24-28, 2012.

[11] Totaro, G. (2012). "Local buckling modeling of isogrid and anisogrid lattice cylindrical shells with triangular cells." *Composite Structures*, 94(2), 446-452.

[12] Morozov, E., Lopatin, A., & Nesterov, V. (2011). "Buckling analysis and design of anisogrid composite lattice conical shells." *Composite Structures*, 93(12), 3150-3162.

[13] Frulloni, E., Kenny, J., Conti, P., & Torre, L. (2007). "Experimental study and finite element analysis of the elastic instability of composite lattice structures for aeronautic applications." *Composite Structures*, 78, 519-528.

[14] Morozov, E., Lopatin, A., & Nesterov, V. (2011). "Finite-element modeling and buckling analysis of anisogrid composite lattice cylindrical shells." *Composite Structures*, 93(2), 308-323.

[15] Haulin, F., & Wei, Y. (2006). "An Equivalent Continuum Method of Lattice Structures." *Acta Mechanica Solida Sinica*, 19(2), 103-113. Retrieved from Science Direct.

[16] Hansen, S. (2004). "Influence of Consolidation and Interweaving on Compression Behavior of IsoTruss® Structures," M.S. Thesis, Brigham Young University, Provo, Utah.

[17] Allen, D. (2011). "Damage Tolerance of Unidirectional Basalt Composites Encased in an Aramid Sleeve," M.S. Thesis, Brigham Young University, Provo, Utah.

[18] Wisnom, M. (1999). "Suppression of Splitting and Impact Sensitivity of Unidirectional Carbon-Fibre Composite Rods Using Tensioned Overwind," *Composites Part A: Applied Science and Manufacturing*, Vol. 30, No. 5, pp. 661-665.

[19] Embley, M. (2011). "Damage Tolerance of Buckling-Critical Unidirectional Carbon, Fiberglass, and Basalt Fiber Composites in Co-Cured Aramid Sleeves," M.S. Thesis, Brigham Young University, Provo, Utah.

[20] Sika, C. (2012). "Damage Tolerance of Unidirectional Carbon and Fiberglass Composites with Aramid Sleeves," M.S. Thesis, Department of Civil and Environmental Engineering, Brigham Young Univ., Provo, Utah, 2012.

[21] Jensen, D., Sika, S., Hinds, K. and Jensen, M., (2013). "Compression Strength After Impact of Unidirectional Carbon/Epoxy Rods Consolidated with Aramid Sleeves," presented at the *American Society of Composites- Twenty-Eighth Technical Conference*, Sept. 9-11, 2013.

[22] TCR Composites (2013). "UF3369 TCR™ Resin Technical Data Sheet," Revision 13. http://www.tcrcomposites.com/pdfs/resindata/uf3369_v11_912.pdf

[23] Agate (October 2002). "Toray T700GC-12K-31E/#2510 Unidirectional Tape [SI Units]," http://www.niar.wichita.edu/agate/

[24] Jensen, M., and Jensen, D., (2010). "Continuous Manufacturing of Cylindrical Composite Lattice Structures," presented at the International Conference on Textile Composites (TEXCOMP10), Oct. 26-28, 2010.

[25] Keller, Brandon S. (2002). "Tension, Torsion, and Flexure of an IsoTruss Structure with an Integral Cylindrical End," M.S. Thesis, Brigham Young University, Provo, Utah, April 2002.

[26] Jensen, C. and D. W. Jensen (2000). "Flexural Behavior of a Graphite/Epoxy IsoTruss," *CASC Report*, January 2000.

[27] Holman, J., & Gajda, W. (1989). "Analysis of Experimental Data." *In Experimental Methods for Engineers* (5d ed.). New York: McGraw-Hill.

[28] S. Peters, (2011). "Filament Winding— Introduction and Overview ." *Composite Filament Winding* (pp. 1-6). Materials Park, Ohio: ASM International.

[29] Branscomb, D., Beale, D., & Broughton, R. (2013). "New Directions in Braiding." *Journal of Engineered Fibers and Fabrics*, 8(2). Retrieved September 16, 2014, from http://jeffjournal.org/papers/Volume8/JEFF8-02-02.Branscomb.D.pdf

APPENDIX A. MANUFACTURING, MATERIAL AND STRAIN GAGE DATA

Table A-1 contains the manufacturing data for the carbon fiber/epoxy used in weaving all the specimens. The dates that the specimens were cured are listed on Table A-2. Table A-3 contains the batch data for all of the types of strain gages used for data acquisition.

Table A-1: Carbon Fiber/Epoxy Material Data

Part-Lot	3353418
Date of Manufacturing	5/29/2013
Date Removed from Freezer	11/11/2013
Resin	UF3369-100
Fiber	T700SC-12K-50C
Resin Content (%)	31.42
Net Weight [lb (kg)]	15.87 (7.2)
Comments	1ST RUN OF DAY. SHIFT, High RC%.

Table A-2: Date Specimens Cured

Specimen	Date Cured
1	1/20/2014
2	2/3/2014
3	2/14/2014

Table A-3: Strain Gage Batch Data

Strain Gage Type	Lot Number	Test Conditions	Resistance (OHMS)	Gage Factor	Transverse Sensitivity	Lead Wires
CEA-06-125UN-120	R-A58AD828	24° C	120.0 ± 0.3%	2.065 ± 0.5%	(+0.6 ± 0.2)%	-
EA-06-062AK-120	R-A56AD137	24° C	120.0 ± 0.15%	2.04 ± 0.5%	(+0.8 ± 0.2)%	-
FLA-2-11-3LT	A51541A	23° C at 50% RH	120.0 ± 0.5%	2.11 ± 1%	(+0.5 ± 0.2)%	10/0.12 3W 3m

APPENDIX B. MEMBER SIZES

Every member of each specimen was measured to compare consolidation quality of members. The cross-sections of the longitudinal members were measured vertically (v) as well as horizontally (h) due to their oval shape. The diagonal members were smaller and thus, closer to a circular member so only one dimension was measured on these members. The longitudinal members were measured in three places: the left, middle and right. Due to limited access to the middle longitudinal members, they were only measured horizontally and on the left and right of the node. These values were averaged and used to calculate the cross-sectional area of each member. Table B-1 and Table B-2 contain the average diameter and area measurements for the Outer and Middle Longitudinal members, respectively.

Table B-1: Outer Longitudinal Member Average Measurements

	Outer Longitudinal							
Specimen	**V Diameter**		**H Diameter**		**Total Diameter**		**Area**	
	[in.	**(mm)]**	**[in.**	**(mm)]**	**[in.**	**(mm)]**	**[in^2**	**(mm^2)]**
1	0.411	10.4	0.373	9.47	0.392	10.0	0.113	72.8
2	0.406	10.3	0.369	9.37	0.387	9.84	0.118	75.9
3	0.413	10.5	0.378	9.60	0.396	10.0	0.123	79.1
Average	0.410	10.42	0.373	9.48	0.392	9.95	0.118	75.9
Std. Dev.	0.00354	0.0900	0.00467	0.119	0.00405	0.103	0.0049	3.18
[%]	0.864		1.25		1.03		4.19	

Table B-2 : Middle Longitudinal Member Average Measurements

Specimen	Middle Longitudinal Diameter		Area	
	[in.	(mm)]	[in^2	(mm^2)]
1	0.367	9.32	0.106	68.3
2	0.376	9.55	0.111	71.7
3	0.375	9.53	0.111	71.4
Average	0.373	9.47	0.109	70.5
Std. Dev.	0.0050	0.127	0.0029	1.851
[%]	1.34		2.63	

The vertical outer diagonal members were measured in three places: the top, middle and bottom of each member. The horizontal outer diagonal members were measured in two locations: the front and the rear of each member. These values were averaged and used to calculate the cross-sectional area. Table B-3 contains the average Vertical and Horizontal, Outer Diagonal diameter and area measurements.

Table B-3: Outer Diagonal Members Average Measurements

Specimen	Vertical, Outer Diagonal Diameter		Area		Horizontal, Outer Diagonal Diameter		Area	
	[in.	(mm)]	[in^2	(mm^2)]	[in.	(mm)]	[in^2	(mm^2)]
1	0.212	5.39	0.0355	0.901	0.215	5.5	0.0365	23.6
2	0.210	5.34	0.0347	0.882	0.214	5.43	0.0359	23.1
3	0.217	5.52	0.0371	0.943	0.220	5.6	0.0379	24.5
Average	0.213	5.42	0.0358	0.908	0.216	5.49	0.0368	23.7
Std. Dev.	0.00362	0.0920	0.00123	0.0312	0.00308	0.0781	0.00105	0.68
[%]	1.700		3.44		1.42		2.86	

Due to limited access and generally consistent size, the inner diagonal members were only measured in the center of each member. These values were averaged and used to calculate the cross-sectional area. Table B-4 contains the average diameter and area measurements for the Inner Diagonal members.

Table B-4: Inner Diagonal Members Average Measurements

Specimen	Inner Diagonals			
	Diameter		Area	
	[in.	(mm)]	[in^2	(mm^2)]
1	0.199	5.06	0.030	19.6
2	0.199	5.05	0.031	19.9
3	0.195	4.95	0.030	19.3
Average	0.198	5.02	0.030	19.6
Std. Dev.	0.00224	0.0570	0.00047	0.305
[%]	1.14		1.56	

APPENDIX C. MEMBER MATERIAL PROPERTIES

As previously described, members were removed from the specimens and cut with a Leco CM-10 cutting jig. The ends of the members were sanded flat using a Leco Spectrum 2000 with a fixture designed to align the members perpendicular to the sander. The sanding schedule for members being analyzed for cross-sectional area and voids was 60, 120 and 800 grit paper. Each was applied until flat and smooth, making sure that no planes formed in between sanding. Additionally, the members analyzed for fiber volume fractions were sanded with 1200 and 1200-fine grit paper.

C.1 Cross-sectional Area Measurements

The cross-sectional areas were measured for each end of the members by drawing a polygon along the edge of the cross-section. This area can be viewed in Table C-1.

C.2 Void Content Measurements

A summary of the void analysis can be viewed in Table C-1. Following the summary, the pictures and void data for the top and bottom of each member analyzed with the Leco Olympus SZX12 microscope at 7X are included. The voids are averaged by member type and by beam specimen in Table C-2 and Table C-3, respectively.

Table C-4 shows the area and void areas of the center of the longitudinal members. The pictures of the voids in each member are displayed in Figure C-1-Figure C-6.

Table C-1: Summary of Void Analysis

Specimen	Member		Area [in^2 (mm^2)]		Void Area [in^2 (mm^2)]		%
1	Longitudinal	Top	0.126	81.1	0.011	7.06	8.70
		Bottom	0.115	74.2	0.0043	2.80	3.77
1	Diagonal	Top	0.027	17.6	0.0008	0.544	3.08
		Bottom	0.024	15.7	0.0019	1.23	7.82
2	Longitudinal	Top	0.114	73.7	0.0074	4.78	6.48
		Bottom	0.112	72.0	0.0079	5.12	7.11
2	Diagonal	Top	0.024	15.4	0.0014	0.907	5.90
		Bottom	0.024	15.7	0.0018	1.13	7.21
3	Longitudinal	Top	0.118	76.2	0.0098	6.32	8.29
		Bottom	0.114	73.6	0.0044	2.86	3.89
3	Diagonal	Top	0.023	15.0	0.00021	0.138	0.920
		Bottom	0.024	15.2	0.00022	0.139	0.917

Table C-2: Summary of Average Voids by Member Type

Member	Average Area [in^2 (mm^2)]		Average Void Area [in^2 (mm^2)]		Average %
Longitudinal	0.12	75.1	0.0075	4.82	6.37
Diagonal	0.024	15.8	0.0011	0.682	4.31

Table C-3: Summary of Average Voids by Specimen

Member	Longitudinal Average %	Diagonal Average %
Specimen 1	6.23	5.45
Specimen 2	6.79	6.55
Specimen 3	6.09	0.919
Average	6.37	4.31
Std. Dev.	0.371	2.99
[%]	5.8	69.3

Table C-4: Longitudinal Member Voids at the Middle of Member Summary

Specimen	Area [in^2 (mm^2)]		Void Area [in^2 (mm^2)]		%
1	0.120	77.7	0.0034	2.21	2.85
2	0.114	73.8	0.0048	3.12	4.22
3	0.113	73.2	0.0019	1.23	1.68
Average	0.116	74.9	0.00339	2.19	2.92
Std. Dev.	0.00378	2.44	0.00146	0.944	1.27
[%]	3.3		43.2		43.63

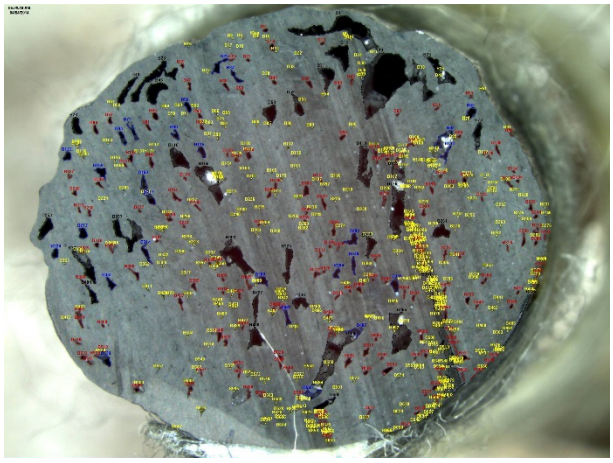

(A)

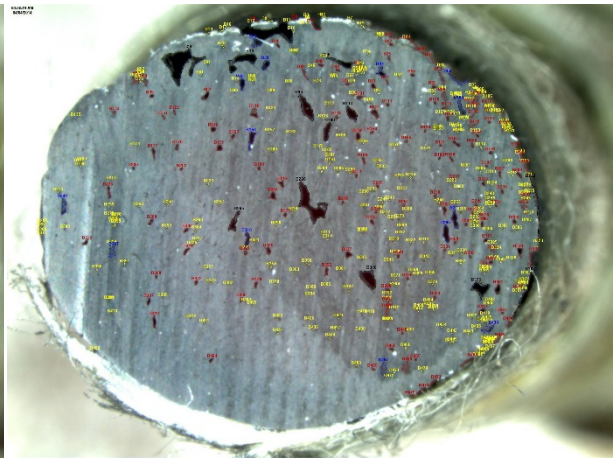

(B)

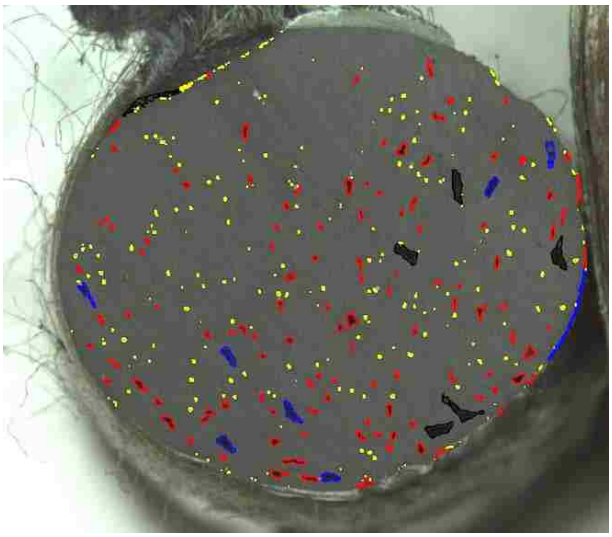

(C)

Figure C-1: Specimen 1 Longitudinal Void Content Analysis Picture: A) Top; B) Bottom; and, C) Middle

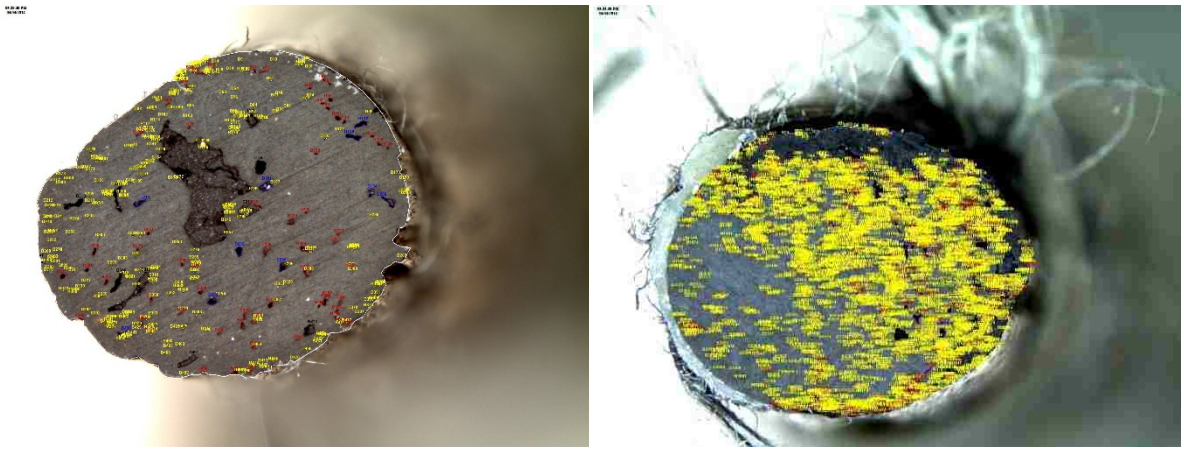

(A) **(B)**

Figure C-2: Specimen 1 Diagonal Void Content Analysis Picture: A) Top; and, B) Bottom

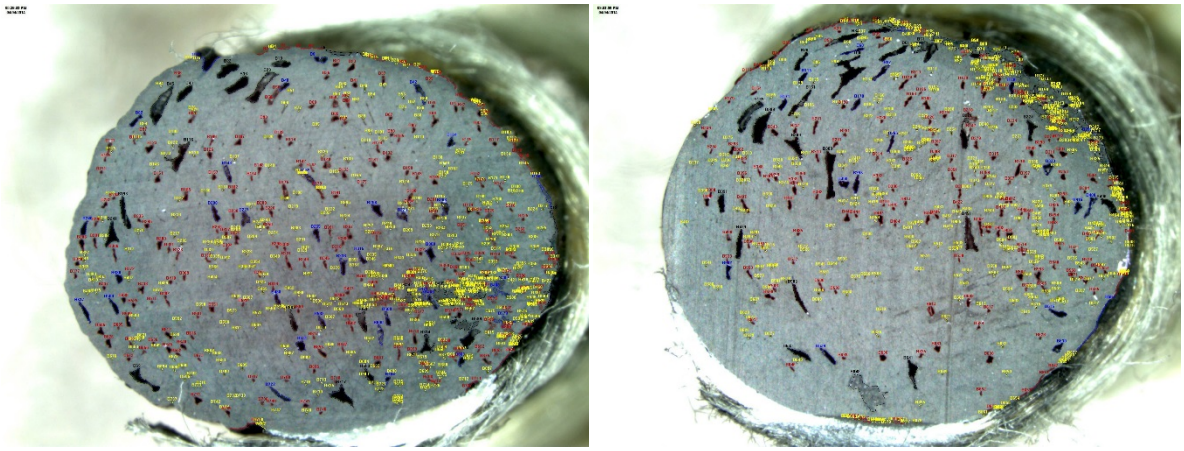

(A) **(B)**

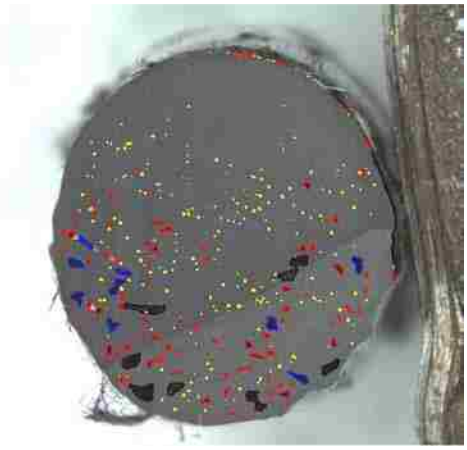

(C)

Figure C-3: Specimen 2 Longitudinal Void Content Analysis Picture: A) Top; B) Bottom; and, C) Middle

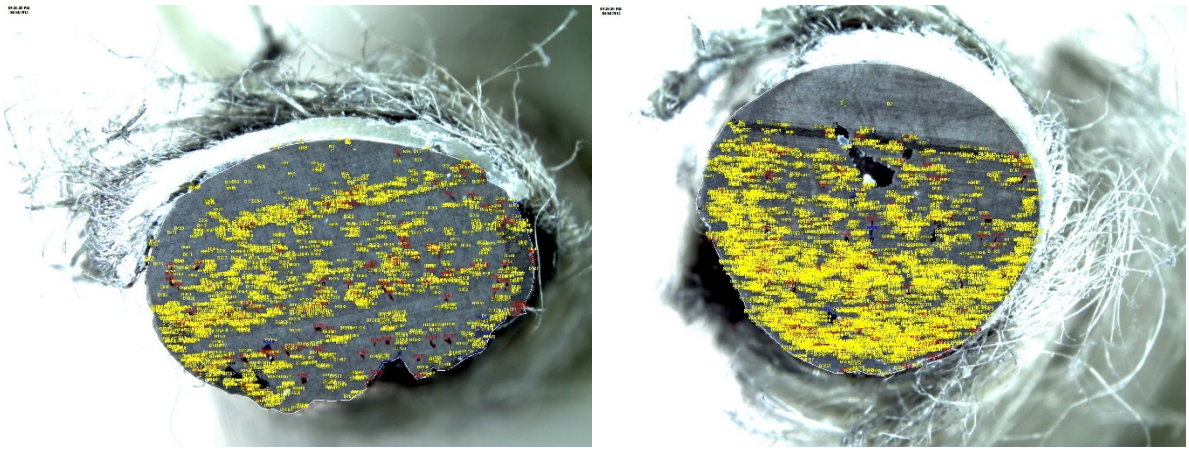

(A) **(B)**

Figure C-4: Specimen 2 Diagonal Void Content Analysis Picture: A) Top; and, B) Bottom

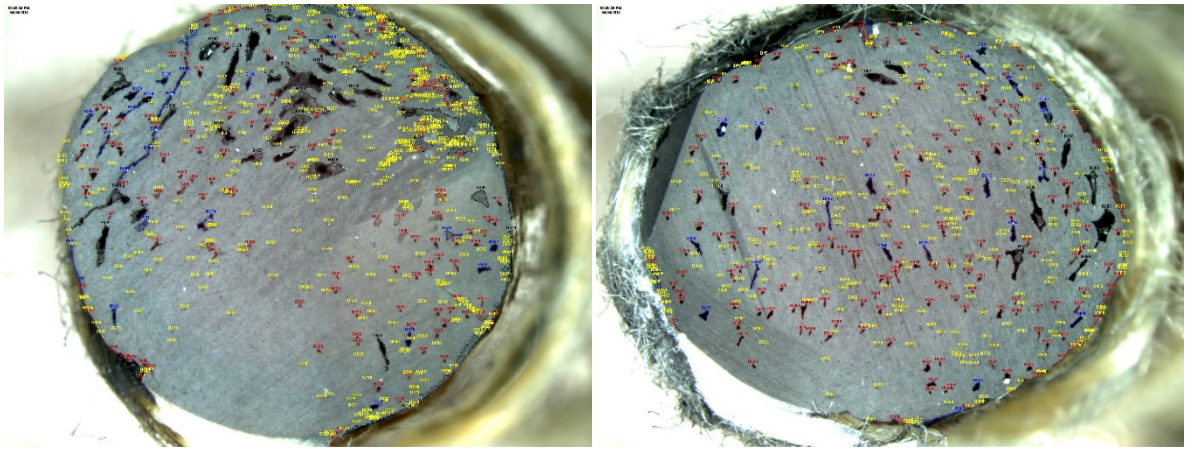

(A) **(B)**

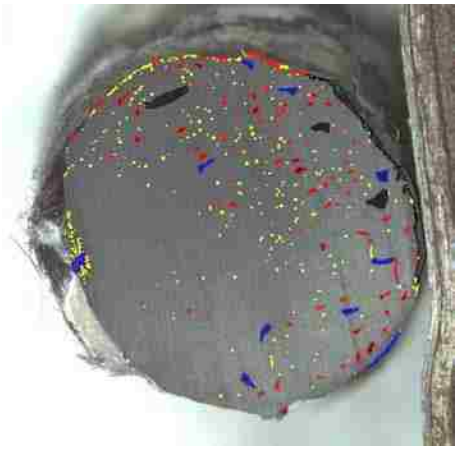

(C)

Figure C-5: Specimen 3 Longitudinal Void Content Analysis Picture: A) Top; B) Bottom; and, C) Middle

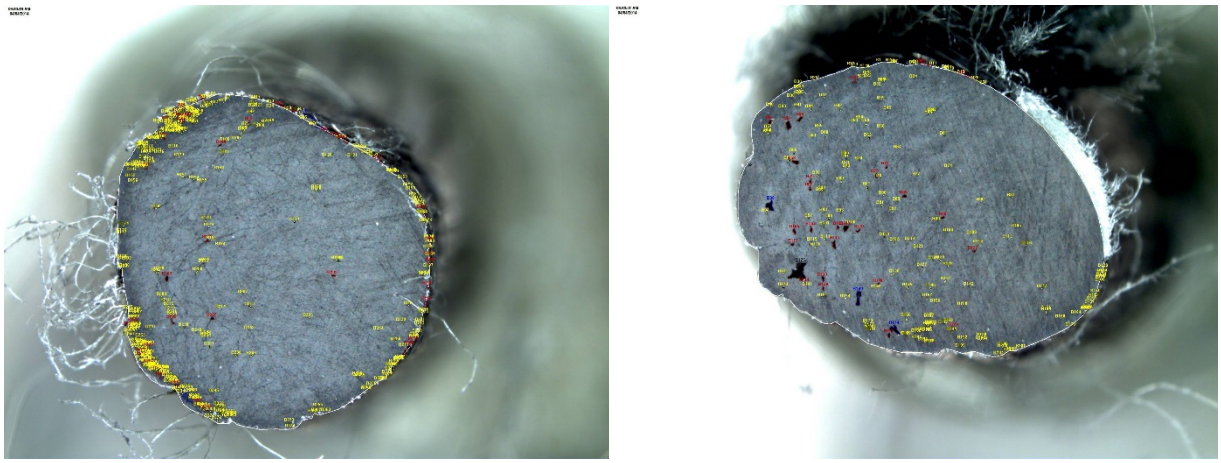

(A) (B)

Figure C-6: Specimen 3 Diagonal Void Content Analysis Picture: A) Top; and, B) Bottom

C.3 Fiber Volume Fraction Measurements

A summary of the fiber volume fraction analysis can be viewed in Table C-5. Following the summary, the pictures of the composite fiber taken with the Leco Olympus GX51 at 50X are included (Figure C-7-Figure C-12). The in focus section of each picture was selected as the area of evaluation and is highlighted in green.

Table C-5: Fiber Volume Fraction Percentage

Specimen	Member	% Fiber
1	Longitudinal	42.0
1	Diagonal	39.0
2	Longitudinal	41.5
2	Diagonal	36.1
3	Longitudinal	37.5
3	Diagonal	31.2
	Average	37.9
	Std. Dev.	3.97
	[%]	10.5

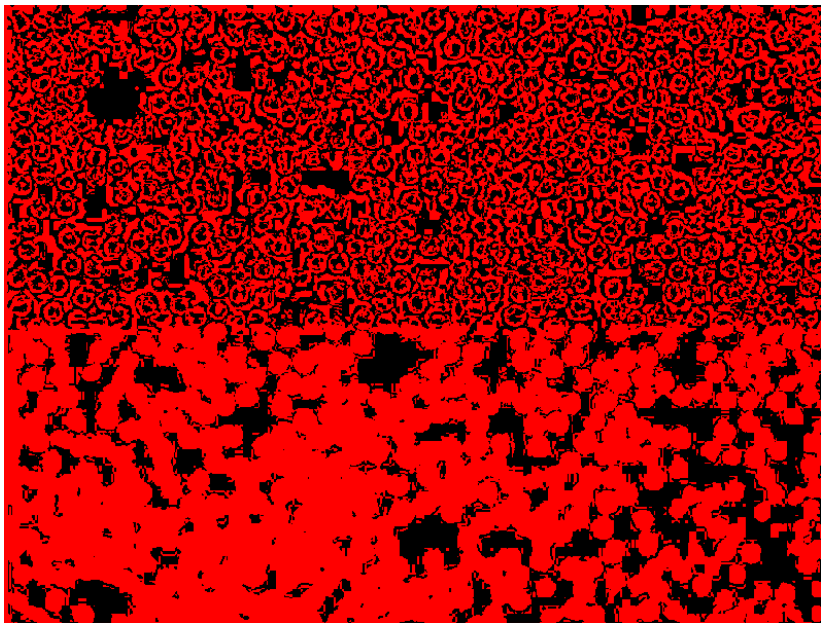

Figure C-7: Fiber Volume Fraction Picture for Specimen 1 Longitudinal

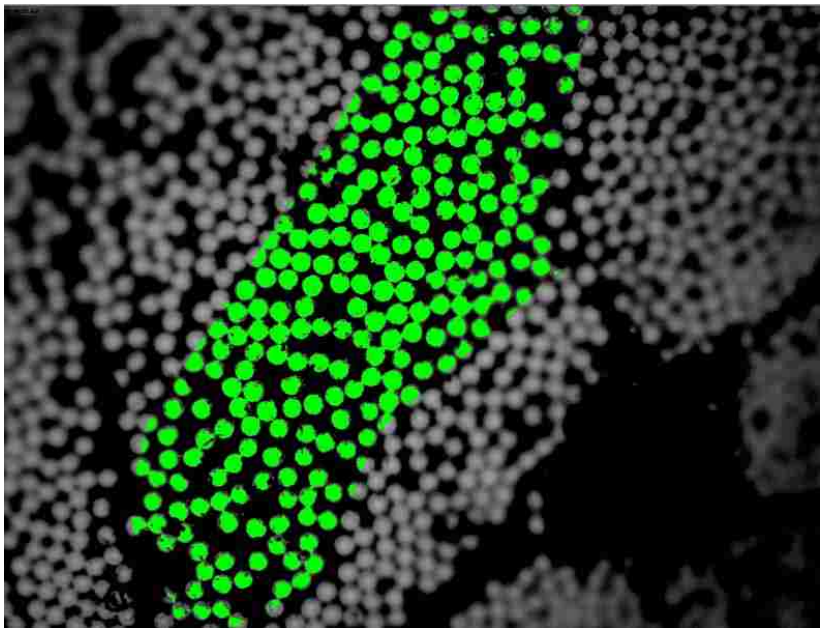

Figure C-8: Fiber Volume Fraction Picture for Specimen 1 Diagonal

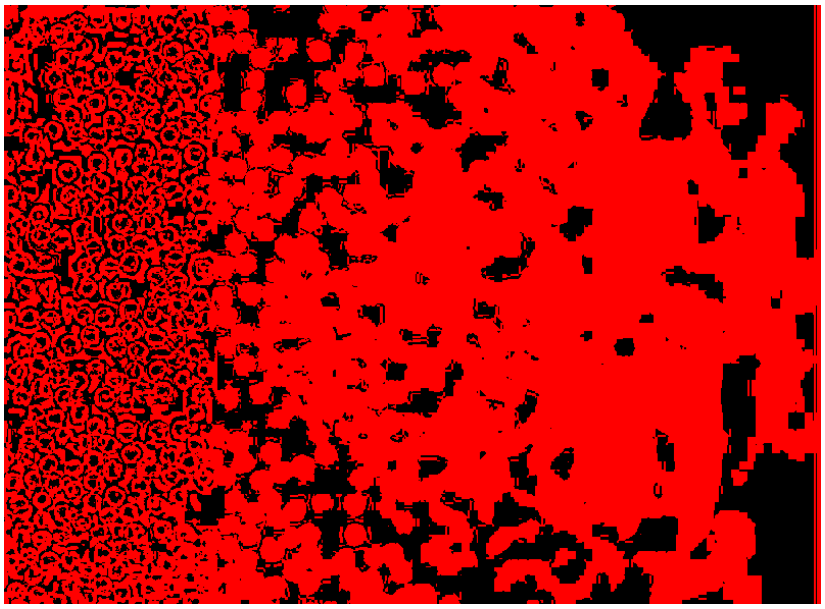

Figure C-9: Fiber Volume Fraction Picture for Specimen 2 Longitudinal

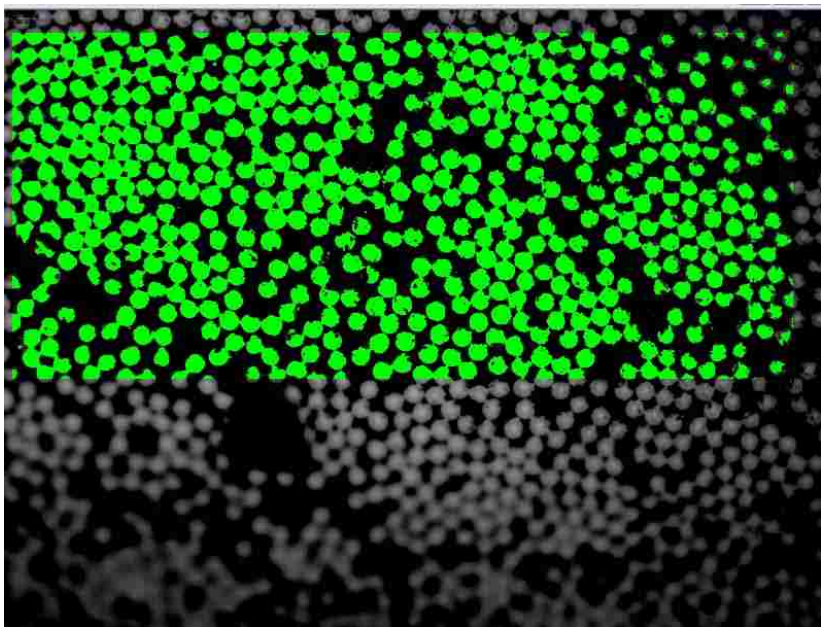

Figure C-10: Fiber Volume Fraction Picture for Specimen 2 Diagonal

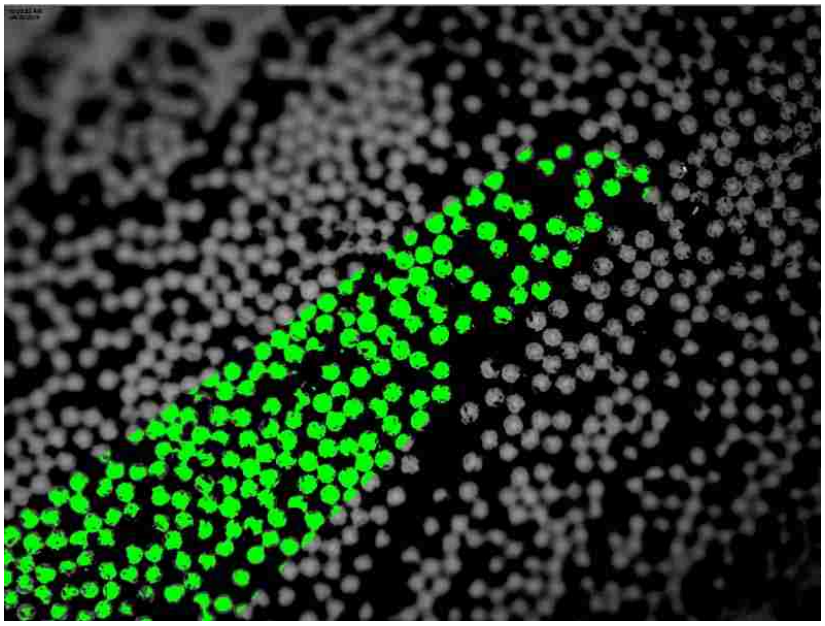

Figure C-11: Fiber Volume Fraction Picture for Specimen 3 Longitudinal

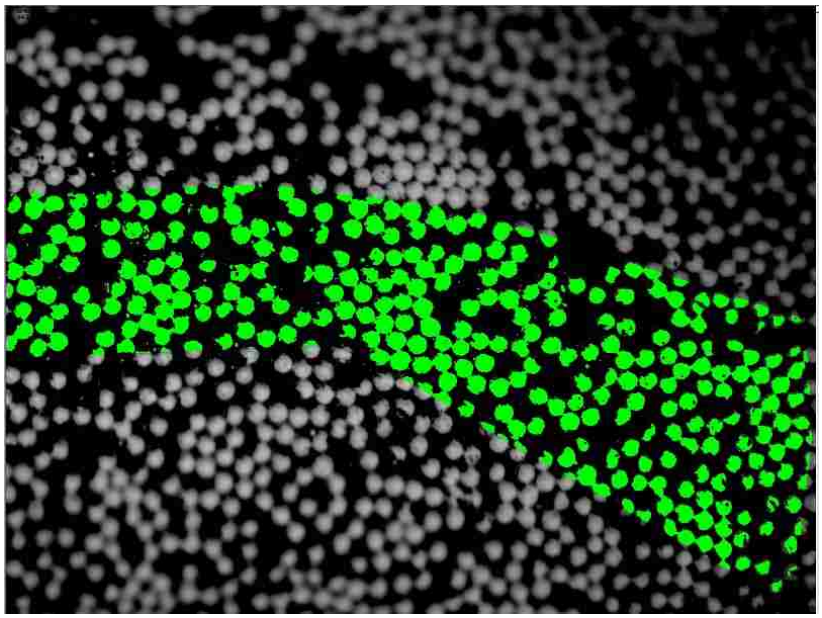

Figure C-12: Fiber Volume Fraction Picture for Specimen 3 Diagonal

APPENDIX D. MEMBER TEST RESULTS BY BEAM SPECIMEN

The following section contains the plots and tables for the members tested in compression organized by IsoBeam specimen.

D.1 Specimen 1 Member Compression Test Results

The results for Specimen 1 members are summarized in Table D-1 and presented in the stress-strain plot shown in Figure D-1. The average compression stress is 85.4 ksi (589 MPa) with a standard deviation of 37.3 ksi (257 MPa). The average strain at ultimate strength is 5.05×10^3 με with a standard deviation of 2.13×10^3 με. The average Young's modulus is 19.4×10^6 psi (133 GPa) with a standard deviation of 5.92×10^6 psi (40.8 GPa).

Table D-1: Summary Table for Specimen 1 Members

Specimen ID	Cross-Sectional Area		Compression Young's Modulus		Strain at Ultimate Compression Stress	Ultimate Compression Stress	
	[in^2	(mm^2)]	[10^6 psi	(GPa)]	[με]	[ksi	(MPa)]
L1-1	0.123	79.3	18.8	130	3,950	62.4	431
L1-2	0.119	76.9	27.6	190	3,000	65.1	449
D1-1	0.026	16.7	17.4	120	7,900	141	971
D1-2	0.032	20.7	13.6	93.8	5,350	73.2	505
Average	0.075	48.4	19.4	133	5,050	85.4	589
Std. Dev.	0.053	34.4	5.92	40.8	2,131	37.3	257
[%]	71.0		30.6		42.2	43.6	

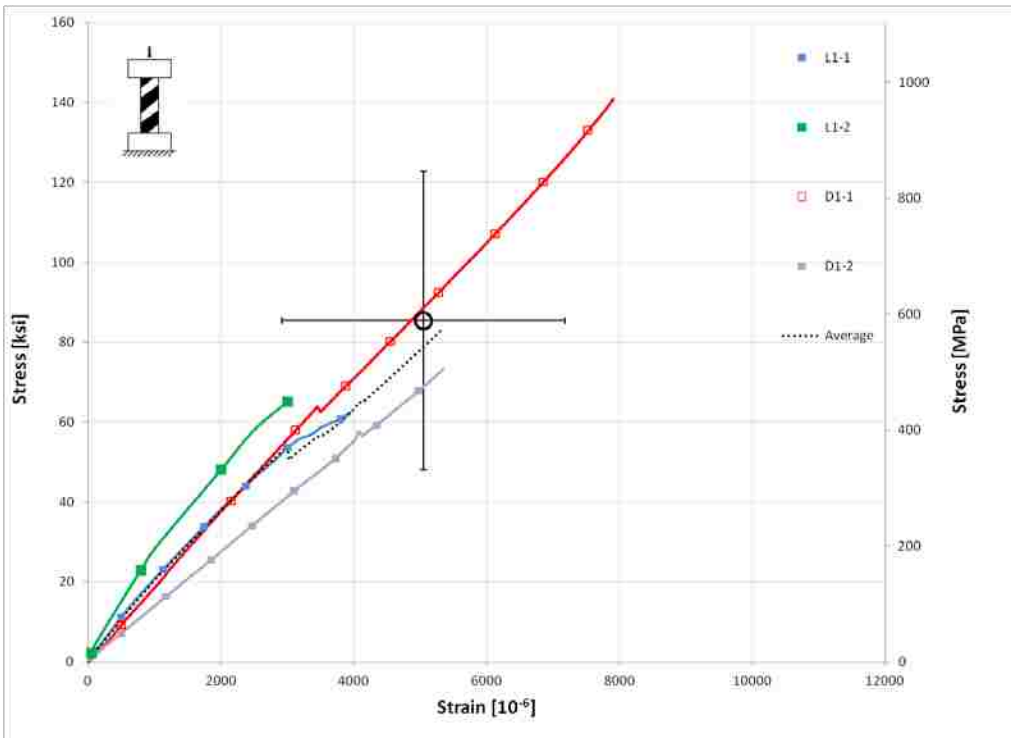

Figure D-1: Stress-Strain Plot for Specimen 1 Members

D.2 Specimen 2 Member Compression Test Results

The results for Specimen 2 members are summarized in Table D-2 and presented in the stress-strain plot shown in Figure D-2. The average compression stress is 83.0 ksi (572 MPa) with a standard deviation of 27.2 ksi (188 MPa). The average strain at ultimate strength is 5.09×10^3 με with a standard deviation of 3.79×10^3 με. The average Young's modulus is 20.9×10^6 psi (144 GPa) with a standard deviation of 5.41×10^6 psi (37.3 GPa).

Table D-2: Summary Table for Specimen 2 Members

Specimen ID	Cross-Sectional Area		Compression Young's Modulus		Strain at Ultimate Compression Stress	Ultimate Compression Stress	
	[in^2]	(mm^2)]	[10^6 psi	(GPa)]	[με]	[ksi	(MPa)]
L1-1	0.123	79.3	18.8	130	3,950	62.4	431
L2-1	0.119	76.9	22.8	157	3,475	61.7	426
L3-1	0.120	77.7	19.1	132	2,750	53.2*	367*
L1-2	0.119	76.9	27.6	190	3,000	65.1	449
L2-2	0.118	76.0	21.0	145	3,175	64.4	444
L3-2	0.124	79.7	15.2	105	4,000	58.6	404
Average	0.121	77.8	20.8	143	3,392	62.5	431
Std. Dev.	0.002	1.48	4.21	29.0	510	2.56	17.6
[%]	1.91		20.3		15.0	4.09	

*Property eliminated using Chauvenet's criterion, values not included in average or standard deviation

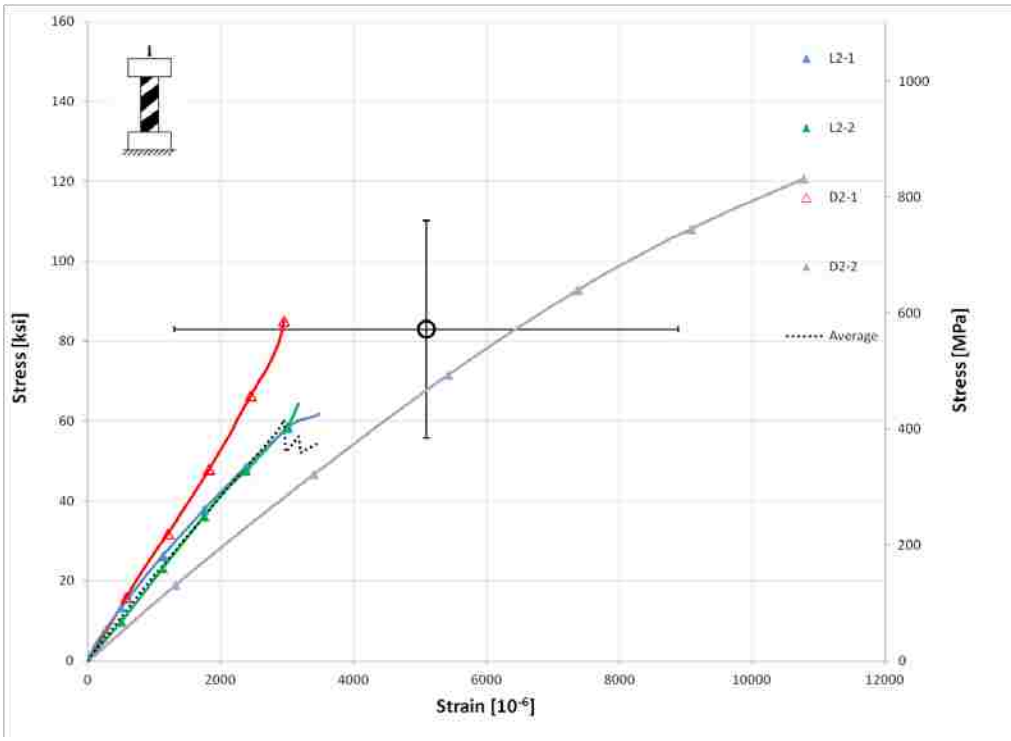

Figure D-2: Stress-Strain Plot for Specimen 2 Members

D.3 Specimen 3 Member Compression Test Results

The results for Specimen 3 members are summarized in Table D-3 and presented in the stress-strain plot shown in Figure D-3. The average compression stress is 89.9 ksi (620 MPa) with a standard deviation of 40.3 ksi (278 MPa). The average strain at ultimate strength is 5.79×10^3 με with a standard deviation of 2.87×10^3 με. The average Young's modulus is 15.9×10^6 psi (110 GPa) with a standard deviation of 2.19×10^6 psi (15.1 GPa).

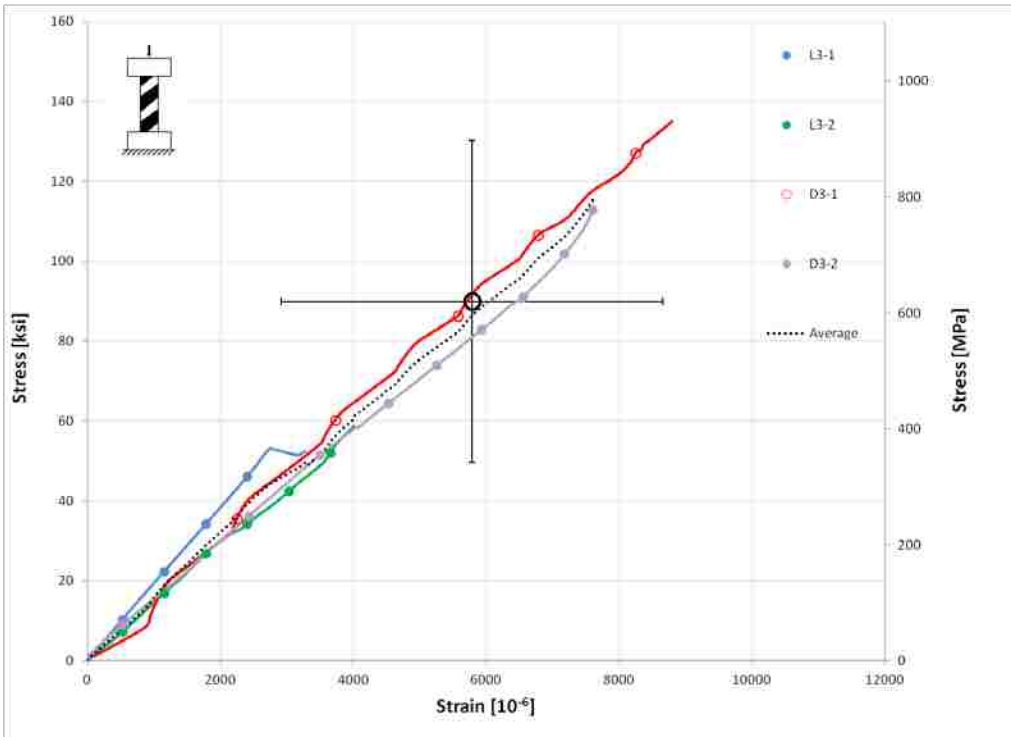

Figure D-3: Stress-Strain Plot for Specimen 3 Members

Table D-3: Summary Table for Specimen 3 Members

Specimen ID	Cross-Sectional Area		Compression Young's Modulus		Strain at Ultimate Compression Stress	Ultimate Compression Stress	
	[in^2	(mm^2)]	[10^6 psi	(GPa)]	[με]	[ksi	(MPa)]
L3-1	0.120	77.7	19.1	132	2,750	53.2	367
L3-2	0.124	79.7	15.2	105	4,000	58.6	404
D3-1	0.023	15.1	15.3	105	8,800	135	931
D3-2	0.031	20.1	14.1	97.2	7,600	113	778
Average	0.075	48.2	15.9	110	5,788	89.9	620
Std. Dev.	0.055	35.4	2.19	15.1	2,874	40.3	278
[%]	73.5		13.7		49.7	44.9	